University of California
Santa Barbara

Four is Not a Crowd: Unexpected Multiphase Separation of Reflectin Proteins

A dissertation submitted in partial satisfaction
of the requirements for the degree

Doctor of Philosophy
in
Molecular, Cellular, and Developmental Biology

by

Reid Gordon

Committee in charge:

Professor Daniel Morse, Chair
Professor Songi Han
Professor Matthew Helgeson
Professor Herbert Waite

December 2023

The Dissertation of Reid Gordon is approved.

Professor Songi Han

Professor Matthew Helgeson

Professor Herbert Waite

Professor Daniel Morse, Committee Chair

December 2023

Four is Not a Crowd: Unexpected Multiphase Separation of Reflectin Proteins

by

Reid Gordon

To my family

Acknowledgements

Many people have been invaluable to my long and arduous Ph.D. journey:

The unrelenting intellectual challenging of my hypotheses, experiments, and data interpretations by Rob Levenson has shown me the importance of never accepting any premise at face value as a scientist.

I would to give a huge thanks to my PI, Dan Morse, for his tireless encouragement of my research, his diligent editing, and reminding me that when I get an experimental effect, *I should push the effect.*

Thank you to my committee, Matt, Herb, and Songi your feedback has helped me focus my ideas and your interest in reflectins has driven me to add as much as I can to with my research.

Thank you to Jerome Santos, who was the first person I worked with in the Morse lab and made me feel welcome.

It was a great pleasure working with Brandon Malady and Yahya Al-Sabeh, who kept the lab running and the recombinant reflectin pipeline flowing while he was with us.

I am grateful for all the training and support I received from Ben Lopez at the NRI microscopy facility, and all the hours spent by Alan Nguyen preparing microscope slides for my confocal experiments.

And finally, thank you to my family for supporting my seemingly endless academic career and especially to my intellectual inspiration and amazing wife Caroline.

Curriculum Vitæ
Reid Gordon

Education

2023	Ph.D. in Molecular, Cellular, and Developmental Biology (Expected), University of California, Santa Barbara.
2022	M.S. in Molecular, Cellular, and Developmental Biology, University of California, Santa Barbara.
2013	B.S. in Biochemistry, University of California, Santa Barbara Reid Gordon

Professional Experience

2014-2017 **Clinical Chemistry Technician**
Pacific Diagnostics Laboratories, Cottage Health Systems. Calibration and quality control of automated high-throughput clinical chemistry and immunochemistry analyzers

Research Experience

2017-present **Graduate Student Researcher**
University of California, Santa Barbara
Principle Investigator: Daniel Morse
Research Area: Oligomerization and Liquid-Liquid phase separation of reflectin proteins A1, A2, B and C that mediate dynamic iridescence in *Doryteuthis opalescens*

2013-2014 **Undergraduate Research Assistant**
University of California, Santa Barbara
Principle Investigator: Herbert Waite
Research Area: Structural characterization of adhesive mussel protein mfp-5 from *Mytilus californianus*

Teaching Experience

Teaching Assistant
MCDB1LL (8 quarters): Introductory Biology Lab I
EEMB 2LL (8 quarters): Introductory Biology Lab II
MCDB 108A (1 quarter): Biochemistry- Structure and Function of Macromolecules
MCDB 108B (4 quarters): Biochemistry-Bioenergetics, Enzymology and Metabolism

Publications

Gordon R, Levenson R, Malady B, Al-Sabeh Y, Nguyen A, Morse DE (TBD) *Electrostatic Screening and Hydrophobicity Drive Progressive Assembly and Liquid-Liquid Phase Separation of Reflectin Protein.* JBC

Gordon R, Morse DE (TBD) *Multiphase Organization of Reflectin Proteins Dictated by Protein Net Charge Density, Salt concentration, and Protein Ratios.* JBC

Abstract

Four is Not a Crowd: Unexpected Multiphase Separation of Reflectin Proteins

by

Reid Gordon

Reflectins are a unique class of proteins found in the specialized iridescent cells, iridocytes, in cephalopods. The colors reflected by dorsal iridocytes from the California market squid Doryteuthis opalascens are neuronally tunable, and these cells are enriched in reflectins A1, A2, B, and C. The phosphorylation of cationic reflectin proteins result in reflectin assembly: the degree of assembly controls the extent of dehydration of the light-scattering Bragg lamellae, adjusting their dimensions and therefore wavelengths of light that are reflected. I show that reflectin A1 assemblies are in dynamic exchange through a dilute monomeric phase and characterize the aging of dynamic exchange using DLS (dynamic light scattering) and FRET (Forster resonant energy transfer). Reflectin A1 phase behavior is determined by protein net charge density and ionic strength. At high net charge densities, increasing salt concentration drives liquid-liquid phase separation of reflectin A1 via nanoscale assembly intermediates. The hydrophobic effect and electrostatic screening of intra- and inter-protein Coulombic repulsion progressively drive reflectin A1 folding, assembly, and LLPS. Using fluorescence recovery after photobleaching (FRAP) and droplet fusion dynamics I demonstrate the liquidity of reflectin A1 condensates is tuned by protein NCD and ionic strength. Reflectins A2, B, and C from tunable iridocytes of Doryteuthis opalascens also show similar phase behavior to reflectin A1. Reflectin C co-phase separates and drastically increases the liquidity of reflectin A1. Condensates formed from physiologically relevant mixtures of reflectins A1, A2, B, and C show complex layered droplet formation in which the relative miscibility of each reflectin

varies with pH, ionic strength, and proportions of reflectin species. The many inputs that define multi-reflectin phase behavior in vivo shows reflectins usefulness for creating soft biomaterials with tunable spatial organizations and liquid properties. These findings also demonstrate that LLPS of reflectins A1, A2, B and C could occur upon iridocyte activation, and that ratios of these reflectin species found in tunable iridocytes could enhance the tunability of lamellar dehydration induced by reflectin phosphorylation.

Contents

Chapter 1

Introduction

1.1 Cephalopod Molecular Strategies for Dynamic Structural Color

Cephalopods are renowned for their rapid, dynamic, and complex displays of color. Their skin is a complex optical system combining both pigmentary and structural coloration working in tandem [1, 2, 3]. Iridocytes and leucophores are specialized dermal cells that produce structural color [4, 5, 6]. Leucophores contain leucosomes: regularly sized spherical sub-cellular bodies of high refractive index structures that scatter broadband light. Iridocytes are marked by their extensive and highly regular membrane invaginations that form intracellular protein-dense lamellae [7, 8, 9]. The regular spacing of these high-refractive index lamellae alternating with low refractive index extracellular fluid create Bragg stacks which produce iridescence by reflecting light coherently in an angle- and wavelength-dependent manner [9, 10, 11]. The leucosomes of leucophores and Bragg lamellae in iridocytes are enriched in reflectin proteins [12, 13].

1.2 Dynamic Iridescence and Broadband Scattering in *Loliginid* Squids

In the recently evolved loliginid squids, both leucophores and iridocytes are dynamic structures under neuronal control [14, 15, 16]. In iridocytes, neuronally released acetylcholine binds muscarinic receptors which activate a G-protein calcium-calmodulin mediated signal transduction pathway [13, 17]. This results in the activation of specific kinases and phosphatases that reversibly alter the phosphorylation of reflectin proteins within the Bragg lamellae, neutralizing the Coulombically-repulsed cationic reflectins to drive their resulting folding and condensation [9, 10, 11, 12, 13].

The release of counter-ions upon reflectin condensation results in the Gibbs-Donnan mediated net efflux of water out of the lamellae upon activation and a net influx upon reversal [18]. This reversible dehydration increases both the refractive index of the lamellae as well as precisely and uniformly tuning their thickness and spacing, thus progressively changing the reflected wavelengths of light [9, 10, 11]. TEM of inactive iridocytes in Doryteuthis opalescens show Bragg lamellae filled with regularly-sized dense spheres of ca. 100 nm size resembling beads on a string whereas Bragg lamellae in activated iridocytes stain uniformly and densely [9, 19].

1.3 Reflectin Protein Family

Found in many cephalopods, reflectin proteins are enriched in arginine, aromatic residues and methionine, while being devoid of lysine and aliphatic residues [12, 13, 20, 21]. They are block-copolymers of cationic linkers and anionic reflectin repeat motifs (RMs) as well as a strongly conserved N-terminal sequence (RMn) [21, 22]. RMs and RMns are strongly conserved methionine-rich sequences (figure 1.3 A,B) that show little

sequence similarity to non-reflectin proteins . The enrichment of arginine and tyrosine residues, specifically RY- and GRY- peptides in reflectins A1 and A2 from Doryteuthis opalescens suggests that pi-cation interactions are a major driving force of reflectin folding and assembly [23, 24]. Similarly, the enrichment of methionine residues in reflectins suggests sulfur-pi bonds could also contribute to inter- and intra-protein interactions in reflectin [25, 26, 27]. NMR of a truncation of reflectin A1 from Doryteuthis pealeii, which has high sequence similarity to reflectin A1 found in D. opalescens, shows significant overlaps of chemical shifts of tyrosine and arginine residues. In these structures, methionines were also shown to cluster around a single tryptophan residue, providing evidence for pi-cation and sulfur-pi bonds in reflectin A1 [28]. Reflectins A1, A2, B, and C are found in leucophores and iridocytes of D. opalescens. Tunable iridocytes in the dorsal epithelium of the mantle respond to exogenous acetylcholine by a dramatic increase in wavelength-specific reflection of light and are enriched in reflectins B and C relative to non-tunable iridocytes in the ventral epithelium that show little or no optical response to acetylcholine [5, 12, 13]. Reflectins B and C from D. opalescens are less enriched in tyrosine and arginine than the A types, and do not share the alternating block copolymeric organization of conserved reflectin motifs (RMs) and linkers seen in reflectins A1 and A2 as well as the entire reflectin protein family (Figure 1.1C). Reflectin B lacks RMs but contains the RMn. Reflectin C lacks the RMn, contains only one weakly conserved RM, and has a unique proline-enriched GMXX repeat region (Figure 1.1C). All four are highly basic, with pKas ranging from 8.59 to 8.88. Upon iridocyte activation with acetylcholine, reflectins A1 and are phosphorylated, reflectin B is dephosphorylated, and no change in phosphorylation has been detected in reflectin C [12, 13]. The net charge density of the reflectins, tuned by phosphorylation, has been shown to correlate with the calibrated dehydration of the Bragg lamellae, determining the wavelength and intensity of light reflected by tunable iridocytes in D. opalescens, as described below.

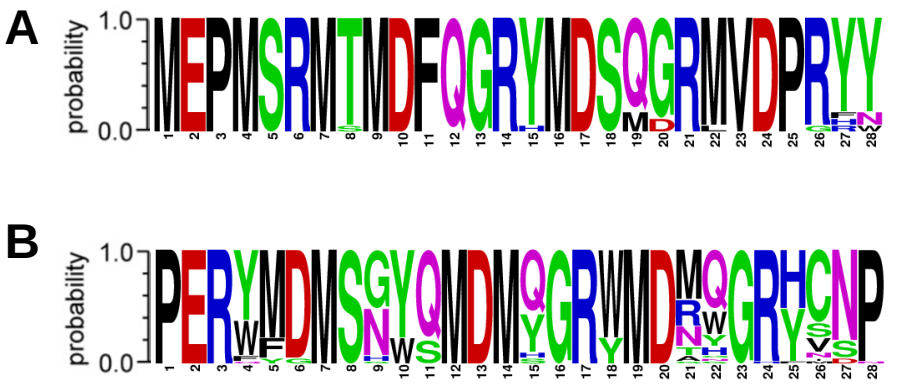

C

Reflectin A1

```
  1-MNRYLNRQRLYNMYRNKYRGVMEPMSRMTMDFQGRYMDSQGRMVDPRYYDHYGRMHDYDR-60
 61-YYGRSMFNQGHSMDSQRYGGWMDNPERYMDMSGYQMDMQGRWMDAQGRYNNPFSQMWHSR-120
121-QGHYPGYMSHHSMYGRNMHYPYHSHSASRHFDSPERWMDMSGYQMDMQGRWMDNYGRYVN-180
181-PFHHHMYGRNMFYPYGSHCNNRHMEHPERYMDMSGYQMDMQGRWMDTHGRHCNPLGQMWH-240
241-NRHGYYPGHPHGRNMFQPERWMDMSSYQMDMQGRWMDNYGRYVNPFSHNYGRHMNYPGGH-300
301-YNYHHGRYMNHPERQMDMSGYQMDMHGRWMDNQGRYIDNFDRNYYDYHMY-350
```

Reflectin A2

```
  1-MNRYMMRHRPMYSNMYRTGRKYRGVMEPMSRMTMDFQGRYMDSQGRMVDPRYYEYGRCHD-60
 61-YDRYNGRSMFNNGPYMDGQRYGGWMDFPERYMDMSGYQMDMHGRWMDSQGRYCNPMGHSW-120
121-SNRQGYYPGSNYGRNMFNPERYMDMSGYQMDMQGRWMDMGGRHVNPFSHSMYGRNMFNPS-180
181-YFSNRHMDNPERYMDMSGYQMDMQGRWMDTQGRYMDPSMSNMYDNYNYWY-230
```

Reflectin B

```
  1-MSSFMDPMHYDGMGMSHSKSGDFSHNCMRSFHKSQRDGMRRDIMGKSSKNRRFGNLMEPM-60
 61-SRMTMDFHGRLIDSQGRIVDPGHYFAMDDHYMENDRFLYPHDMLRNRHGMYGFMQGDYGN-120
121-NMHRGMFADGMYRDMHHSGMNPSSYMHGGSMQNRPMMYMQGRYLDDSYFMNYHDPPVIVH-180
181-SHYNDQEGRHQGMYDRHSDSYGSHRRHGDSHSMPRRPSESHSPQRRPSEGHIIQVRPEGG-240
241-SSRKTSRAQLFPDDKLTDSA-260
```

Reflectin C

```
  1-MNKHSSSHGMHGENYSRTGARGLHRGMEHESKSMYGKGRERSTDHGDMESSRHGMPGGMN-60
 61-PGMYGGMPSGMPGGMYPGMYGGMPGFGVPQMMQCPPDMPRRYIDRHDRSMDMPYGRYMDM-120
121-PQGRYMSSQDRLMHMMHNRHLYGRMMDQGRMGEPMEGNMENRGRNMENYE-170
```

Figure 1.1: Reflectin proteins contain unusual but highly conserved repeat motifs. Sequence logo from the alignment of the (A) N-terminal repeat motif and (B) reflectin repeat motifs from 51 reflectin proteins found in *Octupus bimaculoides, Euprymna scolopes, Sepia officinalis, Doryteuthis opalascens* and *Doryteuthis pealeii*. The reflectin repeat motif begins and ends with completely conserved prolines, suggesting it is a stretch of secondary structure when reflectin is folded. C) Sequences of reflectins A1, A2, B, and C from *Doryteuthis opalascens*. N-terminal motifs are highlighted in green and repeat motifs in red. Reflectin C contains one poorly conserved repeat motif (red) and the GMXX proline-rich region (gray). Sequence logo created using U.C. Berkeley WebLogo

1.4 Protein Net Charge Density Tunes Reflectin Assembly sizes

Increasing pH progressively deprotonates abundant histidine residues in reflectin A1, reducing the number of positive charges and acting as an in vitro surrogate for in vivo phosphorylation of reflectin A1 upon iridocyte activation [22, 29]. This reduction in protein net charge density causes the reversible folding of reflectin A1 and assembly into higher order multimers [22]. Sizes of reflectin A1 assemblies measured as a function of pH, and sizes of assemblies of A1 mutants in which the net charge had been altered by insertion of glutamate or histidine residues demonstrate that the net charge density of the cationic linker regions opposes assembly, and reducing coulombic repulsion by decreasing net charge density controls the sizes of assemblies [29]. Reflectins A2, B, and C also demonstrated pH-dependent assembly, and mixtures of these species in the proportions found in dorsal (tunable) iridocytes reversibly co-assembled [22]. Reflectin A1 folding and assembly sizes have been tuned by electrochemical reduction of native histidine residues, increasing ionic strength [30], and are sensitive to low concentrations of aromatic compounds as well as histidine [31, 32, 33]. Increasing reflectin assembly size reciprocally reduces particle number concentration, thereby regulating osmotic pressure of the membrane-bound Bragg lamellae vesicles of the tunable iridocytes and leucophores. In combination with the Gibbs-Donnan effect, this osmotic motor further increases the efflux of water across the semipermeable membranes of the Bragg lamellae tunability. In combination with the Gibbs-Donnan effect, this osmotic motor could further increase the efflux of water across the cell membrane and drive the dehydration of Bragg lamellae [12]. The remarkable in vivo tunable iridescence of the Bragg lamellae as well as the in vitro tunability of reflectin A1 assembly sizes by pH-titration, genetic engineering, and most recently electrochemical reduction of histidine residues has drawn much bioengineering

interest for creating optically tunable materials. Reflectins have been used to manufacture reflective thin films, diffraction gratings, electronic and protonic-conducting materials, as well as optical biomaterials that can be tuned by electrical, chemical, and mechanical activation [34, 35, 36, 37].

Chapter 2

Reflectin A1 Assemblies Dynamically Exchange Monomer Through Dilute Phase

2.1 Illuminating the Mechanism by Which Protein Net Charge Density Determines Reflectin A1 Assembly Sizes

Reflectin A1 assembly sizes are precisely determined by the extent of coulombic repulsion in the cationic linker regions, with decreasing protein net charge density (NCD) forming progressively larger assemblies [29]. However the physical process that enables this relationship is unknown. The rapid arrest of reflectin A1 assembly size growth, the stability of assembly sizes with time and dilution, and their robustness to AFM probing and TEM sample preparation [22, 29]. These observations are consistent with a kinetic mechanism in which spinodal decomposition is rapidly followed by glass-like ar-

rest which controls the sizes of thermodynamically unstable assemblies, but do not rule out an equilibrium process. Reflectin A1 assemblies can also be described as dynamic equilibrium clusters, where assemblies exist in thermodynamic equilibrium and sizes are determined by a balance of short range attraction and long range repulsion (SALR) [38, 39, 40, 41, 42, 43]. We begin to shine light on these mechanisms by using Forster Resonant Energy Transfer (FRET) to demonstrating that reflectin A1 assemblies are initially in dynamic exchange via a dilute monomeric phase and this exchange ages rapidly. Dynamic light scattering (DLS) shows that the arrest of assembly size growth strongly correlates with the arrest of dynamic exchange between assemblies.

2.2 Reflectin A1 Assemblies Coexist with Dilute Monomer Phase

Following assembly of reflectin A1, a centrifugation assay was used to determine the coexistence of a dilute phase of monomers and a dense phase of assemblies [44]. Reflectin A1 by dilution to a final concentration of 4 μM 25 mM MOPS buffer at pH 7 ,and after 5 d at 20°C, samples were centrifuged at 20,000 x g for 6 hours to remove assemblies (Fig. 2.1A). A Bradford assay revealed that C_{dil} increases with C_{bulk} for C_{bulk} between 1-10 μM (Fig. 2.1B) and the increase is linearly proportional. For reflectin A1, C_{dil} depends on C_{bulk} for a range of C_{bulk} in which the system coexists as monomer and assembly. Although Cdense for reflectin A1 assemblies is unknown, the ratio of moles protein in monomer to moles protein in assemblies is constant for $C_{bulk} \geq 2$ μM. This value decreases from 99.4 $\pm$ 2.7% for $C_{bulk} = 1$ μM to 94.7 $\pm$ 0.1% for $C_{bulk}= 2$ μM and stays relatively constant up to $C_{bulk} = 10$ μM (95.4 $\pm$ 0.18%). This differs from classical bulk phase separation where C_{dil} increases with C_{bulk} until it exceeds the saturation concentration

Csat, and any additional increase in C_{bulk} is partitioned into the dense phase and $C_{Sat} = C_{dil}$ [24, 45]. Reflectin A1 assembly sizes for C_{bulk} between 1-10 μM do not increase with increasing protein concentration as has been recently reported for FUS protein clusters [44]. Instead, reflectin A1 assembly sizes decrease as C_{bulk} is increased from 1-4 μM (Fig. 2.2A-C). Notably, the size distribution of assemblies narrows as C_{bulk} is increased from 1-10 μM (Fig. 2.2A-F) . Assembly sizes range from 70-500 nm diam. for Cbulk of 1 μM. At $C_{bulk} = 2$ μM, size distributions are bimodal with a larger proportion by volume of assemblies in the smaller size distribution (Fig. 2.2B). As C_{bulk} is further increased to 10 μM, this bimodality decreases (Fig. 2.2D-F). Reflectin A1 assembly size as a function of concentration mirrors the dependence of C_{dil} on C_{bulk} . Partitioning of reflectin A1 into assemblies for $C_{bulk} \leq 2$ μM varies from $C_{bulk} \geq 4$ μM which is relatively constant (Fig. 2.1). Assembly sizes for $C_{bulk} \leq 2$ μM vary from assembly sizes for $C_{bulk} \geq 4$ μM, which is then relatively constant (Fig. 2.2), suggesting that the mechanisms for both formation of assemblies and restriction of assembly size are coupled and are incomplete for $C_{bulk} \geq 2$ μM.

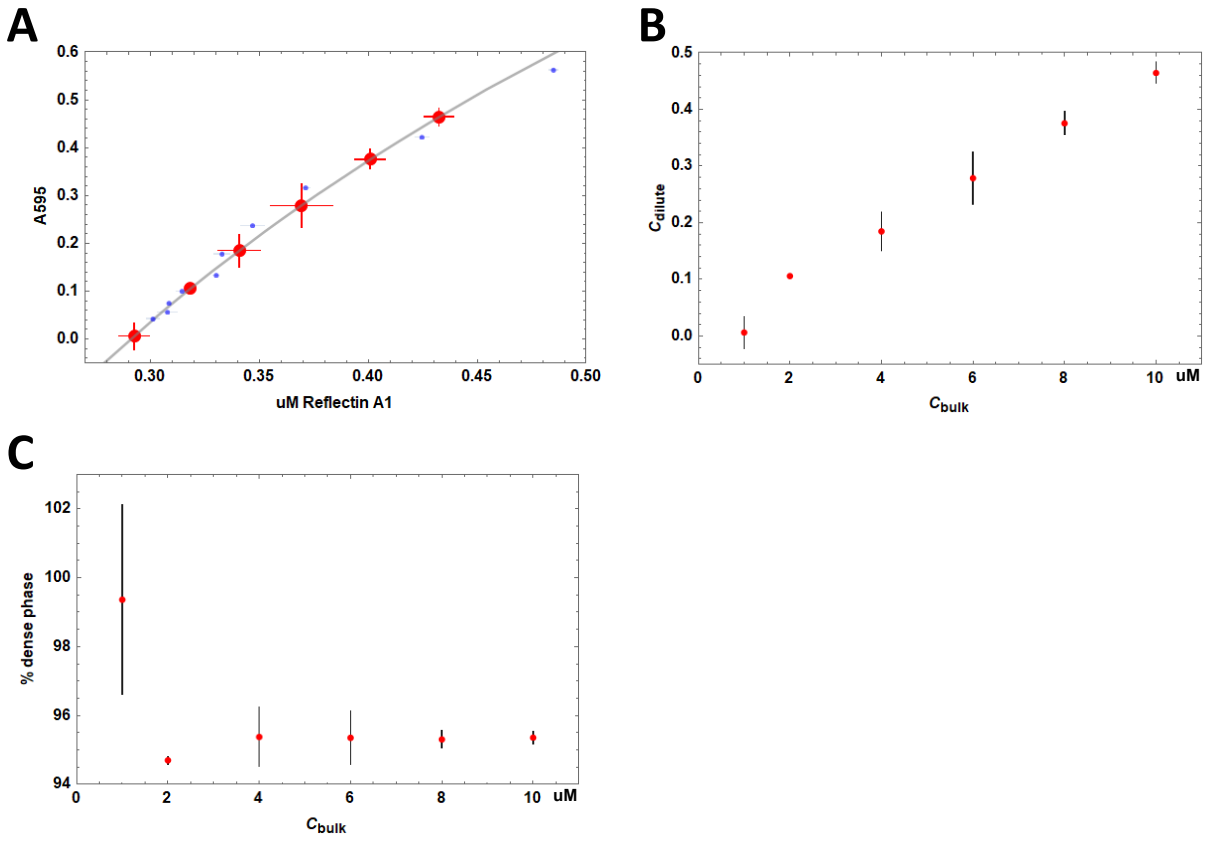

Figure 2.1: Reflectin A1 assemblies coexist with monomer at pH 7 25 mM MOPS. A) Bradford assay showing standards (light blue), the fit curve (light blue), and experimental data points (multiple colors). The y-axis is absorbance at 595 and the x-axis is reflectin A1 concentration in μM. B) Reflectin A1 dilute concentration (y-axis) depends on bulk concentration (x-axis). C) For bulk concentrations between 2-10 μM, the percent of reflectin in the dense phase is constant. All data points represent 3 experimental replicates with 3 measurement replicates each. Error bars represent $\pm$ 1 S.D.

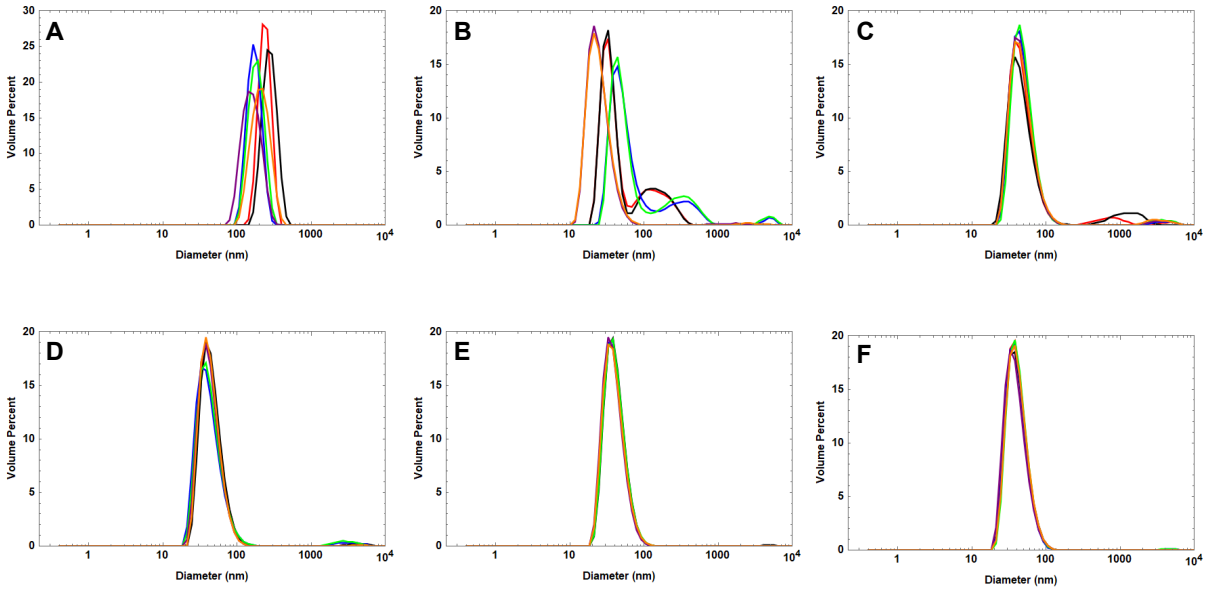

Figure 2.2: Size distributions of reflectin A1 assemblies in MOPS buffer (pH 7, 25 mM) determined by dynamic light scattering for bulk protein concentrations of A) 1 μM, B) 2 μM, C) 4 μM, D) 6 μM, E) 8 μM, F) 10 μM. 3 technical replicates of 3 experimental replicates each were performed for each condition. 3 technical replicates of 3 experimental replicates each are shown as individual lines. Y-axis is volume percent and x-axis is diameter in nm. DLS experiments were performed in parallel to Bradford assays. .

2.3 Reflectin A1 assemblies are in dynamic exchange with dilute phase

FRET (Forster resonant energy transfer) analyses revealed that reflectin A1 assemblies dynamically exchange monomer through the dilute phase. Reflectin A1 assemblies labeled with either fluorescein (donor) or rhodamine (acceptor) were mixed and after excitation at 488nm showed FRET exchange as seen by rhodamine emission at 590nm (Fig. 2.2B). As the length of time between assembly and mixing of separately labeled assemblies, t_{delay}, increased, the FRET signal decreased (Fig. 2.2B) and is interpreted as a time-dependent decrease in assembly exchange dynamics. However, these data do not rule out the possibility that FRET exchange is due to new formation of non-dynamic assemblies, or unidirectional protein transport into the assemblies. To distinguish bidirectional protein transport between assemblies from these alternative hypotheses , assemblies labeled with both donor and acceptor fluorophores were diluted with unlabeled A1 assemblies (Fig. 2.3A). A decrease in FRET signal would represent a decrease in the concentration of fluorophores within assemblies, which necessitates influx of unlabeled and efflux of labeled reflectin A1. After diluting fluorescently labeled reflectin A1 with unlabeled A1 immediately after assembly formation, a decrease in FRET was observed in emission spectra (Fig. 2.3B). Replotting FRET as a function of time demonstrates the dynamic exchange of reflectin between assemblies ages rapidly (Fig. 2.4A). Reflectin A1 assemblies diluted immediately after formation are completely dynamic as FRET decreases to the positive control value (Fig. 2.4A). Relative to the range of the positive control (fully dynamic) to the negative control (fully arrested), 75.6% of the population of assemblies is dynamic after 1 minute (Fig. 2.3A), while at 2 hours 48% of the population is dynamic, and only 19% was dynamically exchanging after 37 hours. Reflectin A1 assembly sizes increased over the same time scale as FRET measurements of dynamic

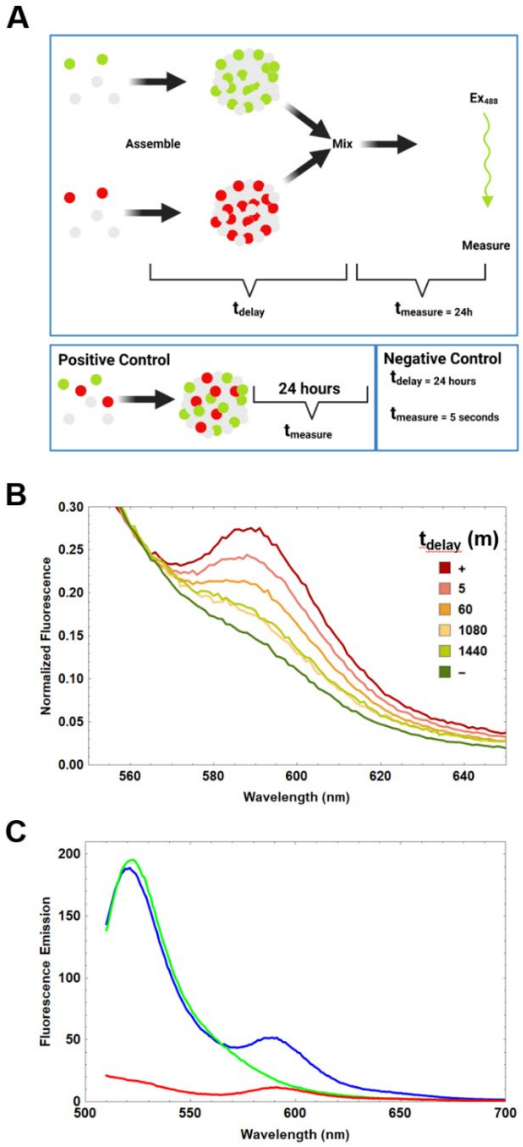

Figure 2.3: A) Design of FRET exchange experiment. Mixtures of reflectin A1 containing either 5% fluorescein-labeled single cysteine mutant C232S (A1 C199-F) or 5% rhodamine sulfate-labeled C232S (A1 C199-R) were separately but simultaneously assembled by dilution into pH 7 25 mM MOPS buffer. After t_{delay} assemblies containing 5% A1 C199-F were mixed with those containing 5% A1 C199-R and incubated 24 hours at 20C. Samples were excited with 488nm light corresponding to the absorption spectra of donor fluorophore fluorescein and emission spectra from 510-700 nm recorded. Mixtures containing both labels were driven to assembly as the positive control. For the negative control t_{delay} was 24 hours and $t_{measure}$ was 5 seconds. B) Spectra normalized to 520 nm (fluorescein emission maximum). C) Fluorescence emission of reflectin A1 assemblies labeled with 5% fluorescein (green), 5% rhodamine sulfate (red) and the positive control (blue) excited at 488 nm.

exchange (Fig. 2.4 B). Initial assembly diameter was 24 ± 1.6 nm diam. and the assemblies grow to 33.9 ± 0.35 nm diam. after 24 hours. Remarkably, the change in assembly size mirrors the decrease in dynamic exchange monitored by FRET, coupling the rate of decrease of dynamic exchange and the rate of change in assembly size. In the following chapter we demonstrate that reflectin A1 does undergo liquid-liquid phase separation into coexisting protein-dense and protein-dilute phases. In terms of the phase diagram for reflectin A1 defined by protein net charge density and NaCl concentration, reflectin A1 assemblies are intermediate to liquid condensates.

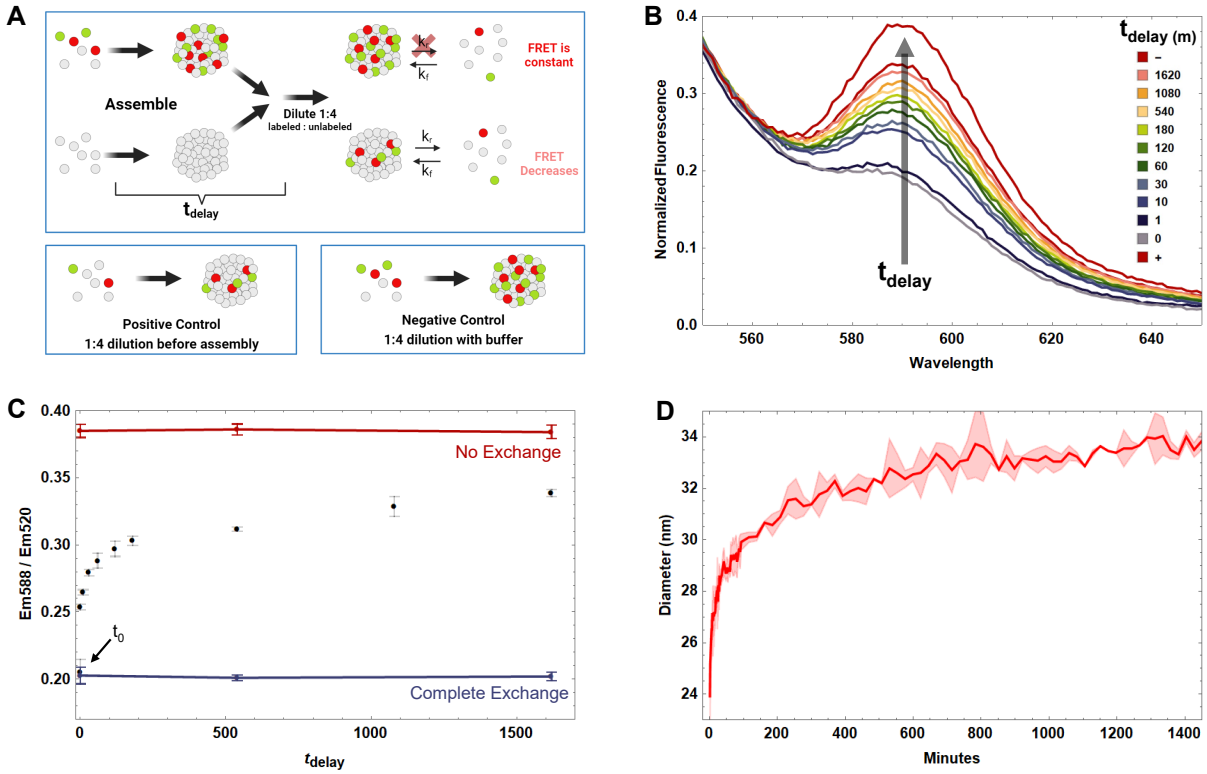

Figure 2.4: A) Design of FRET dilution experiment. Mixtures of 100 μM reflectin A1 containing 5% fluorescein-labeled single cysteine mutant C232S (A1 C199-F) and 5% rhodamine sulfate-labeled C232S (A1 C199-R) were driven to assemble by dilution into MOPS buffer (pH 7, 25 mM). Simultaneously, unlabeled reflectin was driven to assembly under the same conditions. As a function of post-assembly time, labeled assemblies were diluted 1:4 with unlabeled assemblies, then incubated 24 h. Samples were excited at 488 nm light corresponding to the absorption maximum of the donor fluorophore fluorescein and emission spectra from 510-700 nm recorded. For the negative control, fluorescently labeled assemblies were diluted 1:4 with buffer only. Reflectin A1 solutions containing 5% A1 C199-R and 5% A1 C199-F were diluted 1:4 with unlabeled reflectin prior to assembly for the positive control. B) Emission spectra normalized to 520 nm (Em_{Max} of fluorescein) as a function of t_{delay}, the time between assembly and mixing of labeled and unlabeled assemblies. C) FRET emission at 588 nm normalized to 520 nm plotted as a function of time. The red line is the negative control representing zero dynamic exchange and the blue line is the positive control representing complete dynamic exchange. D) In parallel, assemblies of reflectin A1 were formed by dilution of same protein stock into MOPS buffer (pH 7, 25 mM) and sizes determined by dynamic light scattering. For DLS, data points represent 3 experimental replicates. Error bars (C) and error bands (D) represent $\pm$ 1 S.D.

Chapter 3

Reflectin A1 Condensates Tuned by Net Charge Density and Ionic Strength

3.1 Cellular Liquid-Liquid Phase Separation

Intrinsically disordered proteins and proteins with disordered regions can exert their function not only through direct structural interactions, but through their dynamic properties by undergoing liquid-liquid phase separation (LLPS) into coexisting dense and dilute phases [46, 47, 48]. Recently, phase separation of proteins into protein-dense and protein-dilute phases has been demonstrated to form membraneless organelles in living cells that are often regulated by post translational modifications such as phosphorylation [49, 50, 51, 52]. These can act to sequester other proteins and RNA, organize and regulate signaling complexes, and buffer intercellular protein concentrations [53, 54, 55]. Intracellular protein-driven LLPS is increasingly associated with neurodegenerative diseases [56]. Liquid condensates of tau act to seed cytotoxic insoluble amyloid fibrils implicated

in Alzheimer's [57] and aging of FUS condensates produces insoluble aggregates that are found in the neurons of those afflicted with ALS [58], however these processes are increasingly seen as probable secondary effects rather than causes of such diseases [59] . For intrinsically disordered proteins such as FUS, LAF-1, and DDx4, low complexity domains (LCDs) enriched in glycine, arginine, and aromatic residues drive LLPS [23, 24, 60, 61]. In the 'sticker and spacer' model pi-cation interactions, typically between tyrosine and arginine, and electrostatic interactions act as intermolecular stickers between proteins. Smaller and more flexible residues such as serine and glycine serve as relatively weakly interacting spacers that confer flexibility to LCDs. The patterning, valence, and strength of stickers often dominates the phase behavior of IDPs, with increasing valency or clustering of stickers driving LLPS [62, 63]. Reflectin A1 is an intrinsically disordered protein enriched in arginine and tyrosine residues and exhibiting pronounced charge patterning, all of which are consistent with proteins that undergo LLPS [23, 62].

3.2 Increasing Ionic Strength Drives Liquid-Liquid Phase Separation of Reflectin A1

The dilution of 100 μM reflectin A1 containing 5% single cysteine mutant C232S co- valently labeled with fluorescein (referred to as A1 C199-F to denote the location of fluo- rescein) into acetic acid buffer (pH 4, 25 mM) in 250 mM NaCl forms liquid condensates that wet untreated glass coverslips (Fig. 3.1A). Wetting is prevented using polyethylene glycol (PEG) passivated coverslips (Fig. 3.1B) and the condensates are spherical and undergo fusion and relaxation to sphericity upon contact (Fig. 3.1C). The rate of change of aspect ratio of newly fused droplets fits well to an equation of exponential decay that is commonly used to characterize liquid droplet dynamics [54, 64] (Fig. 3.1D)

yielding a relaxation time, tau, of 1.95 ± 1.16 seconds. Surface wetting and relaxation of newly fused droplets indicate that the condensates exhibit surface tension which is characteristic of a liquid. These results show that under these conditions, reflectin A1 undergoes liquid-liquid phase separation to form protein-dense and protein-dilute liquid phases. Comparison of the mean fluorescence intensity of reflectin A1 containing 2% A1 C199-F in acetic acid buffer (pH 4 25 mM) 250 mM NaCl to that of 100% A1 C199-F monomeric standards in acetic acid buffer (pH 4 25 mM) determined the dense phase protein concentration to be 9517 ± 965 μM, or 416 ± 42 mg/mL (Fig. 3.1D). This concentration is within the range of dense phase protein concentrations reported for many other liquid protein condensates [65, 66, 67] and is physiologically relevant: reflectin protein concentration within the Bragg lamellae of *Doryteuthis opalescens* iridocytes was previously estimated to be 381 mg/mL [18].

3.3 Reflectin A1 Phase Diagram Defined by Ionic Strength and Protein Net Charge Density

The phase diagram for reflectin A1 as a function of ionic strength and calculated net charge density (NCD) of the protein is defined by three species: monomer, multimer (both of which are colloids), and liquid-like condensates (Fig. 3.2A). DLS was used to determine the boundary between monomer ($R_H = 4.45 \pm 2.3$ nm) and assembly using the previously established R_H of reflectin A1 monomer (Fig. 3.2D). This experimentally determined R_H is slightly smaller than 6.5 nm, the R_G calculated using worm-like coil theory [68, 69, 70]. The boundary between reflectin A1 assemblies and liquid condensates was determined by confocal microscopy of reflectin A1 containing 5% A1 C199-F. Droplets with the previously mentioned liquid characteristics (Fig. 3.1) were easily distinguished from

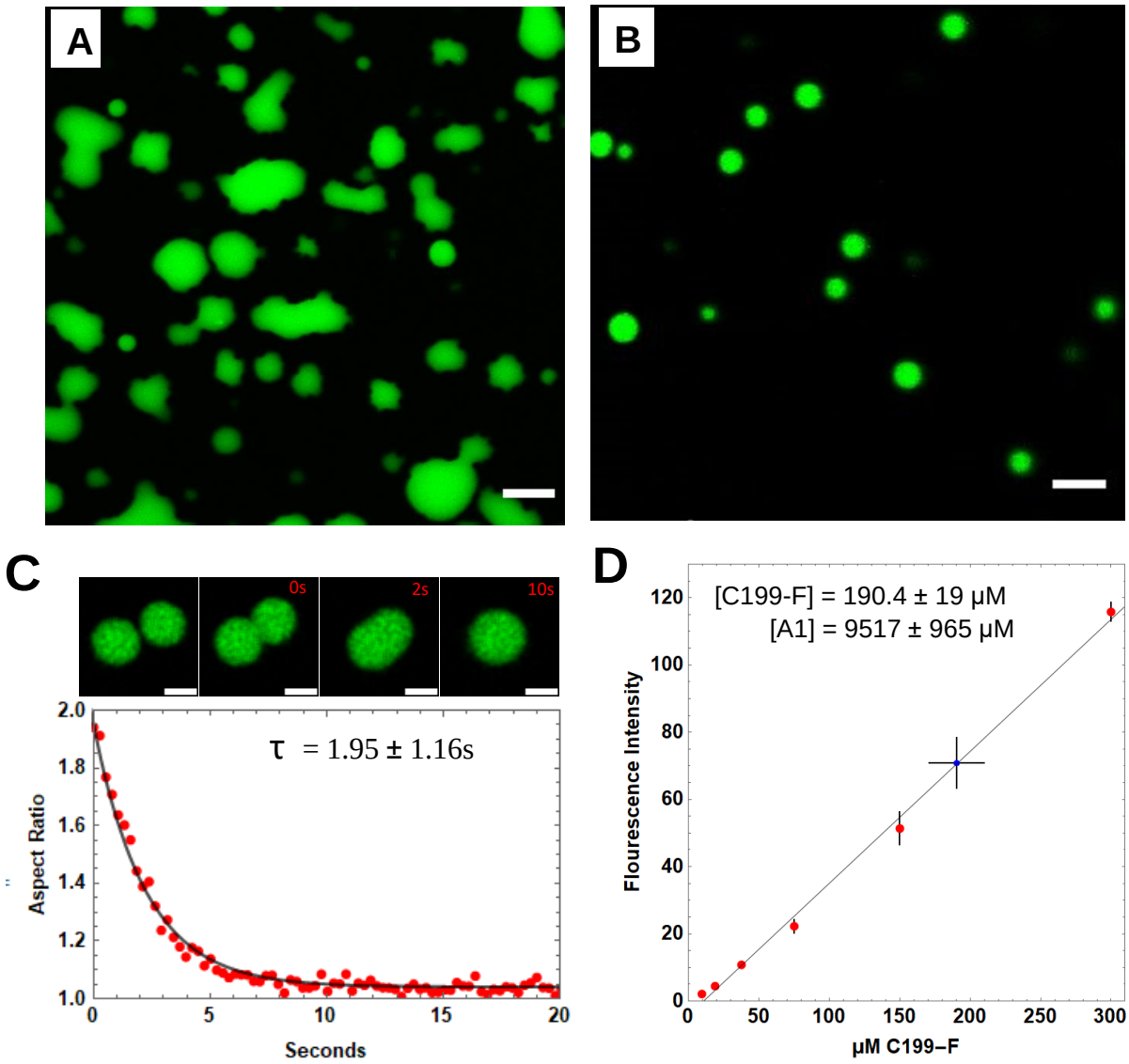

Figure 3.1: Reflectin A1 undergoes LLPS. 100 μM reflectin A1 containing 5% fluorescently labeled single-cysteine mutant C232S (referred to as C199-F for the amino acid location of fluorescein) was diluted to a final protein concentration of 4 μM in pH 4 25 mM acetic acid 250 mM NaCl. A) Reflectin condensates were untreated glass coverslips. B) Condensates are spherical. C) Condensates fuse and relax to sphericity. The change in aspect ratio over time can be quantified and fit to an equation of exponential decay to obtain the characteristic relaxation time τ. C) Reflectin A1 droplet protein concentration is 9517 $\pm$ 965 μM, or 416 $\pm$ 42 mg/mL . Monomeric standards of 100% A1 C199-F in pH 4 25 mM acetic acid were used to relate fluorescence intensity to concentration. Intensities of droplets of 2% C199-F were averaged (n=147 droplets from 5 experiments). Error bars represent $\pm$ 1 S.D. All scale bar = 5μm.

observable and sub-resolution assemblies (Fig. 3.2 B, C). As the liquid phase boundary was approached by increasing ionic strength at a given pH (and its corresponding protein NCD), assemblies increased from sub-resolution (Fig. 3.3A) to microscopically resolvable (Fig. 3.3B) sizes. Upon crossing the liquid phase boundary, partitioning into the dense phase increased markedly (Fig. 3.3 B, C, D). At high protein NCDs (pH 4-5) reflectin A1 can exist as monomer, multimer, or liquid droplet. The decreasing slopes of both phase boundaries at high NCDs reveal that decreasing protein NCD requires lower ionic strength to drive assembly or LLPS. For lower protein NCDs (pH 5.5-8), reflectin A1 is not monomeric at any salt concentration in 25 mM buffers. For all protein NCDs tested, the assembly/LLPS boundary shares the same trend of decreasing protein NCD requiring decreasing ionic strength to drive LLPS. This trend at relatively low to moderate salt concentrations suggests ionic screening may contribute to salt-driven assembly and LLPS [71, 72, 73].

Notably, as a function of salt concentration, assemblies always precede LLPS for high NCDs (Fig. 3.2A, 3.3A-C),suggesting that salt-driven reflectin A1 assembly and LLPS may result from a continuum of the same physical process. The finding that reflectin A1 assembly sizes progressively increase with increasing NaCl concentration until liquid droplets are formed (Fig. 3.3A-D) is consistent with the hypothesis that salt-driven reflectin A1 assemblies are caused by spinodal decomposition immediately followed by dynamic arrest [40, 74, 75, 76] and that above a threshold protein NCD to ionic strength ratio, dynamic arrest of assemblies is bypassed and spinodal decomposition forms liquid droplets. The observed trend of decreasing ionic strength for decreasing protein NCD is consistent with a reduction in the repulsive protein net charge density that is required to drive liquid phase separation. However, the sequence of reflectin A1 suggests a plethora of molecular interactions could dictate the response of reflectin A1 phase behavior to increasing ionic strength [23].In addition to increasing ionic strength's contribution to

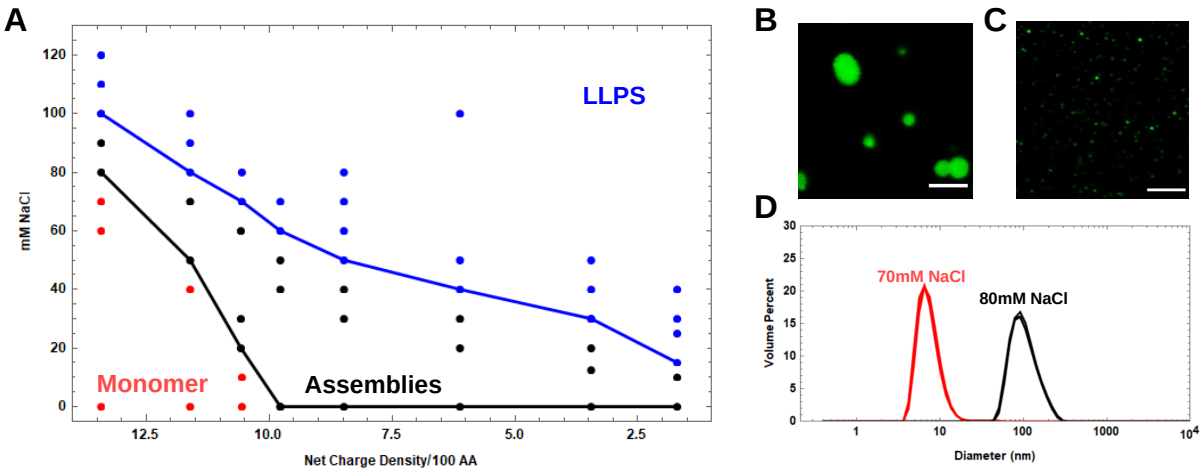

Figure 3.2: A) Depending on the pH and ionic strength, reflectin A1 can exist as a colloid of monomers or assemblies, or a liquid two-phase system. Net charge density is calculated from the pKa of reflectin A1 at each experimentally manipulated pH. 100 μM reflectin A1 was diluted to a final protein concentration of 4 μM for each data point. At high pH deprotonation of histidines decreases the protein net charge density per 100 amino acids. B) Liquid droplets were distinguished from (C) light-resolvable assemblies by size discrepancy as well as surface wetting and droplet fusion. D) Assemblies were distinguished from monomer by using DLS to measure particle size distributions. At pH 4 70 mM NaCl reflectin A1 forms 7.9 $\pm$ 3.5 nm d. monomers and at pH 4 80 mM NaCl reflectin A1 forms 106 $\pm$ 39 nm d. assemblies. 3 DLS replicates at each condition are shown cumulatively. Scale bars are 5um.

screening of repulsive charges, it can also strengthen pi-cation and pi-pi interactions between arginine and tyrosine residues within reflectin A1 [77, 78, 79] and increase surface tension, thereby increasing the strength of the hydrophobic effect. It should be noted that the dielectric constant within protein condensates is not equal to that of the dilute phase. Estimates for the dielectric constant of protein-dense condensates range from 40-50 [80, 81]. The high concentration of protein will decrease the polarity within the droplet, especially with reflectins' high concentration of aromatic residues and methionine. This will change the chemical potential of any ionizable side chains that define the calculated net charge density of reflectin within condensates [82]. Incorporating pH-sensitive fluorophores into reflectin liquid droplets would allow for determination of the pH of the dense phase [83], however fluorophores with quantum yields that are relatively insensitive to the surrounding dielectric constant should be used [84].

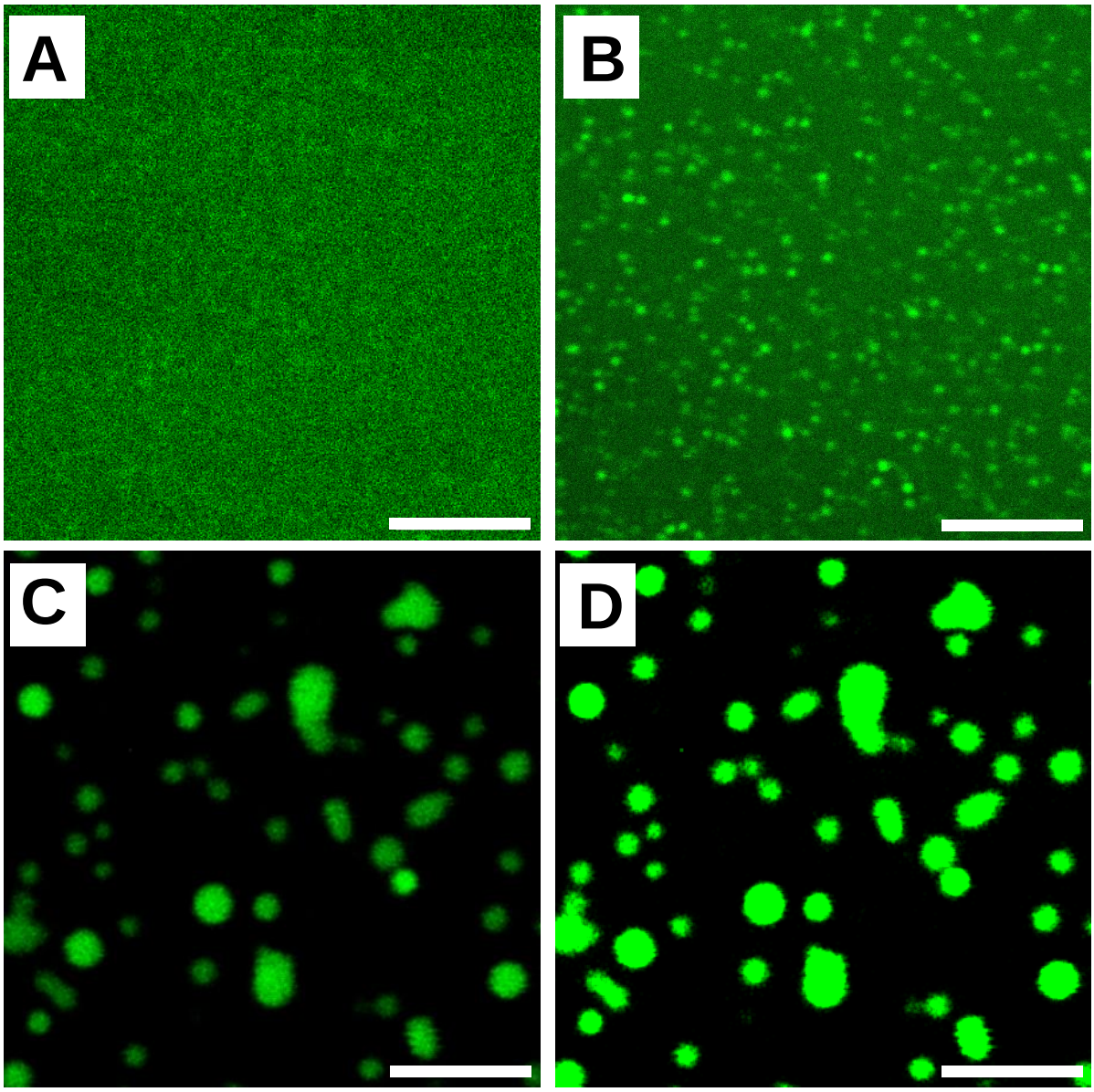

Figure 3.3: Reflectin A1 assembly sizes increase until strongly partitioned liquid droplets are formed. 100 μM reflectin A1 containing 5% A1-C199F diluted into increasing NaCl concentrations at pH 4 25 mM acetic acid until the liquid phase boundary is crossed. A) At 80 mM NaCl no light-resolvable structures are detected but assemblies are present as determined by DLS. B) At 90 mM NaCl 500 nm d. particles are present. C) at 100 mM NaCl surface-wetting liquid droplets are present with stronger partitioning into the dense phase. D) Same image as C but at the same exposure values as (A,B) to confirm strong protein partitioning into dense phase. Scale bars = 5 μm.

3.4 Surface Tension and Electrostatic Screening Contribute to Salt-Driven Assembly and LLPS of Reflectin A1

To determine the possible role of the hydrophobic effect in driving reflectin A1 assembly and liquid-liquid phase separation (LLPS), the protein's behaviors were compared in the presence and absence of 5% 1,6- hexanediol (1,6-HD). This water-soluble aliphatic alchohol lowers the surface tension of water [53] and has been shown to dissolve liquid protein condensates that are formed by the hydrophobic effect [53, 77, 85, 86]. Turbidity measurements of reflectin A1 diluted into acetic acid buffer (pH 4 25 mM) from 80 to 100 mM NaCl demonstrate that 5% 1,6-HD inhibits the salt-driven formation of large, light-scattering particles of reflectin A1 (Fig. 3.4A). In the absence of 1,6-HD, turbidity increased at 90 mM NaCl and reaches approximately 2.5 at 130 mM NaCl. In marked contrast, In the presence of 5% 1,6-HD, turbidity increases at 110 mM NaCl and reaches only 1.5. Similarly, while the dilution of reflectin A1 into pH 4 80 mM NaCl formed 52.7 $\pm$ 18.3 nm D. assemblies, the inclusion of 5% 1,6-HD prevented assembly (Fig. 3.4B). In 100 mM NaCl at pH 4, reflectin A1 formed liquid droplets (Fig. 3.4C), but the inclusion of 5% 1,6-HD abrogated LLPS and droplets were no longer observed (Fig. 3.4D).

These results indicate that increasing ionic strength drives reflectin A1 assembly and LLPS in part by increasing the strength of the hydrophobic effect. This would be expected because of the large gain in entropy typically resulting from burying hydrophobic side chains away from water [82, 87, 88] and LLPS is primarily a segregative process [24] driven by differences in polymer and solvent polarity. Although the primary sequence of reflectin A1 does not have any significant stretches of hydrophobic amino acids, computational analyses of hydrophobic moments show the RMs have maximal hydrophobic moments at

side chain angles consistent with α-helical (100^o) and β-sheet (160^o) secondary structures [21], and these secondary structures emerge upon folding and assembly of reflectin A1 [29, 33]. In contrast, the analyses of hydrophobic moments show that the linker domains of the protein exhibit no significant hydrophobicity in any possible conformation [21]. Thus, the emergent hydrophobicity of the RMs likely provides the main contribution to the protein's overall hydrophobicity,, and decreasing solvent quality increases the energetic contributions of these segments in driving folding, assembly, and LLPS of reflectin A1 .

It previously was demonstrated that the progressive increase in size of reflectin A1 assemblies with salt concentration is well predicted by the concentration of the anionic species as opposed to total ionic strength of the solution (30). To investigate if this relationship is also true for salt-induced LLPS of reflectin A1, the liquid phase boundary of reflectin A1 was determined as a function of CaCl2 concentration in addition to NaCl concentration for pH values 4-5 (Fig. 3.4 D). The liquid phase boundaries as a function of Cl- concentration (Fig. 3.4F) differ by 9.6% for pH 4, 21% for pH 4.5, and are identical for pH 5. In comparison, the liquid phase boundaries as a function of ionic strength (Fig. 3.4 C) vary by 62% for pH 4, 48.9% for pH 4.5, and 20.4% for pH 5. Therefore, the concentration of anionic species better predicts the liquid phase boundary determined by addition of either NaCl or $CaCl_2$ than does ionic strength, strongly suggesting that electrostatic screening of cationic Coulombic repulsion within and between reflectin A1 molecules contributes to the drive of reflectin A1 to undergo LLPS. I conclude that the screening of long-range repulsion at high protein NCDs allows short-range attractive forces such as cation-pi, sulphur-pi, and hydrophobic interactions to drive reflectin A1 folding, assembly, and LLPS.

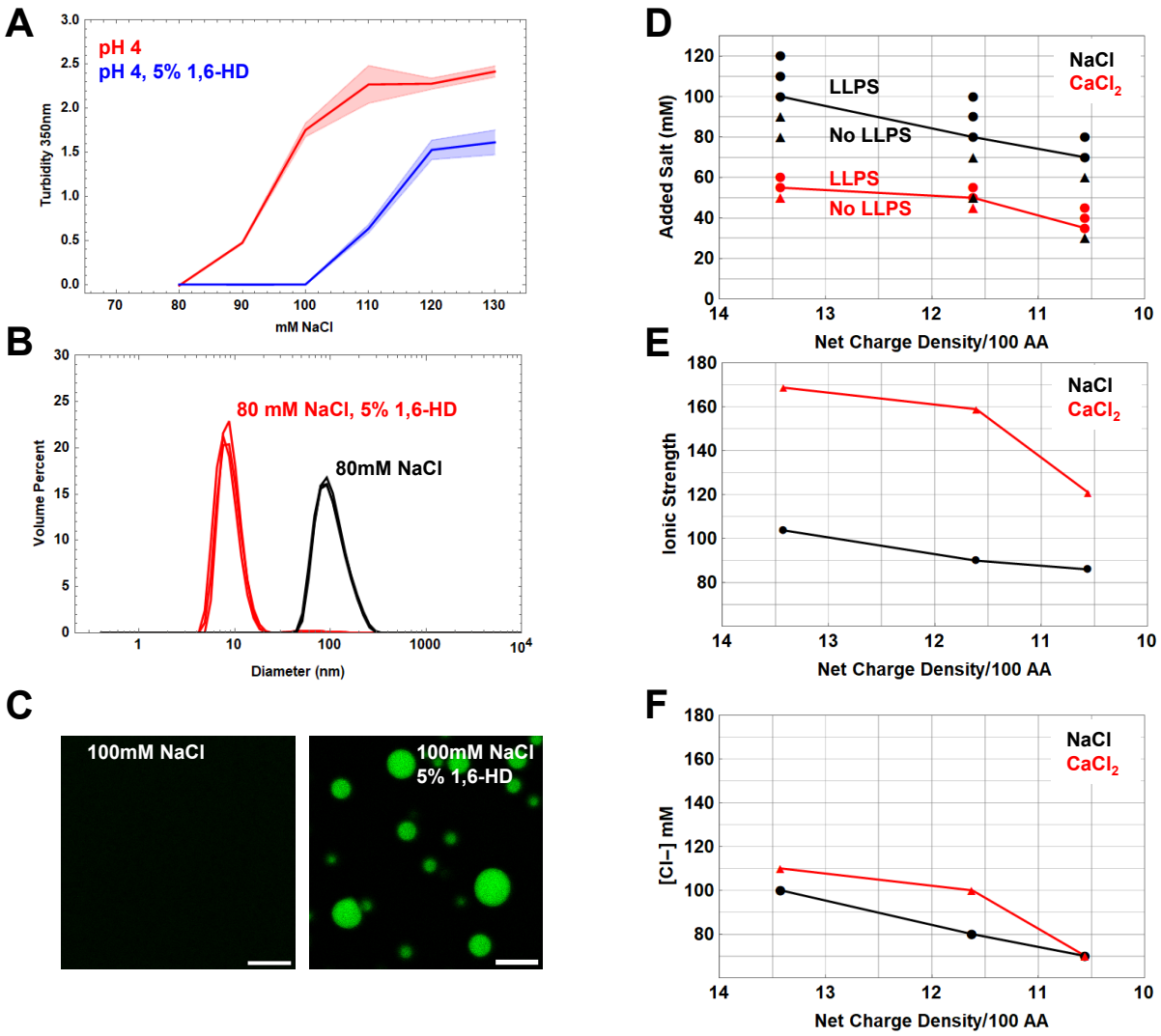

Figure 3.4: Effects of 1,6-hexanediol and anion concentration on reflectin A1 phase transitions. . A) Turbidity measured at 35 0nm for reflectin A1 solutions in acetic acid buffer (pH 4, 25 mM) in 80 mM NaCl (red) with 5% 1,6-HD (blue) B) DLS of dilution of reflectin A1 into pH 4 80 mM NaCl (black) results in 106 ± 39 nm d. assemblies and dilution into pH 4 80 mM NaCl, 5% 1,6-HD with yields monomers of 9.0 ± 2.6nm diam. C) Reflectin A1 droplet formation upon dilution into pH 4 100 mM NaCl and pH 4 100 mM NaCl 5% 1,6-hexanediol. Turbidity measurements are shown as the average of 3 experimental replicates with 3 measurement replicates each; error bands represent ± 1 S.D. The same numbers of DLS replicates are shown cumulatively, and images in (C) are characteristic of 3 experimental replicates. Scale bar = 10 μm. D) Liquid phase boundaries determined presence or absence of droplets upon addition of NaCl (Black) or $CaCl_2$ (Red). E) Same data as (D) displayed as a function of ionic strength and (F) Cl- concentration . X-axis for (D,E,F) is calculated protein net charge density. Data for NaCl addition is the same as that used for Figure 3.2.

3.5 Net Charge Density and Ionic Strength Tune Reflectin Liquid Condensate Dynamics

Using FRAP (Fluorescence Recovery After Photobleaching) and droplet fusion dynamics, we determined that the liquidity of reflectin A1 condensates is tuned by protein NCD and ionic strength. Videos of reflectin A1 condensates in 250 mM NaCl at pH 4, 6, and 7 (Fig. 3.5A, B, C) were used to determine the change in aspect ratio over time of newly fused droplets. Fitting of this data to an equation of exponential decay (Fig. 3.5D, E, F) reveals that relaxation time τ increases from 1.95 ± 1.16s at pH 4 to 36.95 ± 29.32s at pH 6, and ultimately to 84.86 ± 22.77s at pH 7 (Fig. 3.5G). Droplet fusion and relaxation rates increase by almost two orders of magnitude from pH 4 to pH 7, demonstrating that liquidity (64) of reflectin A1 condensates decreases as protein NCD decreases.

For FRAP experiments a small region in liquid droplets at pH 4, 6, and 7 at 250 mM NaCl was photobleached (Fig. 3.6A) and fluorescence recovery in that region was characteristic relaxation τ for each experiment. The proportion mobile component of the droplets decreases as pH increases (Fig. 3.6D), indicating that the population of liquid-like protein molecules in the droplet is decreasing. Fluorescence recovery rates τ increase from 192.3 ± 31.1s at pH 4 to 641.6 ± 220.2s at pH 6, and at pH 7 the dynamics within reflectin condensates are too slow to determine accurate τvalues (Fig. 3.6C). These demonstrate that the liquidity of reflectin A1 liquid condensates decreases as protein net charge density decreases for range of conditions tested. This could be due to more rapid aging of non-covalent inter-protein cross-links at lower protein NCDs (higher pHs) than higher protein NCDs (lower pHs), as more extensive protein-protein interactions would be expected for decreasing Coulombic repulsion at low protein NCDs.

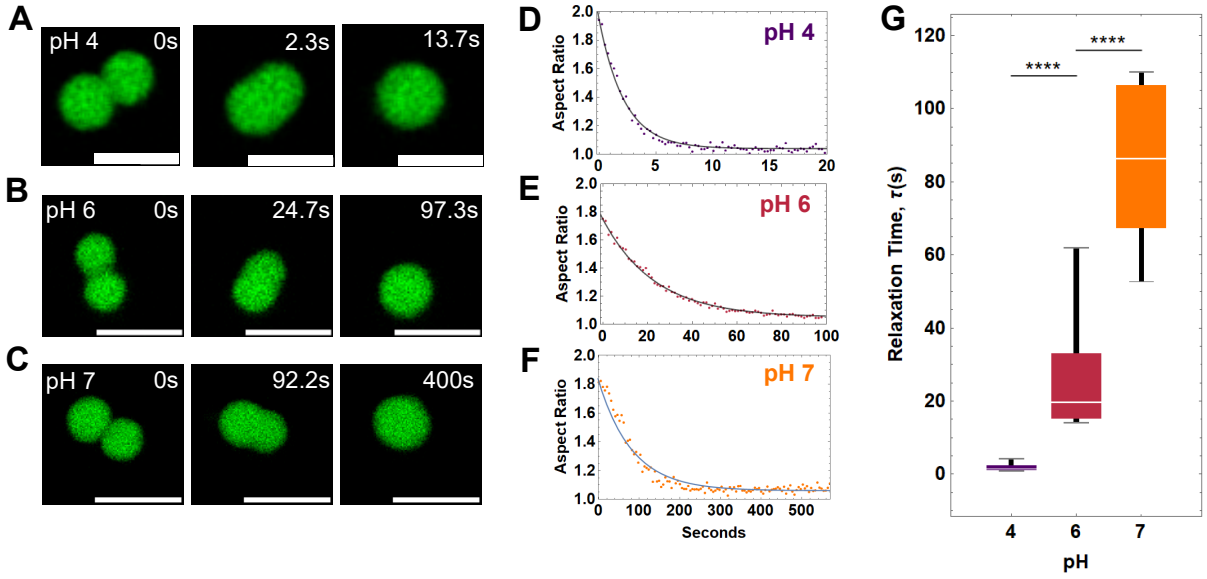

Figure 3.5: Aspect ratios of newly fused droplets in 250 mM NaCl were calculated from videos at pH 4, 6 and 7. Representative time series of droplet fusion and relaxation at (A) pH 4, (B) pH 6 and (C) pH 7. Aspect ratio as a function of time was fit to an exponential equation of decay to determine τ for (D) pH 4, (E) pH 6, and (F) pH 7. G) Changes in aspect ratio over time between each pH were found to be statistically significantly different using a one-way ANOVA test. Box and whisker plots display the median (center line), 2nd and 3rd quartile (solid box) and the complete range (black fences) of the data. N=23 for pH 4, n=26 for pH 6, and n=22 for pH 7. Total protein concentration is 4 μM. Scale bars = 5 μm.

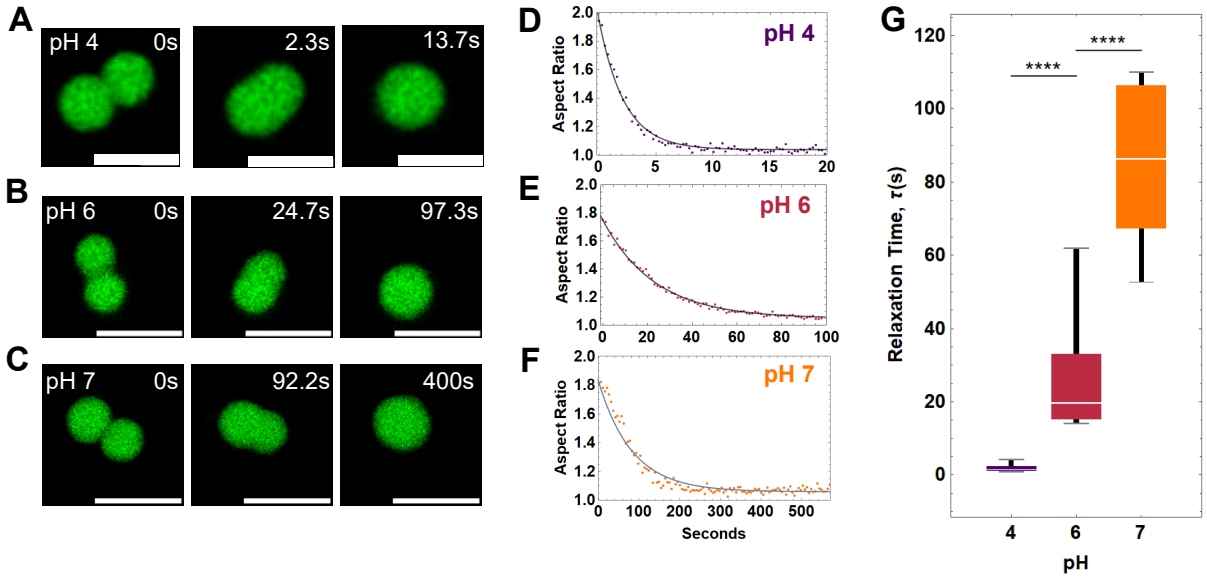

Figure 3.6: FRAP of reflectin A1 condensates demonstrate pH-dependent FRAP recovery. A) characteristic images of droplets before, immediately and 1400 s post photobleaching for pH 4,6, and 7. B) Data were corrected for photobleaching and fully normalized fluorescence intensity of bleach spots plotted as a function of time. C) Fitting of individual experiments to an exponential decay equation shows the characteristic relaxation time τ decreases as pH increases. D) Percent fluorescence recovery for pH 4, 6, and 7 also decreases as pH increases. Examples of fits to individual experiments at (E) pH 4, (F) pH 6 and (G) pH 7. N=8 for pH 4, n=9 for pH 6 and n=7 for pH 7. τ for pH 4 and pH 6, as well as percent recovery for all pHs were found to be statistically significant using a one-way ANOVA test. Accurate τ values for pH 7 could not be obtained by fitting. Error bands in FRAP plots represent $\pm$ 1 SD. Scale bars = 5 μm. Total protein concentration is 4 μM.

3.6 Effect of pH on Droplet Liquidity is Ionic Strength Dependent

FRAP of reflectin A1 liquid condensates at pH 4,6, and 7 at varying NaCl concentrations reveal a complex relationship between droplet liquidity, pH, and ionic strength. For increasing ionic strength from 200 mM to 250 mM Nacl at pH 4 τ decreases, then does not change significantly upon increasing NaCl concentration to 300 mM (Fig. 3.7A). A similar trend is seen for pH 6 where droplets were not liquid enough to estimate τ at 200 mM NaCl and increasing NaCl concentration to 250 mM increases liquidity (fluorescence recovery increases enough to estimate τ) then no significant change comparing 250 mM to 300 mM NaCl (Fig. 3.7B). Percent fluorescence recovery for pH 4 and 6 followed the same trend, demonstrating that liquidity has a non-monotonic response to increasing NaCl concentrations (Fig. 3.7C, D). Contrary to pH 4 and 6, fluorescence recovery for pH 7 does not significantly change for 200 mM vs. 250 mM NaCl but decreases when ionic strength is increased to 300 mM NaCl (Fig. 3.7E). There is an optimal ratio of pH to ionic strength that maximizes droplet liquidity. In terms of salt concentration, conditions farther from the liquid phase boundary become more liquid-like (increasing ionic strength from 200 to 250 mM at pH 4 and 6), then less dynamic even further into the liquid phase (increasing ionic strength from 250 to 300 mM at pH 7).

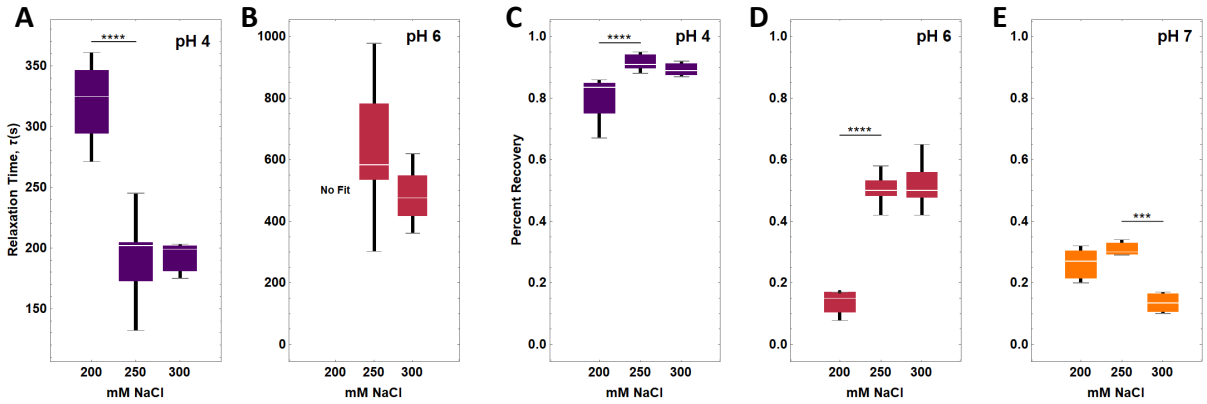

Figure 3.7: Effect of ionic strength on A1 droplet liquidity is dependent on pH. A,B) FRAP demonstrates that at pH 4 and 6, relaxation time τ decreases from 250 to 300 mM NaCl. C,D) Percent mobile component for pH 4 and pH 6 follow the same trend. E) Percent mobile component decreases significantly from 250 to 300 mM NaCl for pH 7. All pH 7 conditions and pH 6 200mM NaCl were not dynamic enough to obtain accurate values for τ.

3.7 Reflectin A1 Droplets Show Liquid Characteristics Up To 96 Hours

The percent fluorescence recovery from FRAP of reflectin A1 condensates in pH 4 25 mM acetic acid 250 mM NaCl decreases significantly from 0-24 hours and 72-96 hours, while there is no significant change from 24 to 72 hours (Fig. 3.8A, B). Remarkably, τ does not change significantly from fresh droplets to 72 hours, then increases drastically from 72-96 hours (Fig. 3.8C). From 0-72 hours the liquid-like population of the droplets decreases (Fig. 3.8C) . Reflectin A1 droplets show no visible changes in morphology such as jaggedness or fibrillization for the duration of the experiment (Fig. 3.8D). Interestingly, despite the stability of τ in these conditions, droplet size did not change significantly over 96 hours suggesting that Ostwald ripening is either arrested or too slow to detect (Fig. 3.8D) [74, 89, 90]. An arrest of ripening for droplets between 2-24 hours could explain the stability of τ up to 72 hours despite a significant decrease in the mobile component from 91.6 $\pm$ 3.6% at 0-2 hours to 64.8 $\pm$ 8.4% at 24 hours. This decrease in mobile component may represent the contribution of diffusion of monomer between the dense and dilute phase to the fluorescence recovery in fresh droplets. Reflectin A1 FRAP experiments performed on droplets between 10-120 minutes old did not demonstrate a time dependence and show slow and incomplete fluorescence recovery compared to many other in vitro and in vivo protein systems [50, 54, 55, 57, 91, 92, 93, 94, 95]. Coupled with the lack of Ostwald ripening observed over 96 hours, these observations suggest that reflectin A1 condensates have already aged significantly between the time of formation and time of FRAP measurement. Although 96 hours well exceeds the seconds it takes for iridocytes to respond to acetycholine by expelling water from the Bragg lamellae, this demonstrates promise for bioengineered systems based on reflectin A1 condensates.

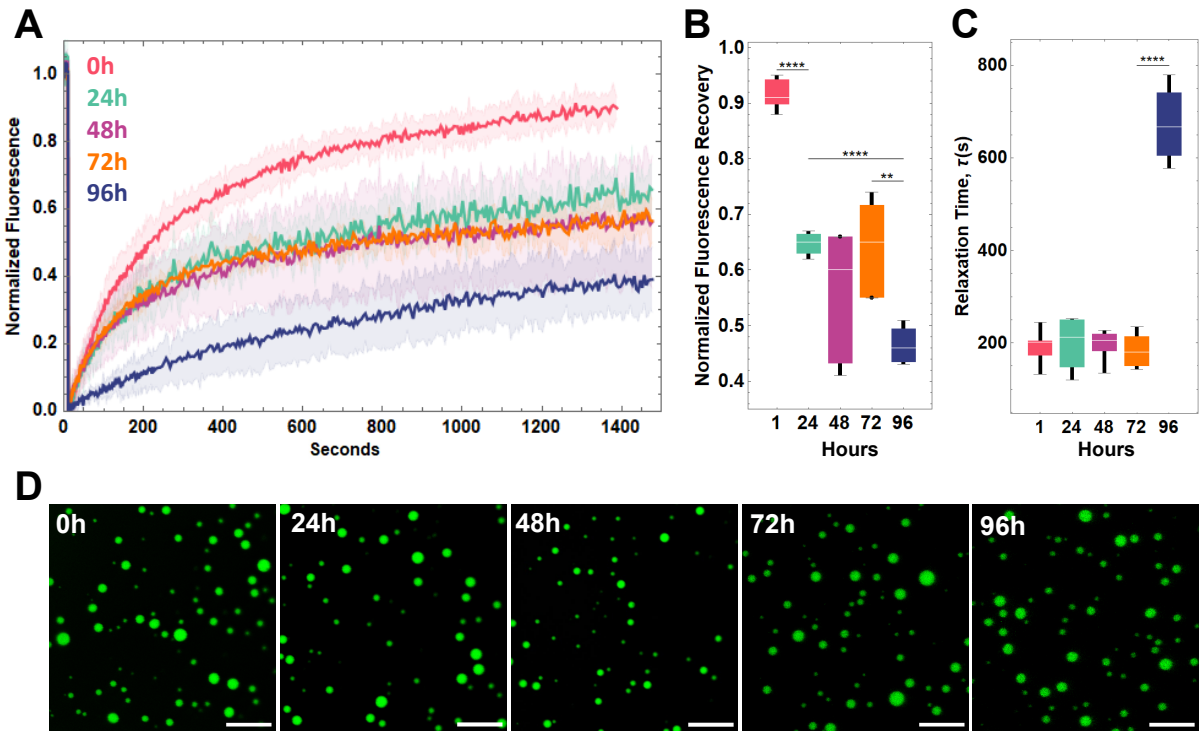

Figure 3.8: A) FRAP of reflectin A1 liquid condensates in pH 4 25 mM acetic acid 250 mM NaCl for 0-4 (red), 24 (green), 48 (purple), 72 (orange), and 96 hours (blue). B) Data were corrected for photobleaching and fully normalized fluorescence intensity of bleach spots plotted as a function of time. C) Fitting of individual experiments to an exponential decay equation yields the characteristic relaxation time τ. Statistical significance determined by one-way ANOVA testing. Box and whisker plots display the median (center line), 2nd and 3rd quartile (solid box) and the complete range (black fences) of the data. D) Droplet morphologies for 0-96 hours. N=8 for 0h, N=8 for 24h, N= 6 for 48h, N=7 for 72h, N=7 for 96h. Total protein concentration is 4μM. Scale bars = 10 μm

Chapter 4

Reflectins A1, A2, B and C Form Multiphase Liquid Condensates

4.1 Reflectins A2, B and C Undergo Liquid-Liquid Phase Separation in Ionic Strength and Protein Net Charge Density Dependent Manner

In addition to reflectin A1, lamellae of iridocytes in *D. opalescens* contain reflectins A2, B, and C (Fig. 4.1 D) which also undergo liquid-liquid phase separation (LLPS) upon dilution into high ionic strength buffers. Reflectin A2 (Fig. 4.2A.), reflectin B (Fig. 4.2B) and reflectin C (Fig. 4.2C) form liquid droplets that wet untreated glass slides and fuse and relax to sphericity upon contact (Fig. 4.3I, J, K). To investigate the possibility that the lamellar contents in tunable iridocytes could exist, conditions, in a liquid state, reflectins A2, B, and C were each mixed with reflectin A1 in the molar ratios found in dorsal (maximally tunable) iridocytes (Fig. 4.1B). Reflectins A2 (Fig. 4.2D), B (Fig. 4.2E) and C (Fig. 4.2F) all liquid phase-separated with reflectin A1

when diluted into high ionic strength buffers to form homogeneous droplets at 4 μM final protein concentration.

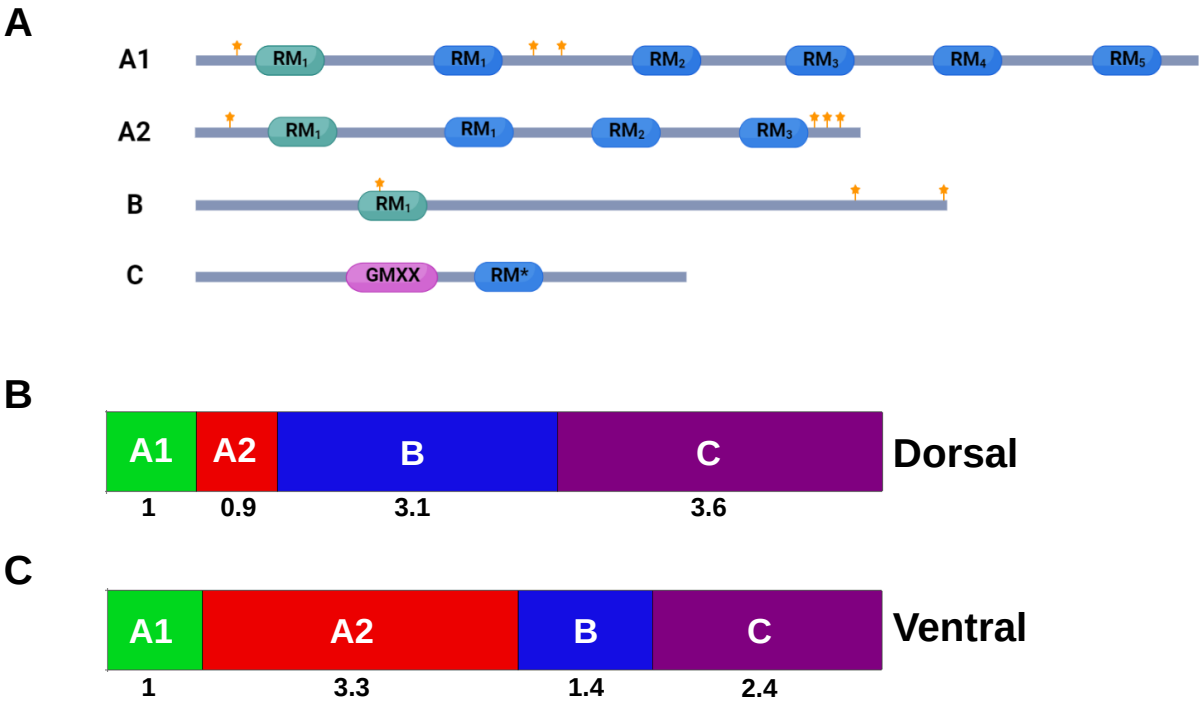

Figure 4.1: Reflectins A1, A2, B and C are enriched in iridocytes of *D. opalascens*. A) Diagrams of reflectins A1, A2, B and C showing the location of RMns (green), RMs (blue) and GMXX motif (purple). Stars mark the known phosphorylation sites *in vivo* in dorsal iridocytes. B) Molar ratios of the four protein species in the tunable (dorsal) and (C) non-tunable (ventral) iridocytes.

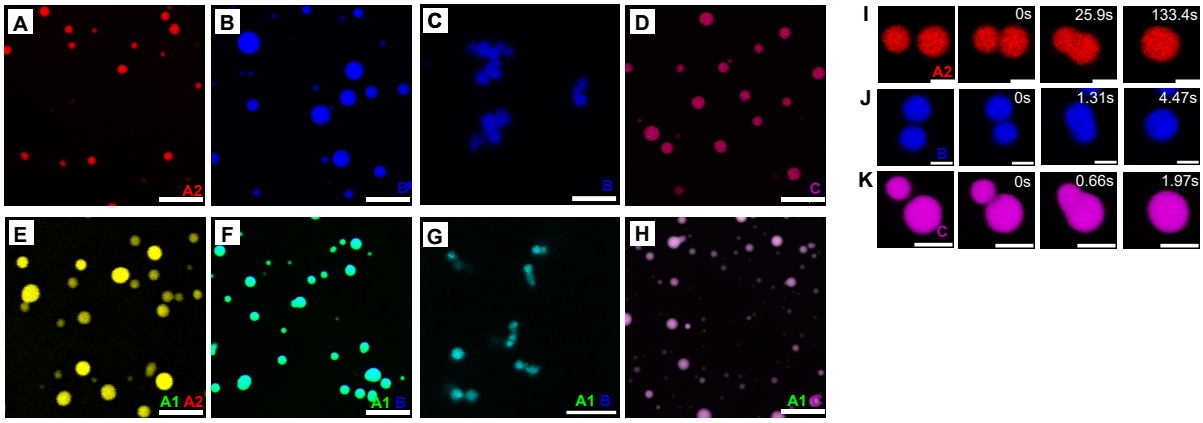

Figure 4.2: A) Reflectin A2 diluted into 250 mM NaCl at pH 6. B) Reflectin B diluted into 150 mM NaCl at pH 6. C) Reflectin B diluted into 400 mM NaCl at pH 4. D) Reflectin C diluted into 150 mM NaCl at pH 6. Co-phase separation of: (E) 53% reflectin A1 with 47% reflectin A2 in same conditions as (A). E) 75.6% reflectin B with 24.4% reflectin A1 in same conditions as (B). F) 75.6% reflectin B with 24.4% reflectin A1 in same conditions as (C). H) 78.3% reflectin C with 21.7% reflectin A1 in same conditions as (D).Time series of fusion and relaxation of two droplets of (I) reflectin A2, (J) reflectin B and (K) reflectin C. Stock solutions of 100 μM total protein concentration in acetic acid buffer (pH 4, 25 mM) were diluted to final protein concentrations of 4 μM in respective buffers. Covalent fluorescent protein labeling for reflectins A1, A2, B and C respectively: 5% A1 C199-F, 2% rhodamine, 1% Alexafluor 405 and 1% Alexafluor 660. These labeling percentages were used for all experiments unless stated otherwise. Scale bars= 5 μm.

4.2 Diffusivity is Greatly Increased in Liquid Condensates of Reflectins B and C

FRAP analyses of reflectin C containing 5% fluorescein labeled protein (to ensure power settings for photobleaching as that used for reflectin A1) diluted into 250 mM NaCl at pH 6 (Fig. 4.3A) and pH 7 (Fig. 4.3B) reveal that the diffusivity within reflectin C liquid condensates is dependent on protein net charge density. Fluorescence recovers completely for both conditions (Fig. 4.3C) demonstrating that 100% of reflectin C liquid droplets are mobile under these conditions.

At pH 6 $\tau = 3.9 \pm 0.7$s and pH 7 $\tau = 12.2 \pm 5.3$ for reflectin C (Fig. 4.3D). FRAP analyses of reflectin B containing 1% Alexafluor 405-labeled reflectin B (Fig. 4.4 A, B) reveal that the diffusivity of reflectin B liquid condensates is intermediate between to that of reflectins A1 and C. A comparison of the extent of fluorescence recovery for reflectins A1, B and C in 250 mM NaCl at pH 6 shows that the proportion of mobile components in liquid condensates of reflectins B and C is significantly greater than in the liquid condensates of reflectin A1. The liquid condensates of reflectins B and C each exhibit faster diffusivity than seen in

Reflectin A1 may exhibit the slowest dynamics because it has a greater number of potential arginine and tyrosine residues, as well as RMs, and possibly thus potentially more extensive inter-protein interactions than reflectins B and C [74, 47]. It is also the largest of the three proteins followed by reflectins B and then C. Reflectin C contains the unique GMXX motif with proline occurring every 5-6 residues in this glycine-rich stretch. This region may remain disordered in the liquid phase, potentially conferring greater flexibility and increased dynamics of reflectin C in liquid condensates [88] relative to reflectins A1 and B, although increased backbone flexibility does not necessarily increase the translational dynamics of proteins within condensates [47].

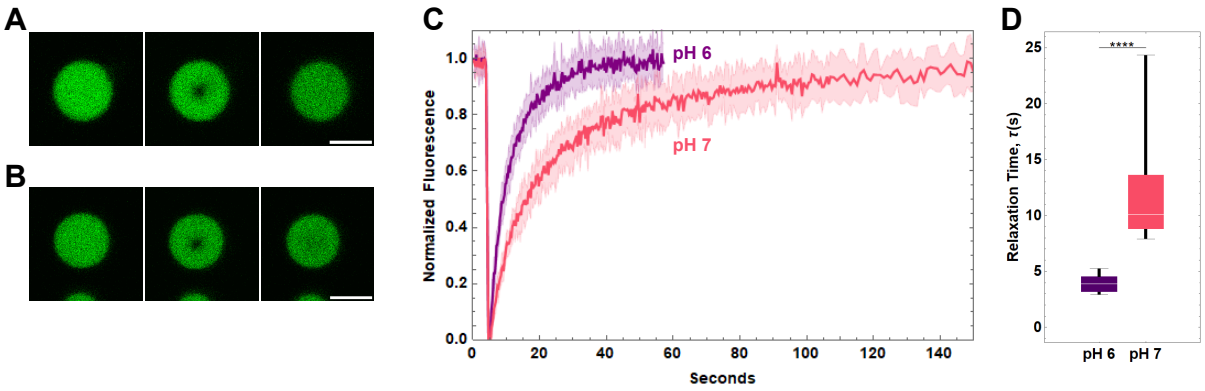

Figure 4.3: Reflectin C condensates demonstrate pH-dependent FRAP recovery. Characteristic images of reflectin C containing 5% fluorescein labeled reflectin C showing droplet pre-bleach, immediately post- bleach, and final in (A) 250 mM NaCl at pH 6 and (B) 250 mM NaCl at pH 7. C) Fluorescence intensity of the photobleached regions were corrected for photobleaching, fully normalized and the average of experiments plotted as a function of time. D) Fitting of individual experiments to an exponential decay equation yields the characteristic relaxation time τ. Differences of τ and percent recovery were found to be statistically significant using a one-way ANOVA test. Box and whisker plots display the median (center line), 2nd and 3rd quartile (solid box) and the complete range (black fences) of the data. N=12 for each condition. Error bands in FRAP plots represent $\pm$ 1 SD. Scale bars =5 μm.

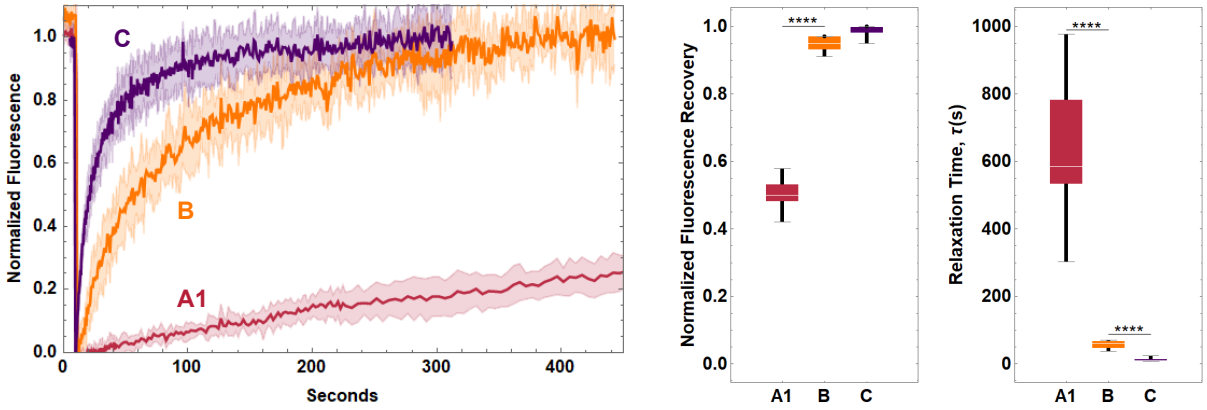

Figure 4.4: FRAP analyses of reflectins A1, B and C in 250 mM NaCl at pH 6. A) Fluorescence intensity of the photobleached regions were corrected for photobleaching, fully normalized and the average of experiments plotted as a function of time for reflectins A1, B and C C) Comparison of normalized fluorescence recovery for reflectins A1 (orange), B (blue) and C (purple). D) Comparison of relaxation time τ for reflectins A1 (orange), B (blue) and C (purple). Statistical significance tested for as previously described. N=9 for reflectin A1, n= 6 for reflectin B and n=12 for reflectin C. Error bands in FRAP plots represent $\pm$ 1 SD. Scale bars= 5 μm.

4.3 Reflectin C Increases Liquidity of Reflectin A1 in Liquid Condensates

FRAP analysis of reflectin A1 combined with reflectin C in the ratio found in maximally tunable dorsal iridocytes (21.7% reflectin A1, 78.3% reflectin C) shows that reflectin C greatly increases the rate and extent of fluorescence recovery for reflectin A1 at pH 6 and 7 (Fig. 4.5A, B). For reflectin A1, $\tau = 641.6 \pm 220.2$s at pH 6 , yet in mixtures of reflectin A1 and C τ decreases to 141.7 ± 26.3s at pH 6 and 182.6 ± 13.2s at pH 7 (Fig. 4.5C). Similarly, reflectin C increases the mobile component of reflectin A1 in condensates of both species from $50.5 \pm 4.4\%$ to $93 \pm 8.2\%$ at pH 6 and remarkably from $31 \pm 2.6\%$ to $90.7 \pm 1.7\%$ at pH 7 (Fig. 4.5D). Reflectin C may increase the diffusivity of reflectin A1 by increasing the overall liquidity of the condensate, although it also could do so through heterotypic interactions with reflectin A1 that would disrupt homotypic interactions of reflectin A1 [96]. The enrichment of reflectin C in the maximally tunable dorsal iridocytes thus could have the effect of increasing the diffusivity of the lamellar condensates, facilitating activation of the signal activated assembly of the reflectins and its consequent tuning of photonic behavior on the observed sub-second timescale.

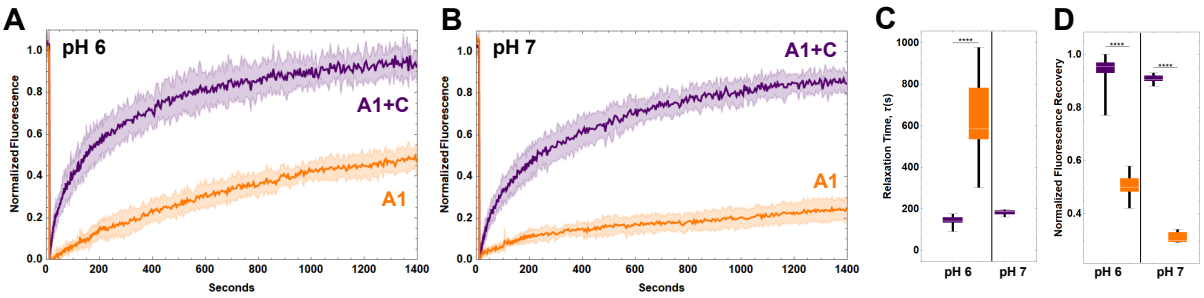

Figure 4.5: FRAP analyses of selective photobleaching of reflectin A1 in dorsal mixture with reflectin C. Fluorescence intensities in the bleached region were corrected for photobleaching, fully normalized and plotted as a function of time from FRAP experiments of reflectin A1 mixed in dorsal ratio with reflectin C at (A) pH 6 and (B) pH 7. C) Comparison of relaxation times and (D) normalized fluorescence recovery for reflectin A1 (orange) and reflectin A1 mixed with reflectin C (purple) at pH 6 and 7. N= 11 for reflectin A1+C at pH 6, N=8 for reflectin A1+C at pH 7, n=9 for A1 at pH 6, and n=7 for pH 7. Statistical significance tested for as previously described. Error bands in FRAP plots represent ± 1 SD.

4.4 Diverse Responses of Liquid Phase Boundaries of Reflectins A2, B and C to Changes in Ionic Strength and Protein Net Charge Density

The liquid phase boundaries of reflectins A2, B, and C are dependent upon protein net charge density (NCD) and ionic strength (Figs. 4.6A, B, A.1, A.2). The locations and slopes of these liquid phase boundaries as functions of protein NCD and ionic strength are most similar for reflectins A1 (green line) and A2 (red line) that are most similar in sequence, showing nearly linear responses to ionic strength as a function of protein NCD (Figs. 4.6A, B, A.1). In terms of ionic strength, reflectin A1 exhibits a stronger drive to LLPS than reflectin A2 at any given protein NCD. This is expected in the context of the number of potential intra- and interprotein attractions: reflectin A1 has 38 arginine and 44 tyrosine residues compared to A2's 27 arginine and 28 tyrosine residues. The predicted emergent hydrophobicity of the folded RMs, whether they facilitate interprotein hydrophobic attractions or as simple mediators of the hydrophobic effect, also follows this trend as reflectin A1 contains 5 RMs compared to 3 RMs in reflectin A2. Reflectin B (Fig. 4.6), which contains the N-terminal RMn but lacks internal RMs exhibits a weaker drive to LLPS as a function of increasing ionic strength relative to the A-types at high protein NCDs but a greater drive at lower protein NCDs (Figs. 4.6A, B, A.2). Unlike reflectins A1, A2 and C, reflectin B forms arrested gel-like clusters (Fig. 4.2C) at high protein NCDs for salt concentrations up to 500 mM (Figs. 4.6A, B, A.2). The phase boundary of reflectin C (purple line), which lacks the RMn and contains only one weakly conserved RM, shows the widest range of salt concentrations of these four reflectins, ranging from 600 mM at the highest protein NCD (pH 4) to zero added salt at low protein NCD (pH 7) (Figs. 4.6C, D, A.2). Despite the wide range of salt concentrations that drive LLPS

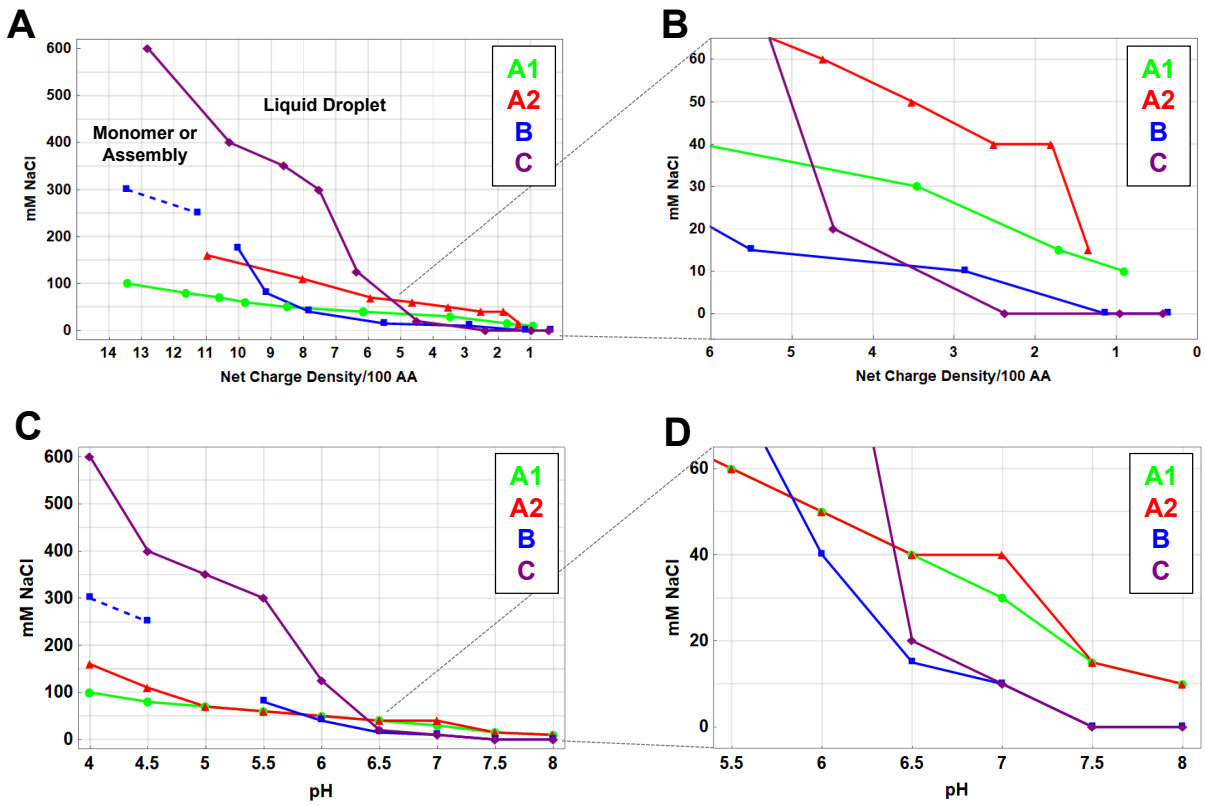

Figure 4.6: A) Liquid phase boundaries of reflectins A1 (green), A2 (red), B (blue) and C (orange) as a function of NaCl concentration and calculated protein net charge density as determined by presence or absence of fluorescently labeled droplets with the previously mentioned liquid characteristics. Reflectin B forms arrested gel-like bodies (blue dashed line) for pH 4-4.5. B) Inset of (A) C) Same data as (A) re-plotted as a function of pH. D) Inset of (C). Total protein concentration is 4 μM for reflectins A1, A2, B and C.

of reflectins A1, A2, B and C at high protein NCDs, the liquid phase boundaries all converge to within 15 mM NaCl as their protein NCDs approach zero (Figs. 4.6, A.2, A.3). This is expected as proteins are typically least soluble as they approach their isoelectric point and zero net charge [87, 88].

Relative to reflectins A1 and A2, reflectins B and C require more salt to liquid phase separate at high protein NCDs and less salt at low protein NCDs (Figs. 4.6, A.2, A.3). They thus exhibit a greater switch-like response to decreasing protein NCD than reflectins A1 and A2. The primary sequences of reflectins B and C differ markedly from those of A1 and A2 as well as from each other, suggesting that analyses of the effects of mutational insertion and deletion of key sequences within reflectins B and C may be needed to further resolve how these sequence features inform their liquid phase boundaries.

It appears that at high protein NCDs (pH values lower than pH 6-6.5, a reasonable assumption for the pKas of native histidine residues) the contribution to the drive to LLPS by non-covalent intra- and inter-protein interactions is greatest, as reflectins A1 and A2 have the highest drive to LLPS. For lower protein NCDs (pH values greater than 6-6.5) this relationship is inverted and the species with the greatest valencies have the weakest drive to undergo LLPS. This relationship is especially evident when viewed as a function of pH (Fig. 4.6C, D), . showing that ionic strength differentially affects the drivers of reflectin LLPS at different protein NCDs. At high protein NCDs, increasing ionic strength may contribute more to the drive to LLPS by increasing intra- and inter-protein interaction strengths by screening Coulombic repulsion and increasing the strength of pi-cation interactions, while at lower protein NCDs, ionic strength may contribute more to the drive to LLPS by decreasing the quality of the solvent [24] .

4.5 Reflectins A2, B and C Enable Switch-like Response of Reflectin Liquid Phase Boundary to Changing Protein Net Charge Density

The liquid phase boundary of reflectin A1 as a function of salt concentration and protein net charge density (NCD) is shifted in mixtures with either reflectin A2, B or C in the ratios found in tunable (dorsal) iridocytes. Such mixtures of reflectins A1 and A2 (53% reflectin A1, 47% reflectin A2) require less salt to drive LLPS than for reflectin A2 at all protein NCDs (Figs. 4.7A, A.3 A). At higher protein NCDs these mixtures require more salt to drive LLPS than reflectin A1, but surprisingly less salt to drive LLPS for protein NCDs less than ca. 9. The ratio of reflectins A1 and A2 found in tunable iridocytes also has a less linear response to salt concentration as a function of protein NCD than either protein alone (Figs. 4.7 A, A.3 A).

The ratio of reflectins A1 and B found in dorsal iridocytes (24.4% reflectin A1, 75.6% reflectin B) reveals that at higher protein NCDs the liquid phase boundary of reflectin B dominates that of the mixture (Figs. 4.7B, A.3B, C). These mixtures required higher salt concentration to drive LLPS relative to reflectin A1 at protein NCDs greater than ca. 8. Arrested gel-like clusters of reflectins A1 and B were observed for protein NCDs greater than ca. 11 (Fig. 4.2G) which is consistent with reflectin B alone (Fig. 4.2C).

The liquid phase boundary of the ratio of reflectins A1 and C found in dorsal iridocytes (21.7% reflectin A1, 78.3% reflectin C) reveals that reflectin C is more effective than reflectins A2 and B at shifting the liquid phase boundary of reflectin A1 (Figs. 4.7C, A.3 D,E). As a function of pH, the liquid phase boundaries of reflectin C and reflectin A1/C mixture are identical except for a 10 mM NaCl deviation at pH 6 (Fig. A.3D ,E). As a function of NaCl, Reflectin C shifts the liquid phase boundary of reflectin A1 up to 6

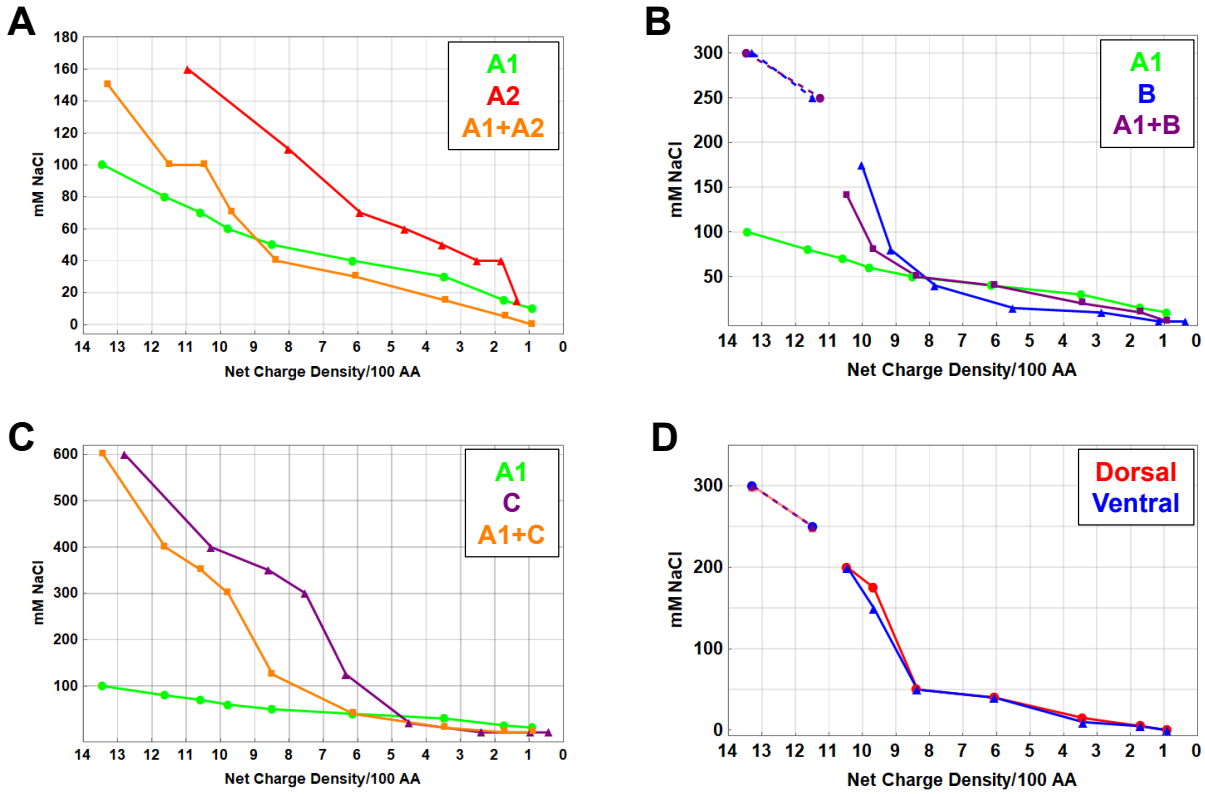

Figure 4.7: Liquid phase boundaries for maximally tunable dorsal iridocyte ratios of reflectins as a function of calculated protein net charge density and NaCl concentration. A) The liquid phase boundary of 53% reflectin A1 and 47% reflectin A2 (orange) compared to those of reflectin A1 (green) and reflectin A2 (red). B) Liquid phase boundary for 24.4% reflectin A1 and 75.6% reflectin B (purple) compared to reflectin B (blue) and reflectin A1 (green). C) Phase boundary for mixtures of reflectin A1 and C (orange) compared to that of reflectin C (purple) and reflectin A1 (green). D) Phase boundaries of reflectins A1, A2, B and C in the molar ratios found in tunable (red) and non-tunable (blue) iridocytes. Reflectin B and mixtures containing it form arrested gel-like clusters at high protein NCDs (dashed lines). Total protein concentration is 4 μM for A-D.

fold for protein NCDs greater than ca. 13 (Fig. 4.7C, Fig. A.3 D,E), demonstrating the significant influence of reflectin C on reflectin A1 phase behavior.

Molar ratios of reflectins A1, A2, B, and C found in both tunable (dorsal) and non-tunable (ventral) iridocytes have highly similar liquid phase boundaries and most closely resemble that for reflectin B alone (Fig. 4.7D, Fig. A.4), despite the enrichment of reflectins B and C in the tunable molar ratios compared to non-tunable (Fig. 4.1B, C). Thus, the relative concentration of reflectin B in both dorsal and ventral molar ratios is sufficient dominate the phase behavior of these mixtures.

Phase diagrams of dorsal and ventral mixtures of reflectins A1, A2, B and C were determined by diluting 100 μM protein stock to 4 μM final protein concentration in respective buffers. For dorsal mixtures, slight heterogeneity suggestive of multiphase separation was observed in 200 mM NaCl at pH 6 (Fig. 4.8A, B). Upon dilution of 200 μM protein stock to 8 μM final protein concentration in the same buffer, striking multiphase separation was observed in which reflectins A1 and A2 became less miscible in reflectins B and C (Fig. 4.8C, D). Droplets rich in reflectins A1 and A2 were present on the interior of larger droplets of reflectins B and C (Fig. 4.8C, D).

Notably, for all mixtures at all conditions tested, the species within each mixture showed coordinated phase behavior (Fig. 4.9), including conditions that produce multi-phase condensates. pH 4 120 mM NaCl is above the liquid phase boundary for reflectin A1 (Fig. 4.9A) but below that of reflectin A2 yet for mixtures of both reflectins, reflectin A1-only droplets are never observed at this condition. Instead, a sub-resolution haze or resolvable assemblies are detected (Fig. 4.9B). The same phenomena are observed for mixtures of reflectins B and C with A1. 100 mM NaCl at pH 5.5 is above the liquid phase boundary for reflectin A1 (Fig. 4.9C) but below that form mixtures of reflectin A1 and B (Fig. 4.9D). In 250 mM NaCl at pH 5 reflectin A1 exists as a liquid condensate (Fig. 4.9 E) yet in in mixtures with reflectin C, reflectin A1-only droplets are not observed (Fig.

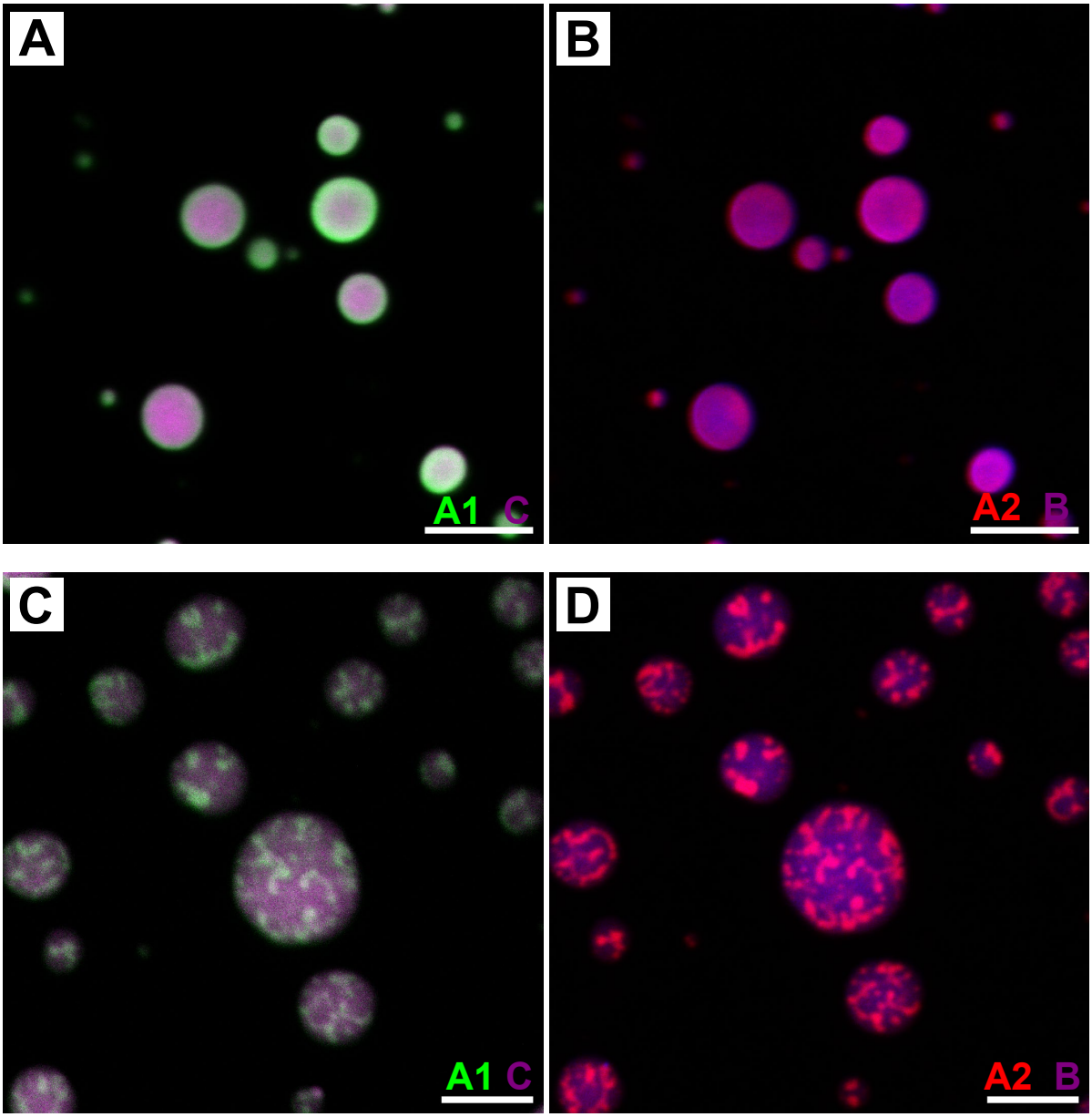

Figure 4.8: Multiphase separation of reflectins A1, A2, B and C at 4 μM and 8 μM final protein concentrations. A) Reflectins A1 (green) and C (magenta), and (B) reflectins A2 (red) and B (blue) at 4 μ M total protein concentration in 200 mM NaCl at pH 6 showing slight heterogeneity in distributions of individual proteins throughout the droplet. C) Reflectins A1 (green) and C (magenta), and (D) reflectins A2 (red) and B (blue) at 8 μM total protein concentration in same buffer conditions as (A). A,B and C,D are separate channels of the two images.

4.9F). Client/scaffold recruitment of reflectins B and C by reflectin A1 is not observed as has been shown for some multicomponent protein condensates [67, 97, 98]. Instead, reflectins B and C inhibit LLPS of reflectin A1 (Fig.s 4.7B, C, 4.9B, C) and reflectin A2 (Fig.s 4.7A, 4.9A).

With respect to the ability of arginine and tyrosine to form inter- and intraprotein cation-pi bonds, reflectin A1 is has the greatest valency (38R : 44Y) followed by reflectin A2 (27R : 29Y), reflectin B (27R:15Y) and reflectin C (18R : 11Y). Unlike reflectins A1 and A2, reflectins B and C do not have near equimolar ratios of R : Y. In mixtures with reflectin A1, reflectins B and C and exert the greatest influence the liquid phase boundary of reflectin A1 (Fig. 4.7A, B) and reflectin B dominates the phase behavior of both dorsal and ventral mixtures of all four reflectins as seen by the similarity of the liquid phase boundaries of these mixtures to those of reflectin B (Fig. 4.7B, D). In the proposed model, when reflectins B and C interact with reflectin A1 and A2, the uneven ratios of arginine and tyrosine of reflectins B and C cap and exhaust the valences of reflectins A1 and A2, arresting condensate growth and subsequently bulk LLPS [74, 99, 100, 101]. Once the liquid phase boundaries of reflectins B and C are reached, homotypic interactions of both reflectins B and C out compete heterotypic interactions of reflectins B and C with reflectins A1 and A2. This leads to dissociation of reflectins B and C from A1 and A2, freeing sufficient valences of the latter to allow LLPS of all species. Importantly, once the liquid phase boundary is crossed at final protein concentrations of 4 μM, mixtures of reflectins A1 and B as well as A1 and C co-phase separate, demonstrating that reflectins B and C have favorable interactions with reflectin A1 that can screen homotypic reflectin A1 interactions.

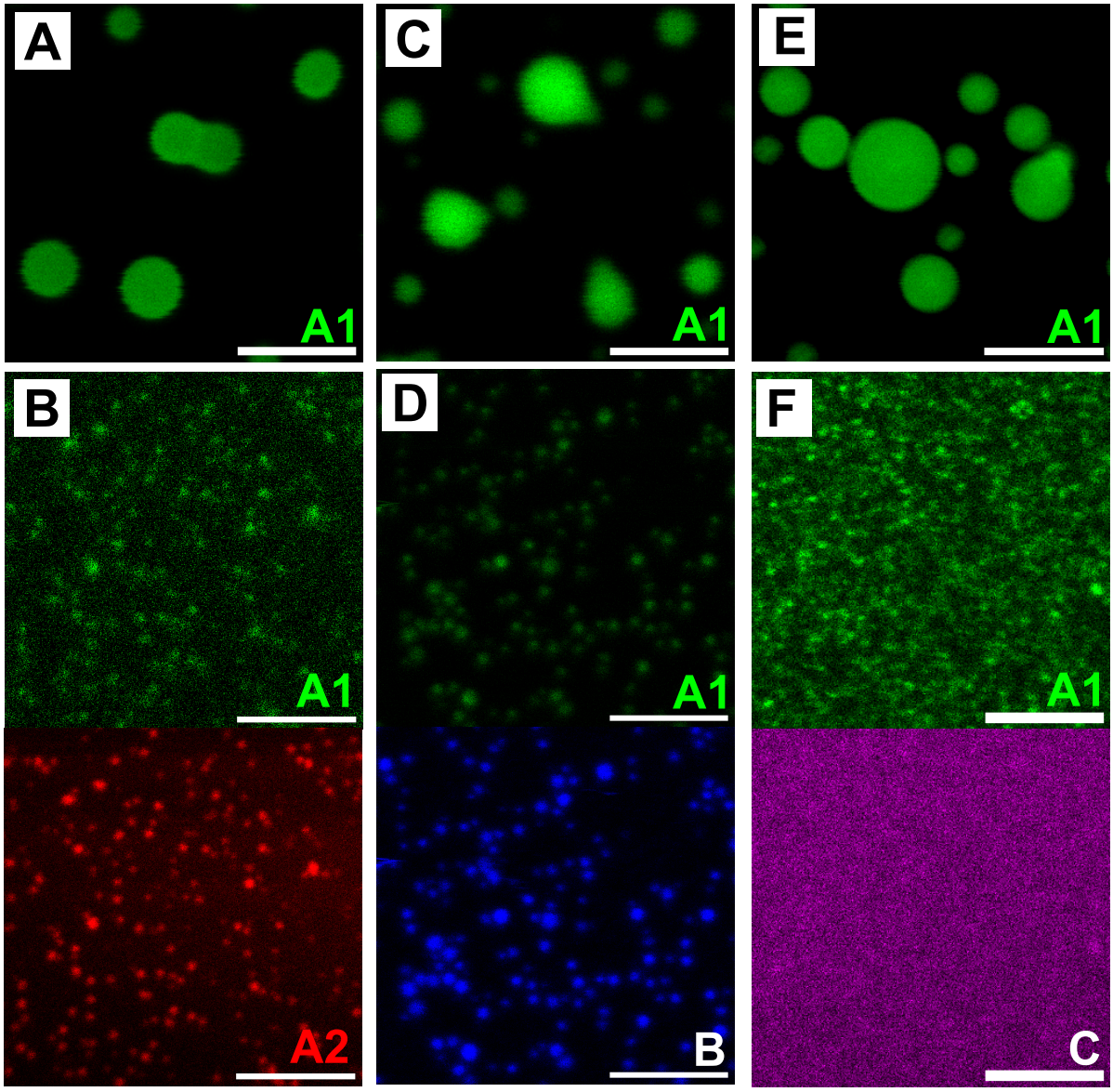

Figure 4.9: Coordinated phase behavior of ratios of reflectins found in maximally tunable iridocytes. A) Reflectin A1 and (B) mixture of reflectins A1 (green) and A2 (red) in 120 mM NaCl at pH 4. C) Reflectin A1 and (D) mixture of reflectins A1 (green) and B (blue) in 100 mM NaCl at pH 5.5. E) Reflectin A1 and (F) mixture of reflectins A1 (green) and C (purple) in 250 mM NaCl at pH 5.5. Exposure values for B, D, F have been increased 190-210 fluorescence intensity units compared to A, C, E. Total protein concentration is 4 μM. All scale bars=5 μm.

4.6 Immiscibility of Reflectins A1, A2, and C in B is Controlled by Ionic Strength

Increasing protein stock concentration from 100 to 200 μM and final protein concentration from 4 to 8 μM exceeded the inter-miscibility of these four species, leading to multi-phase separation of reflectins A1, A2, B, and C (Fig. 4.8). Mixtures of reflectins A1, A2, B, and C in the dorsal ratio show salt-dependent demixing of reflectins A1, A2, and C from reflectin B. At the liquid phase boundary, 20 mM NaCl at pH 7, reflectin A2 is distributed heterogeneously throughout the droplets while A1, B and C appear homogeneous (Fig. 4.10 A). As the salt concentration increases, the heterogeneity of reflectin A2 becomes more pronounced and is also apparent for reflectin A1 (Fig. 4.10B). Increasing the salt concentration further results in heterogeneity of reflectin C (Fig. 4.10C) and this trend continues up to 300 mM NaCl (Fig. 4.10D, E). Thus, at pH 7 reflectin C is the most miscible with reflectin B, followed by reflectin A1 then reflectin A2. Note that for all conditions shown here reflectins A1, A2 and C are partially miscible with reflectin B.

At pH 7 the drive to phase separate as a function of NaCl concentration, from greatest to weakest, is : reflectin B = C > A1 >A2. If the increase in surface tension by increasing ionic strength was the sole driver of reflectin LLPS and these organizations are at thermodynamic equilibrium, then multiphase separation at pH 7 would be expected to produce droplets with reflectins B and C on the interior, shielded from solvent by reflectins A1 and A2 in order to minimize the surface energy of the system [24, 102]. Measurements of the surface tensions of individual reflectin condensates are needed to begin to understand the energies determining droplet organizations. However, if ionic strength drives LLPS at high protein NCDs in part by screening repulsive charges and/or increasing the strength of pi-cation interactions, then the concentration of NaCl needed to drive LLPS of each

reflectin does not solely reflect the surface tension of liquid condensates of each reflectin.

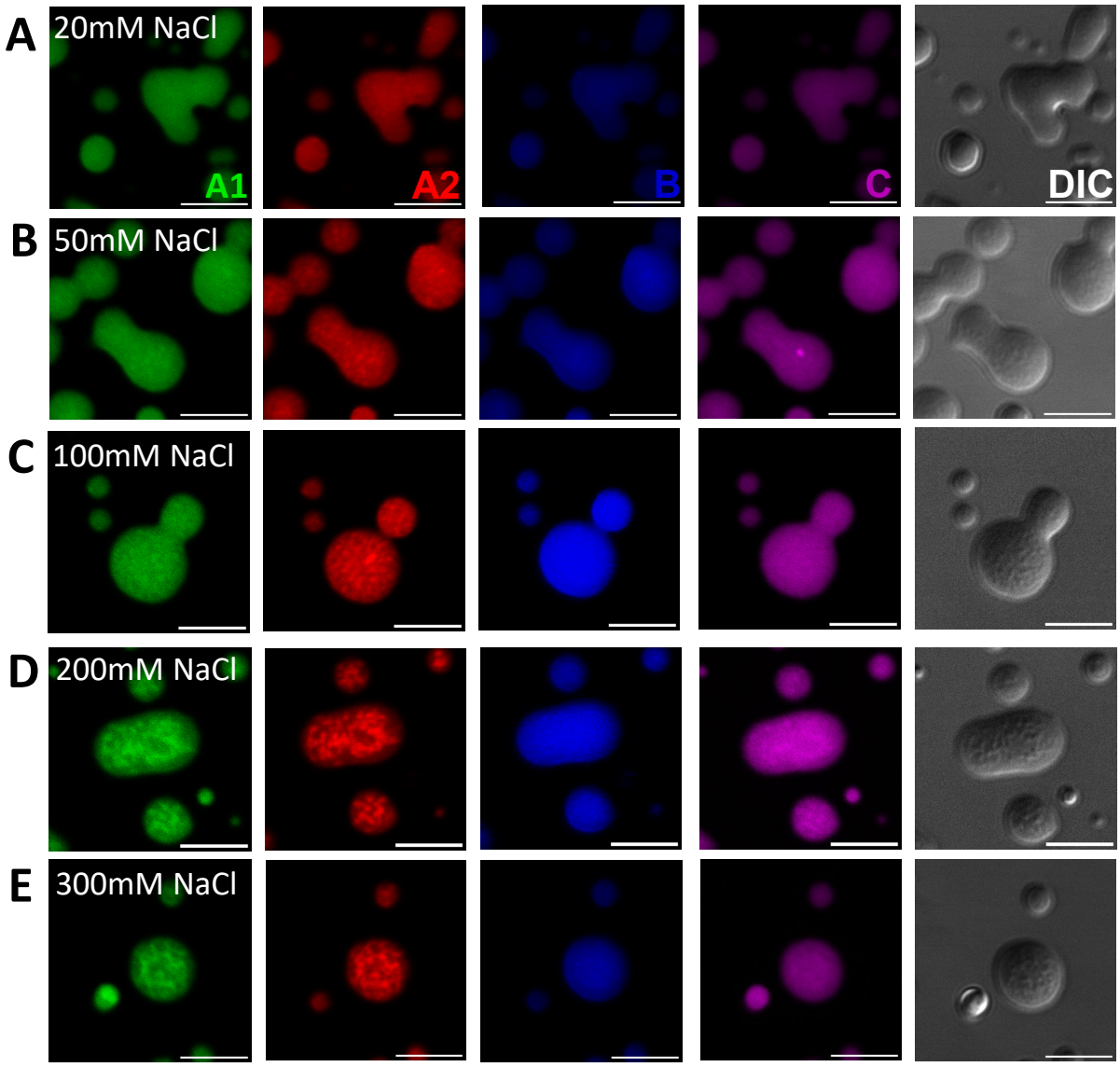

Figure 4.10: : Individual fluorescent channels and DIC images of reflectins A1 (green), A2 (red), B (blue) and C (magenta) in dorsal ratio at pH 7 in (A) 20 mM, (B) 50 mM, (C) 100 mM, (D) 200 mM and (E) 300 mM NaCl on untreated glass coverslips. 200 μM total protein stock was diluted into respective buffers to a final protein concentration of 8 μM. Scale bar = 5 μm.

4.7 Molar Ratio of Reflectins Found in Tunable Iridocytes Shows Greatest Change of Multiphase Organization in Response to Changing Protein NCD

The dorsal and ventral molar ratios of reflectins A1, A2, B, and C demonstrate different pH-dependent morphologies. The dorsal ratio at pH 5.5 250 mM NaCl (Figure 4.11A) appears homogenous and as pH is increased to 7 and 8, the condensates exhibit internal puncta that are relatively devoid of reflectins A1 and A2 (Fig. 4.11B, C). The multiphase organization of condensates formed from the dorsal ratio of reflectins A1, A2, B and C demonstrate a greater change upon increasing pH and differ significantly from those of the ventral ratios. At pH 5.5 250 mM NaCl condensates formed from the dorsal ratios exhibit a shell-like organization of reflectins A1 and A2 around reflectins B and C, although some A1 and A2-rich microdroplets are seen in the interior of the condensates (Fig. 4.11D). As pH increases, the shell-core arrangement is lost and microdroplets of both reflectins A1 and A2 are seen in the interior of the condensates (Fig. 4.11D, E). It is currently unclear if these organizations are at, or are on, the path to thermodynamic equilibrium; however these data were captured on PEG-passivated coverslips up to four hours after droplet formation.

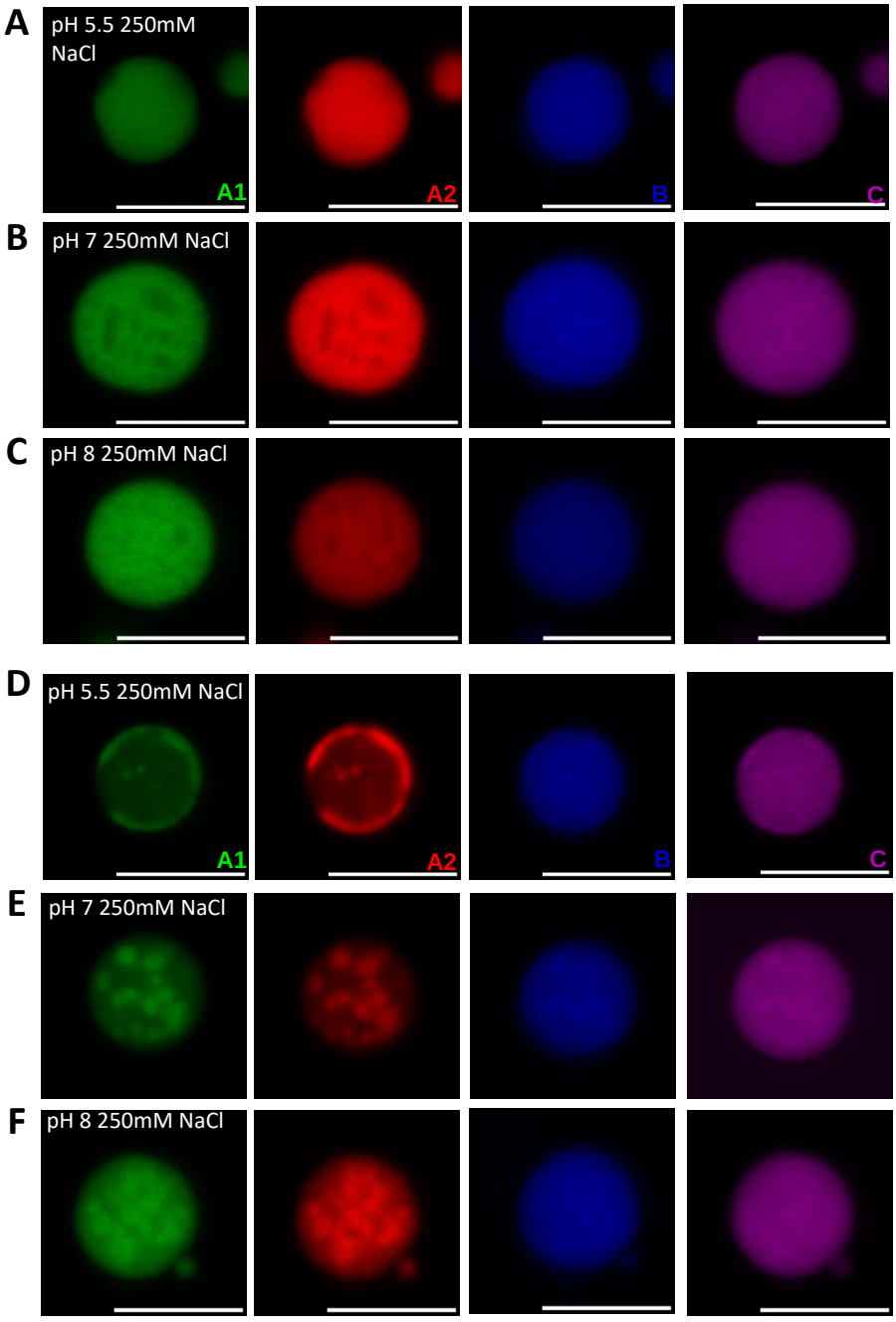

Figure 4.11: Individual fluorescent channels of dorsal and ventral ratios of reflectins at 250mM NaCl as a function of pH. Dorsal ratio of reflectins A1, A2, B and C (A) pH 5.5, (B) pH 7 and (C) pH 8. Ventral ratios of reflectins A1, A2, B and C at (D) pH 5.5, (E) pH 7 and (F) pH 8. Protein stock (200 μM) was diluted to final protein concentration of 8 μM. Droplets imaged in PEG-passivated microchambers. Scale bar=5 μm.

4.8 Reflectins A2, B and C Control Multiphase Organization of Reflectin Condensates at High Protein Net Charge Densities.

The organization of reflectins A1, A2, B, and C also depends on the molar ratios of the species. Of the four protein species, the relative concentrations of reflectins A2 and B change the most between the dorsal and ventral mixture. At pH 5.5 250 mM NaCl dorsal ratios the of the four species have a shell-like layer of reflectins A1 and A2 shielding reflectins B and C from solvent (Fig. 4.11A). A fluorescent intensity profile across the length of the dashed white box confirms that reflectins A1 and A2 co-segregate from reflectins B and C (Fig. 4.11B). However in the same conditions, ventral ratios of the four species are relatively homogeneous (Fig. 4.11C), with very slight increasing distribution of reflectins B and C on the outside of the droplets as seen by the fluorescent line profiles for all four species.

To decipher their roles in organizing the multiphase organization, solutions of dorsal ratios of reflectins absent of reflectin A2, B, or C were driven to LLPS by dilution into pH 5.5 25 mM acetic acid 250 mM NaCl and compared to liquid condensates of dorsal ratios of all four reflectin species. This salt and pH condition was chosen because it showed the greatest differences between dorsal and ventral multiphase organizations. Dorsal mixtures of reflectins that lack reflectin B still demonstrate the layered architecture as seen for dorsal mixtures that do contain reflectin B (Fig. 4.11 E, F), revealing that the increase in reflectin B for dorsal compared to ventral mixtures is not solely responsible for the multi-layered organization of droplets. This organization is abolished in dorsal mixtures that lack reflectin A2 (Fig. 4.11 G, H) These results show that the relative ratios of both reflectins A2 and B dictate the multiphase droplet structures. Reflectin

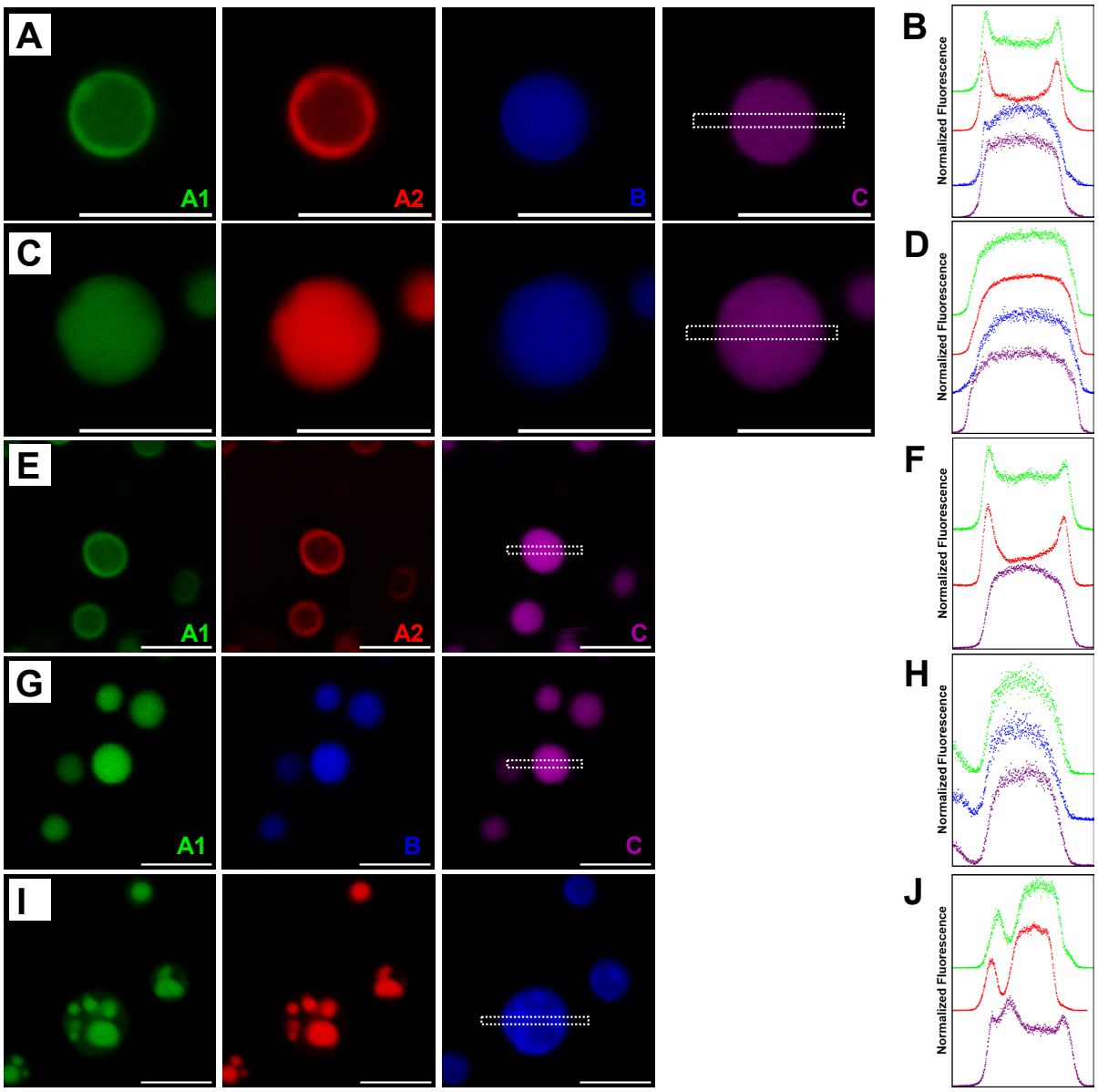

Figure 4.12: Multiphase organization of dorsal mixtures of reflectins with and without reflectins A2, B and C at pH 5.5 25mM acetic acid 250mM NaCl. A) Dorsal ratios of reflectins A1, A2, B and C. B) Fluorescence intensity profile across the length of the white dashed box for reflectins A1, A2, B and C in (A). C) Ventral mixture of reflectins A1, A2, B and C with (D) corresponding fluorescence intensity profile. E) Mixture of dorsal ratios of reflectins A1, A2 and C with (F) corresponding fluorescence intensity profile. G) Mixture of dorsal ratios of reflectins A1, B and C with (H) corresponding fluorescence intensity profile. I) Mixture of dorsal ratios of reflectins A1, A2 and B with (J) corresponding fluorescence intensity profile. 200 μM protein stock was diluted to final protein concentration of 8 μM. Droplets imaged in PEG-passivated microchambers. Scale bar= 5 μm.

A2 is necessary to drive the multiphase structure in these salt and pH conditions (Fig. 4.11 G, H), however it is decreased in the dorsal ratios, where the multiphase organization appears (Fig. 4.11 A). Reflectin B is enriched in the dorsal ratios, however its presence alone does not drive the multiphase organization. The omission of reflectin C reverses the shell/core organization observed in dorsal mixtures of all four reflectin species and microdroplets rich in reflectins A1 and A2 in the interior of reflectin B droplets are observed (Fig. 4.11 I, J).

Remarkably, multiphase separation of this four protein system can be reorganized in constant salt and pH conditions by changing the ratios of reflectins A2, B and C. A systematic analysis of varying the relative concentration of each protein while holding the others constant across a wide pH and salt range would establish consistent organizational rules that would be the basis for a complete model of this multiphase behavior.

4.9 Reflectins B and C Affect Inner-Droplet Morphology at Low Protein Net Charge Densities

Solutions of dorsal and ventral ratios of reflectins absent of reflectin A2, B or C were driven to LLPS by dilution into pH 7 25mM MOPS 250mM NaCl and compared to liquid condensates of dorsal ratios of all four reflectin species. Omitting reflectin B from dorsal ratios at these conditions shows a change in the internal structure formed by the segregation of reflectins A1 and A2 from B (Fig. 4.12 A, 4.10 E). The removal of reflectin C has a similar effect, and seems to form hollow spheres of reflectins A1 and A2 segregated from reflectin C (Fig. 4.12 B, 4.10 E). Omitting reflectin B from ventral mixtures produces a similar inner droplet morphology but with apparent finer structure of reflectins A1 and A2 (Fig. 4.12 C, 4.10 B). Omitting reflectin C from ventral mixtures

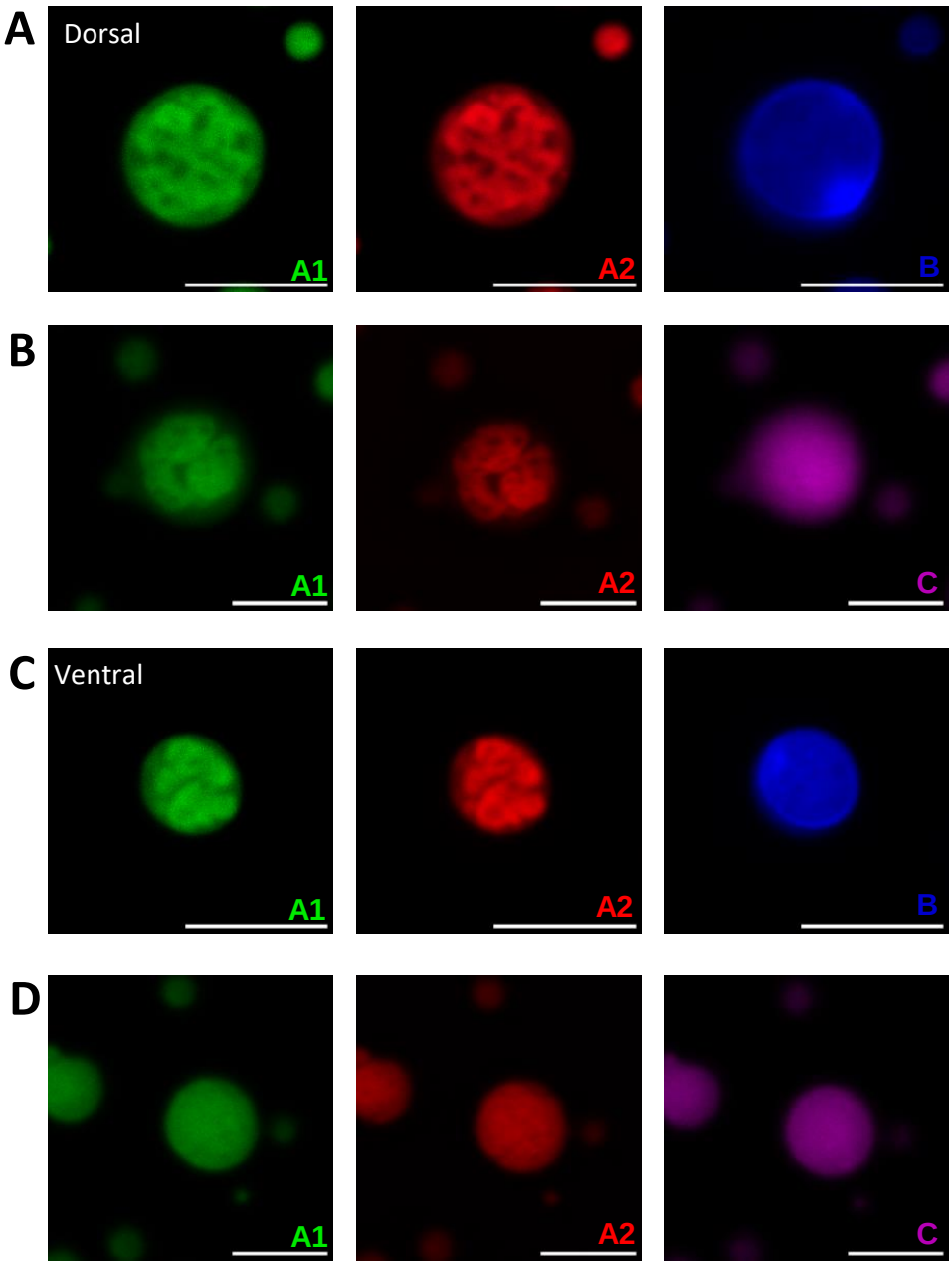

Figure 4.13: Dorsal and Ventral ratios of reflectins lacking reflectin B or C in 250 mM NaCl at pH 7. A) Mixture of reflectins A1, A2 and B in dorsal ratio. B) Mixture of reflectins A1, A2 and C in dorsal ratio. C) Mixture of reflectins A1, A2 and B in ventral ratio. D) Mixture of reflectins A1, A2 and C in ventral ratio. 200 μM protein stock was diluted to final protein concentration of 8 μM. Images captured in PEG-passivated microchambers. Scale bar=5 μm.

produces inner droplet structures of reflectins A1 and A2 that are more similar to that seen for the dorsal ratio (Fig. 4.11 D, 4.10 B). The high surface area presented by these intricate interfaces suggests that this system is not at thermodynamic equilibrium[**?**]. Further considering the role of reflectin C in greatly increasing the liquidity of reflectin A1, these inner structures formed by the omission of reflectin C may be kinetically defined. Further investigation of the liquidity of these inner structures including droplet fusion and FRAP would help determine the role of arrested dynamics in defining these structures.

Chapter 5

Conclusion

5.1 Molecular Mechanisms of Reflectin A1 Assembly and LLPS

The phase behavior of reflectin A1 adds to recent reports of proteins with both assembly and liquid-liquid phase-separation (LLPS) behavior [44, 103, 104]. FUS protein forms heterogeneous 100s nm diameter clusters in solutions when C_{bulk} is less than C_{sat} for LLPS (44). These clusters are described as a pre-percolation state in percolation-coupled phase separation of FUS [44]. Reflectin A1 assemblies differ from FUS clusters in several aspects. 0.15-1% of total FUS protein was partitioned into these clusters, 2-3 orders of magnitude weaker partitioning into clusters than seen with reflectin A1 assemblies (95%). FUS clusters exhibited a broad heavy-tailed distribution of cluster sizes [44] whereas reflectin A1 assemblies are relatively monodisperse and display a normal distribution of sizes as detected by dynamic light scattering (DLS) here and previously [22, 29, 30]. Finally, Reflectin A1 assembly sizes did not increase with increasing concentrations for the range of 1-10 μM (Figure 2.2), in contrast to predictions for the

pre-percolation model in which the size of protein clusters increases with increasing concentration [24, 44]. Therefore, the assembly of reflectin A1 appears to result from a different mechanism.

Comparison of reflectin A1 to IDPs such as FUS and attempts to describe reflectin A1 phase behavior in the context of 'linkers' and 'stickers' used to describe noncovalent associations for other LLPS systems [24, 74, 105] proves to be of limited usefulness. Although reflectin A1 shares key sequence features with proteins like FUS and hnRNPA1, such as an abundance of arginine and tyrosine favoring cation-pi interactions, and a relative lack of aliphatic amino acids [23, 60, 62], the sequence of reflectin A1 differs in key aspects. Typically, 'stickers' (residue pairs capable of noncovalent interactions) are often clustered, and the length, flexibility, and solvation volume of 'linkers' (regions between stickers enriched in small, flexible amino acids such as serine and glycine) modulates phase behavior as well [24, 99]. In contrast, in reflectin A1 tyrosine and arginine are relatively evenly distributed throughout the length of the entire sequence, and charged amino acids capable of inter-protein interactions are abundant in the stretches between tyrosine and arginine (Fig. 1.1). In further contrast, reflectin A1 lacks regions of low complexity such as prion-like domains (PLDs) [62, 104] , exhibits a pronounced block copolymeric organization of alternating cationic and conserved regions at neutral pH, with the methionine-rich, highly conserved reflectin repeat motifs predicted to show emergent hydrophobicity upon folding [21, 29]. Thus, the sequence of reflectin A1 with respect to possible inter- and intra-protein interactions is incompletely described by the 'sticker and linker' framework of multivalent protein LLPS.

Reflectin A1's net charge density (NCD) has been shown to finely control the protein's assembly sizes, and it has been hypothesized that progressive neutralization of the protein's excess cationic charge, minimizing Coulombic repulsion both within and between reflectin molecules, mediates this relationship [29], both physiologically in re-

sponse to neuronally activated phosphorylation [12, 13] and in vitro by various surrogates [29, 32, 33]. The dependence of the liquid phase boundary of reflectin A1 on the concentration of anions at high protein NCDs (Fig. 3.4) supports the hypothesis that ionic screening of Coulombically-repulsed cationic reflectin A1 allows short-range attractive forces (including cation-pi and sulfur-pi interactions and thehydrophobic effect) to drive LLPS of reflectin A1. Importantly, this matches the recent finding that salt induces reflectin A1 assembly by ionic screening [30], and both mechanisms are in line with the findings that reducing reflectin A1 NCD by pH titration or genetic engineering control reflectin A1 assembly sizes [29]. In contrast to my results with reflectin A1, it has been found that solutions of proteins FUS, TDP-43, BrD4, Sox2 and A11 undergo LLPS under low salt concentrations (¡50 mM KCl) and exist as a single phase under intermediate salt concentrations (125 mM-1.5 M KCl), and it was shown that electrostatic screening at intermediate salt concentrations prevent LLPS by disrupting attractive ionic protein interactions [77]. Hence, it is not without precedent that intermediate salt concentrations can dictate liquid phase transitions of proteins by screening ionic interactions.

The physical mechanism by which Coulombic repulsion controls assembly size is incompletely understood. The dynamic exchange of reflectin A1 assemblies ages rapidly (Fig.s 2.3, 2.4), and this aging is tightly correlated with the decrease of the rate of assembly growth (Fig. 2.4), both together suggesting the arrest of Ostwald ripening is limiting assembly sizes (105). Reflectin A1 exhibits a progressive increase in secondary structure as assembly sizes increase with decreasing protein NCD, demonstrating that reflectin A1 folding is incomplete in smaller assemblies [29]. Notably, as salt concentration increases, assemblies increase in size [30] and reflectin A1 assembly always precedes LLPS, suggesting that reflectin A1 assembly and LLPS are on a continuum of the same physical process [74, 105]. Reflectin A1 condensates with liquid properties show no significant growth in size via Ostwald ripening up to 96 hours, demonstrating that ripening arrests after bulk

LLPS. These observations are consistent with the model that salt-driven reflectin A1 assemblies are caused by spinodal decomposition immediately followed by dynamic arrest of assemblies [40, 75, 76], and that above a threshold in the ratio of protein NCD to ionic strength, assembly arrest is bypassed and spinodal decomposition forms a bulk liquid phase. Dynamic arrest could occur due to exhaustion of potential inter-protein interaction sites [74, 106]. In this model reflectin A1 assembly sizes are kinetically determined by the rate of protein transport into assemblies and the rate of dynamic arrest. However, an equilibrium mechanism for controlling reflectin A1 assembly size is also supported by these observations. Thermodynamic equilibrium could define reflectin A1 assembly size by a trade-off between short range attractive forces and long-range repulsive forces (SALR) [39]. Equilibrium protein clusters well described by SALR models have been reported [43, 107] in which long range electrostatic repulsion competes with Van der Waals forces and the hydrophobic effect to control cluster size. The strong dependence of reflectin A1 assembly sizes on protein net charge density can be described as long-range repulsive forces that, in tandem with short range attractive forces such as cation-pi and hydrophobic interactions, define assembly sizes. Screening of coulombic repulsion, which is proportional to equilibrium cluster sizes in both lysozyme and hemoglobin solutions [43, 107, 108, 109], could control reflectin A1 assembly sizes similarly. In model lysozyme systems the formation of equilibrium clusters can be followed by a glass transition that arrests cluster dynamics [43], which is consistent with the formation and arrest of reflectin A1 assemblies as demonstrated by FRET. In silico modeling demonstrated that mesoscopic metastable clusters can be intermediates to the condensation of a bulk liquid phase, and that increased ionic screening lowers the repulsive energy barrier and allows bulk transition to two liquid phases [110]. Reflectin A1 phase behavior is likely influenced by the valency of potential interprotein non-covalent bonds, and thus one shortcoming of relating this behavior to that of lysozyme and hemoglobin-based model systems is that

these do not depend on the valency of such bonds. Further, the observed and predicted numbers of monomers in those cluster are typically in the 10s [43, 107, 111], whereas 30 nm diam. reflectin A1 assemblies contain ca. 500 individual proteins assuming close packing and 4 nm diam. of individual proteins.

5.2 Biological Insights From Dense-Phase Interactions of Reflectins A1, A2, B and C

The liquid phase behavior of reflectins A1, A2, B and C adds to our understanding of the possible states of matter in the tunable iridocytes of D. opalescens. While in vitro analyses did not exceed 8 μM bulk protein concentration, while the reflectin concentration in activated Bragg lamellae of the tunable iridocytes from D. opalescens was estimated to be 381 mg/mL, which near the estimated 416 $\pm$ 42 mg/mL reflectin concentration in the dense phase [18].

There is evidence from TEM analyses of the tunable iridocytes from D. opalescens, and from the iridocytes and purified Bragg lamellae from the related squid, Lolliguncula brevis, that a phase transition from monodisperse 10-100 nm diam. spherical puncta to a gel or liquid may occur upon iridocyte activation, but these may be artifacts from fixation and staining [112, 19]. Further, expression of reflectin A1 from D. pealeii [113] and individual expression of reflectins A1, A2, B and C from D. opalescens, both in HEK 293T cells, results in spherical puncta consistent with liquid-liquid phase separation [114]. In maximally tunable iridocytes, a liquid phase transition would maximize the lamellar protein density relative to a solution of assemblies and therefore enhance the refractive index contrast resulting from activation, while maintaining a dynamic environment essential for the controlling activities of reflectin-specific kinases and phosphatases.

Decreasing the protein's NCD by phosphorylation could provide a mechanism for tuning lamellar dehydration and the consequent photonic behavior [10, 11, 18]) by controlling the dense phase protein concentration.

For ventral and dorsal mixtures of the four reflectins, decreasing protein NCD within the physiological range of 200-300 mM NaCl takes the system farther from the liquid phase boundary and deeper into the two-phase region, thus potentially increasing protein concentration in the dense phase [105]. By increasing the density of reflectin in the condensed phase this effect could thereby increase lamellar dehydration and the consequent photonic response to reduction of reflectin's NCD by phosphorylation. The finding that reflectin C increases the diffusivity of reflectin A1 in the dense phase suggests the possibility that reflectin C could act to increase the diffusivity the lamellar contents and therefore facilitate the rapid reactions that tune lamellar dehydration. The increased liquidity of reflectin A1 imposed by reflectin C could also maintain a fluid, non-arrested condensate and facilitate reversibility of lamellar dehydration. Optically active but non-tunable iridocytes are found in many cephalopod families [7, 8, 115] and the evolution of an 'off' state is what likely enables reversible tunability in iridocytes only observed in the Loliginidae family. The in vitro inhibition of LLPS of reflectins A1 and A2 by reflectins B and C, which are unique to Loliginidae, may represent this 'off' state that allows the lamellar contents to exist as a colloid of assemblies at the physiologically relevant salt concentration of ca. 250 mM. Multiphase condensates have been previously observed in living cells, most notably in the nucleoulus where rDNA transcription, rRNA processing and ribosome assembly are spatially separated into three distinct immiscible condensate compartments [98, 116]. The specific multiphase organizations of reflectins A1, A2, B and C observed in vitro have limited biological relevance in the absence of a cell membrane. Indeed, previous immune-TEM analyses revealed that reflectin C appears to be preferentially localized adjacent to the inner face of the lamellar membrane, in contrast

to reflectins A1, A2 and B that are uniformly distributed throughout the lamellar lumen [12]. Possible roles of reflectin C as a physical link between the reflectin assemblies and the membrane, or as a buffer or insulator protecting the membrane, may thus be suggested. These multiphase organizations are nonetheless valuable in deciphering the strength and hierarchies of interactions between the four protein species and therefore their roles in facilitating lamellar dehydration in iridocytes. Further, the possibility of multiphase organization of reflectin condensates within the lamellae offers the opportunity for differential phosphorylation/dephosphorylation of reflectins A1 and A2 compared to reflectin B.

Reflectin B is phosphorylated at serine and threonine residues, whereas reflectins A1 and A2 are phosphorylated primarily at tyrosine residues [12, 13], suggesting the actions of different kinases. Further, the targeted serine and threonine residues in reflectin B are contained within a motif (RRPSESH/RRPSEGH) that differs from that of the targeted tyrosine residues in reflectins A1 and A2 [12, 13], further supporting the suggestion that different, specific kinases act on the different reflectins. . Whenever in vitro multiphase separation was observed in reflectin mixtures containing reflectin B, B was always segregated from A1 and A2 (Figs. 4.8-4.10). This spatial segregation might increase the rate of phosphorylation of reflectins A1 and A2 as well as the dephosphorylation of reflectin B upon iridocyte activation, and thereby might enhance the rate of lamellar dehydration and its photonic consequences by concentrating kinases and phosphatases with their respective reflectin targets. Similar effects have been documented in other cellular systems in which LLPS of proteins can increase kinase or phosphatase activity when these enzymes co-partition into the condensate with their target proteins [51, 117, 118, 119, 120]. Additionally, multiphase separation of reflectins A1 and A2 from reflectin B could modulate the 'off' response of tunable iridocytes. Rehydration of the Bragg lamellae occurs upon removal of exogenous acetylcholine [18], suggesting constitutive dephosphorylation

of reflectins A1 and A2, concomitant with phosphorylation of reflectin B in the 'off' state [13]. Positive or negative feedback loops controlling these rates could be enhanced or disrupted by multiphase segregation and thus further contribute to the rapid tunability and reversibility of lamellar dehydration.

Because reflectin B is dephosphorylated while reflectins A1 and A2 are phorphorylated upon activation of the tunable iridocytes, and phosphorylation of reflectin C has not been detected [12, 13], simultaneous pH titration or electroreduction of mixtures of all 4 reflectins cannot recapitulate the complex changes in phosphorylation and its control of protein NCD in vivo. True dynamic recapitulation of the differential phosphorylation and dephosphorylation of reflectins A1, A2 and B thus far can only be achieved by employing and controlling reflectin-specific kinases and phosphatases.

The findings summarized above illuminate a significant extension of the remarkable tunability of the reflectin system. Reflectin A1 can be driven to liquid-liquid phase separate by changing protein net charge density and ionic strength. The phase boundary of this transition can be tuned by the addition of reflectins A2, B and C. The liquidity of reflectin condensates and their multiphase organization can similarly be tuned, presenting promise for increasing the control over the design of more complex reflectin-based tunable materials.

5.3 Future Directions

These analyses have provided a narrow window into complex multiphase behavior defined by colloidal reflectin A1 assembly and liquid-liquid phase separation. A combination of thermodynamic analyses, solution state NMR, and molecular modeling would illuminate the molecular mechanism by which increasing ionic strength drives the phase behavior of reflectin A1. Van't Hoff analyses of the saturation concentrations for re-

flectin A1 LLPS at varying temperatures would determine the entropic and enthalpic contributions of the transition of reflectin from the dilute phase to the dense phase [99] . This would begin to resolve the role of the entropic hydrophobic effect from the role of enthalpic pi-cation and salt-bridge interactions. Such analyses would need to encompass a range of pH values (protein NCDs) as well as salt concentrations as the molecular drivers likely change across these conditions. Combining this approach with solution state NMR would correlate changes in reflectin A1 structure and overlaps of chemical shifts of amino acids such as arginine and tyrosine with phase transitions [28, 47, 65]. Finally, a combination of molecular simulations and analyses of form factors of reflectin A1 assemblies would begin to distinguish between hypotheses that reflectin A1 assembly sizes are kinetically determined by the rate of dynamic arrest or are thermodynamically determined by a combination of short-range attraction and long range repulsion (SALR) [43, 121, 122, 123]. The phase behaviors of reflectins A1, A2, B and C in the Bragg lamellae and in the cellular environments of both tunable and non-tunable iridocytes from D. opalescens are currently unknown. The determination of the pH and salt concentration within the lamellae would be valuable in guiding future in vitro investigations of biologically relevant reflectin phase behavior. Cryo-EM could characterize the condensate or assembly state of reflectin within the Bragg lamellae as well as structural interactions between reflectins and the membranes of the lamellae [124, 125]. Time-resolved Cryo-EM could also be a powerful tool in characterizing physical phase transitions both in vivo [126, 127] and in vitro [128]. Super-resolution microscopy of fixed and immunostained tunable iridocytes could determine any possible multi-phase organization of reflectins within their membrane enclosures.

Chapter 6

Materials and Methods

6.1 Protein Expression and Purification

Reflectins A1, A1 C232S, A1-6E, A2, B, and C were purified as previously described (29). Codon-optimized sequences of reflectins A1, A2, B, and C were cloned into pj411 plasmids. Proteins were expressed in Rosetta 2 (DE3) cells grown in 1 or 2 liter LB cultures at 37° C from plated and sequenced transformants in the presence of 50mg/mL kanamycin. Expression was induced at OD 0.06-0.07 with 5 mM IPTG. After 16 hours, cultures were pelleted by centrifugation and frozen at -80 C. All four reflectins expressed in inclusion bodies, with similar yields for reflectins A1 and A2, and decreasingly smaller yields for C and B as judged by SDS-PAGE. Inclusion bodies were purified using Bug-Buster medium (Novagen, Inc., Madison, WI) per manufacturer protocol, then resolubilized in 8 M urea 5% acetic acid. All reflectins were purified using cation exchange with a 10mL Hitrap cation-exchange column (Cytiva, Marlborough, MA) and eluted using a step gradient of 5% acetic acid, 6 M guanidinium chloride. Reflectins A1 and A2 were loaded at 5% eluting buffer whereas reflectins B and C were loaded onto the column with no eluting buffer. All reflectins eluted at 10% eluting buffer. Purity of collected

fractions was determined by A260/A280 and SDS-PAGE, then pooled and concentrated. Concentrated reflectin was loaded onto reverse-phase HPLC waters Xbridge 4.6 mL C4 column equilibrated with 10% (reflectins A1 and A2) or 5% (reflectins B and C) acetonitrile with 0.1% trifluoroacetic acid and eluted over a gradient of 100% acetonitrile 0.1% TFA. Fractions were frozen at -80° C or shell frozen using an ethanol and dry ice bath, lyophilized, and stored at -80° C until solubilization. Purity was determined by SDS-PAGE and A260/A280. Lyophilized reflectin was solubilized using 0.22 μm-filtered acetic acid buffer (pH 4 25 mM) and dialyzed using 2 changes (12 hours each) of 1000X sample volume of the same buffer at 4C. Protein concentration was calculated using absorbance at 280 nm and molar extinction coefficients for each protein.

6.2 Bradford Assay

0.5, 1, 2, 3, 4, and 5μL of 100μM reflectin A1 in pH 4 25mM acetic acid was driven to assembly by dilution into neutralizing buffer to a total volume of 50uL and final protein concentrations of 1, 2, 4, 6, 8, and 10μM, then incubated at 20C for five days. Samples were then centrifuged at 20C 20,000g for 6 hours and a small portion of supernatant immediately removed. Supernatant was combined with Bradford dye and absorbances at 450 and 595nm recorded after 30 minutes. A serial dilution of BSA standard was used to create standard curve. All experimental data points represent averages of three experimental replicants with three measurements each.

In parallel, centrifugation was omitted, and sizes were determined by dynamic light scattering (DLS) using a Malvern Zetasizer Nano. All DLS measurements were replicated with three individual experiments, each with three technical replicates spanning 15 minutes each.

6.3 Fluorescent Labeling

Reflectin A1 C232S, A1 6E, A2, and C were covalently labeled using cysteine specific fluorescein- or rhodamine-methanethiosulfonate. 50μM proteins were incubated with 500 μM FMTS or MTSR in pH 4 25 mM AcoH with gentle orbital stirring for 4 hours RT then overnight at 4C. Reflectin B was labeled with maleimide-based Alexafluor-405 and Reflectin C labeled with maleimide-based Alexafluor-660. To ensure reflectins B and C stayed monomeric, protein was dialyzed to pH 4 25 mM acetic acid 8 M urea then dialyzed to pH 7 25 mM MOPS 8 M urea, each step over night. 50 μM proteins were incubated with 500μM malemide-based probe with gentle orbital stirring for 4 hours RT then overnight at 4C. They were then dialyzed to pH 4 25 mM acetic acid 8 M urea then pH 4 25 mM acetic acid. All Labeled reflectins were concentrated using 10K MWCO amicon spin filters, and excess label removed using the previously described HPLC method. Labeling efficiencies for FMTS and RMTS were between 70-80% and maleimide probes 100%.

6.4 FRET

For FRET dilution experiments, 100 μM Reflectin A1 and 100 μM reflectin A1 containing 5% C199-F and 5% C199-R were separately but simultaneously diluted into pH 7 25 mM MOPS to final protein concentrations of 4 μM. Fluorescently labeled reflectin A1 assemblies were then diluted 1:4 with unlabeled reflectin A1 assemblies after a time tdelay, and incubated in protein LoBind tubes at 20 C for 24 hours before measurements. Using a Cary Eclipse fluorescence spectrometer (Agilent Technologies, Australia), samples were excited at 488nm and emission spectra recorded from 510-700 nm. Each data point consists of a single measurement per three experimental replicates. For the positive

control, solutions of 100 μM A1 and 80 μM A1, 10 μM of each C199-R and C199-F in pH 4 25mM acetic acid were mixed, then assembled by dilution into neutralizing buffer. For the negative control fluorescently labeled assemblies were formed as per the experimentals but diluted 1:5 with pH 7 25 mM MOPS. All spectra are normalized to 488nm (Emmax of fluorescein).

For mixing of assemblies separately labeled with donor and acceptor fluorophores, 100 μM reflectin A1 containing 5% C199-F and 100 μM reflectin A1 containing 5% C199-R were separately but simultaneously driven to assembly by dilution into pH 7 25mM MOPS to final protein concentrations of 4 μM. After a time tdelay fluorescein labeled and rhodamine labeled A1 assemblies were mixed, and at this point treated identically to samples in the dilution experiment. For the positive control a solution of 100 μM reflectin containing both 5% C199-F and 5% C199-R was driven to assembly. The negative control mixed assemblies containing 5% C199-R with assemblies containing 5% C199-F 24 hours after assembly, and measured immediately upon mixing.

6.5 Phase Diagrams

LLPS boundaries for reflectins A1, A2, B, and C were determined using confocal microscopy. To determine the liquid-liquid phase separation boundary, 0.6 μL 100 μM reflectin containing 5% (A1), 2% (A2), or 0.5% (B,C) fluorescently labeled protein in acetic acid buffer (pH 4 25 mM acetic acid) were diluted into 9.4 μL of respective buffers to a final concentration of 4 μM, pipette mixed, and incubated for 10 minutes using 0.5 mL protein LoBind tubes. The solutions were pipetted onto cleaned glass coverslips and imaged immediately after deposition using Leica SP8 resonant confocal microscope with 63X objective (NRI-MCDB Microscopy Facility) . For protein stock solutions containing more than one reflectin type, reflectins in acetic acid buffer (pH 4 25 mM acetic acid)

were mixed in the noted ratios then diluted into respective buffers. To determine the boundary for transition from monomer to assembly, 2 μL of 100 μM reflectin in pH 4 25 mM acetic acid were diluted into 48 uL respective buffer to a final protein concentration of 4 μM and incubated as above. Sizes were determined by dynamic light scattering (DLS) using a Malvern Zetasizer Nano. All DLS measurements were replicated with three individual experiments each with three technical replicates spanning 15 minutes each. All buffers were freshly 0.22 μm-filtered before use.

6.6 Glass Coverslip Passivation

For FRAP, droplet fusion, and certain examinations of LLPS of mixtures of reflectins A1, A2, B, and C, glass coverslips were passivated to prevent reflectin from wetting the surface. Glass slides and coverslips were sonicated in near-boiling 1% Hellmanex cleaning solution for 15 minutes. After thorough rinsing with Milli-Q water, glass slides were dried with CO2 and stored with Drierite dessicant. Coverslips were immersed in 0.1M NaOH for 15 minutes, thoroughly rinsed with Milli-Q water, then dried with CO2. They were then heated to 100C in closed glass Petri dishes containing Drierite for 10 minutes, after which 20uL of 1% methoxy-PEG silane was pipetted onto each 18X18mm coverslip and incubated for 20 minutes at 100C. After allowing to cool, coverslips were thoroughly rinsed, sonicated in Milli-Q water for 10 minutes, and rinsed again. After drying with CO2, glass chamber microscope slides were constructed using two strips of Scotch double sided tape to secure the coverslip against the slide.

6.7 FRAP Experiments and Analysis

100μM partially fluorescently labeled reflectin (A1: 5% C199-F, A2: 2% A2-rhodamine sulfate, B: 0.5% Alexafluor 405, C: 5% C-F or 1% Alexafluor 660) was diluted into respective high ionic strength buffers, then quickly pipetted into passivated chamber slides which were sealed with fast drying clear nail polish. Using the FRAP module in a Leica SP8 scanning confocal microscope, a 1μm diameter circular ROI ("point ROI" in software) was selectively photobleached at 45-50% laser power for 150-200ms to avoid heating the droplet. Concentrations of fluorophores for all four reflectins were chosen such that they could be bleached with similar settings. FRAP was compared for Alexafluor-660 and fluorescein labeled reflectin C to ensure slight difference in bleaching settings did not effect data. The bleached ROI was monitored for 10s before bleaching, and for 5-25 minutes post bleaching. For data analysis, the fluorescence intensity of the bleached region, an unbleached region in the droplet, and background were used to correct for photobleaching:

$$F_{corrected}(t) = \frac{F_{raw} - F_{background}}{F_{nonbleached} - F_{background}}$$

then fully normalized using the equation:

$$I_{norm} = \frac{(I_{bleach})_t - (I_{bleach})_0}{(I_{bleach})_{pre} - (I_{bleach})_0}$$

where $(I_{bleach})_t$ is the intensity of the photobleached region at time t

$(I_{bleach})_0$ is the intensity of the photobleached region at the time of photobleaching

$(I_{bleach})_{pre}$ is the intensity of the photobleached region prior to photobleaching. To determine the characteristic relaxation time τ data was fit to the equation:

$$y = A_1(1 - e^{-\tau_1 t}) + B_1(1 - e^{-\tau_2 t})$$

using NonLinearRegression function in Mathematica

6.8 Droplet Fusion Analysis

Frame rates and resolutions varied greatly due to the wide range of relaxation times across reflectin species and conditions. Reflectin protein and slides were prepared as described for FRAP, and imaging occurred immediately after chamber slide was prepared. Only fusion events of equally sized droplets were analyzed. Using Fiji ImageJ software, the threshold function was used to create binary videos. Aspect ratios were calculated by using the "Fit Ellipse" measurement in "Analyze Particles". Using NonLinearRegression function in Wolfram Mathematica, the change in aspect ratio over time was fit to the equation:

$$A.R. = 1 + (A.R._0 - 1) \cdot exp(-t/\tau)$$

where A.R.$_0$ is the intial aspect ratio, t is the time, and τ is the characteristic relaxation time.

Appendix A

Supplemental Figures

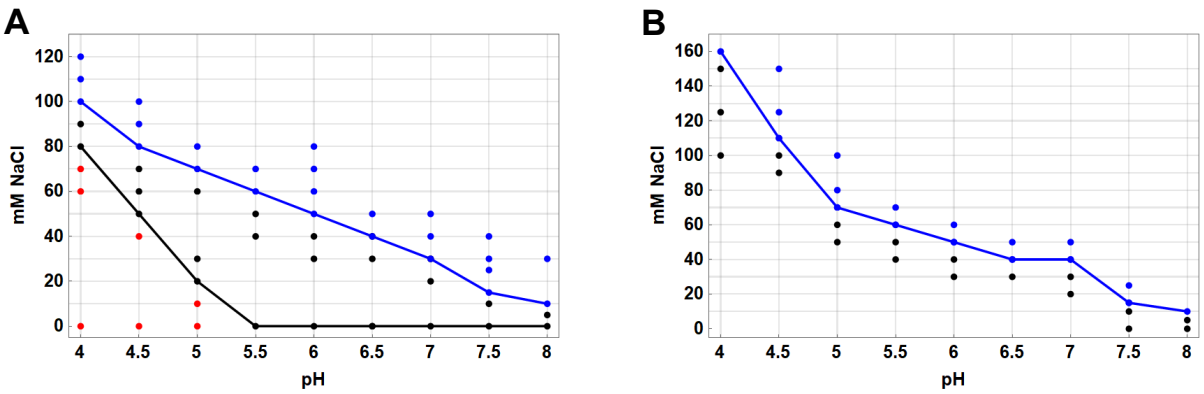

Figure A.1: Phase diagrams of (A) reflectin A1 and (B) reflectin A2 as functions of NaCl concentration and pH. Blue points denote the presence of droplets as detected by confocal microscopy and black points the absence of droplets. Red points denote monomer as determined by DLS. For (A) black points at pH 4-5.5 and black line denote assemblies as characterized by DLS. 100 μM stock protein concentration was diluted to final protein concentration of 4 μM in respective buffers.

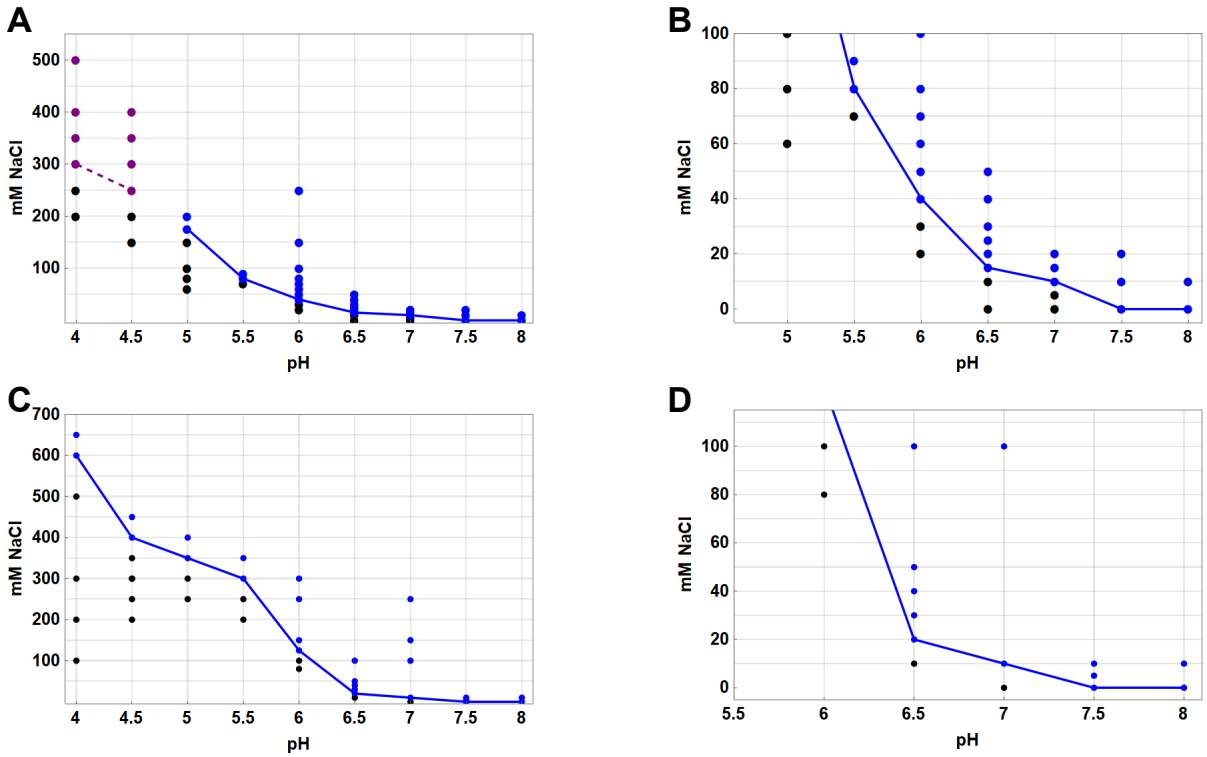

Figure A.2: Phase diagrams of (A) reflectin B and (B) zoom-in of reflectin B phase diagram for high pH values, as well as (C) reflectin C and (D) zoom-in of reflectin C phase diagram for high pH values. Black points denote the presence of droplets as detected by confocal microscopy and black points the absence of droplets. 100 μM stock protein concentration was diluted to final protein concentration of 4 μM in respective buffers.

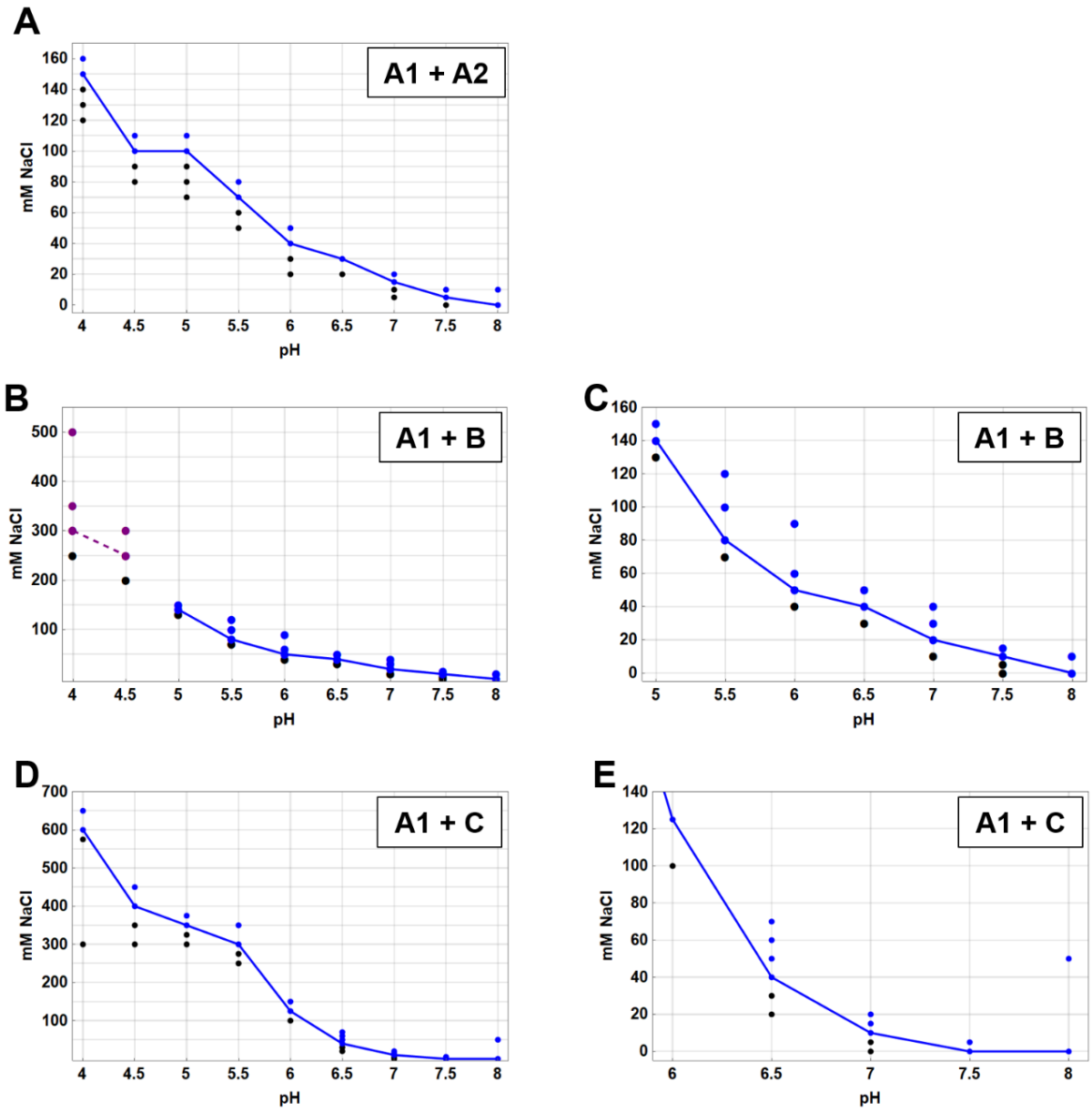

Figure A.3: Phase diagrams of mixtures of (A) reflectin A1 and A2, (B,C) reflectin A1 and B, (D,E) reflectin A1 and C. Black points denote the presence of droplets as detected by confocal microscopy and black points the absence of droplets. 100 μM stock protein concentration was diluted to final protein concentration of 4 μM in respective buffers.

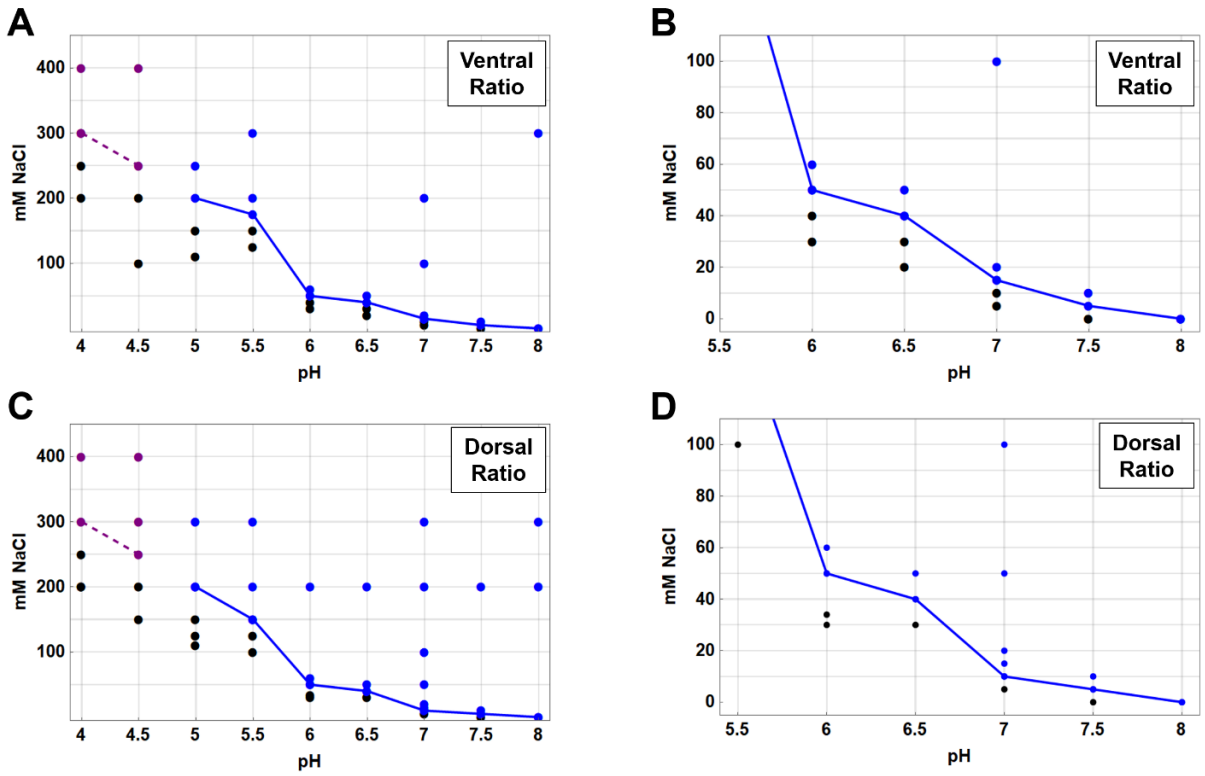

Figure A.4: Phase diagrams of mixtures of reflectins A1, A2, B and C in the (A, B) dorsal molar ratio and (C, D) ventral molar ratio. Black points denote the presence of droplets as detected by confocal microscopy and black points the absence of droplets. 100 μM stock protein concentration was diluted to final protein concentration of 4 μM in respective buffers.

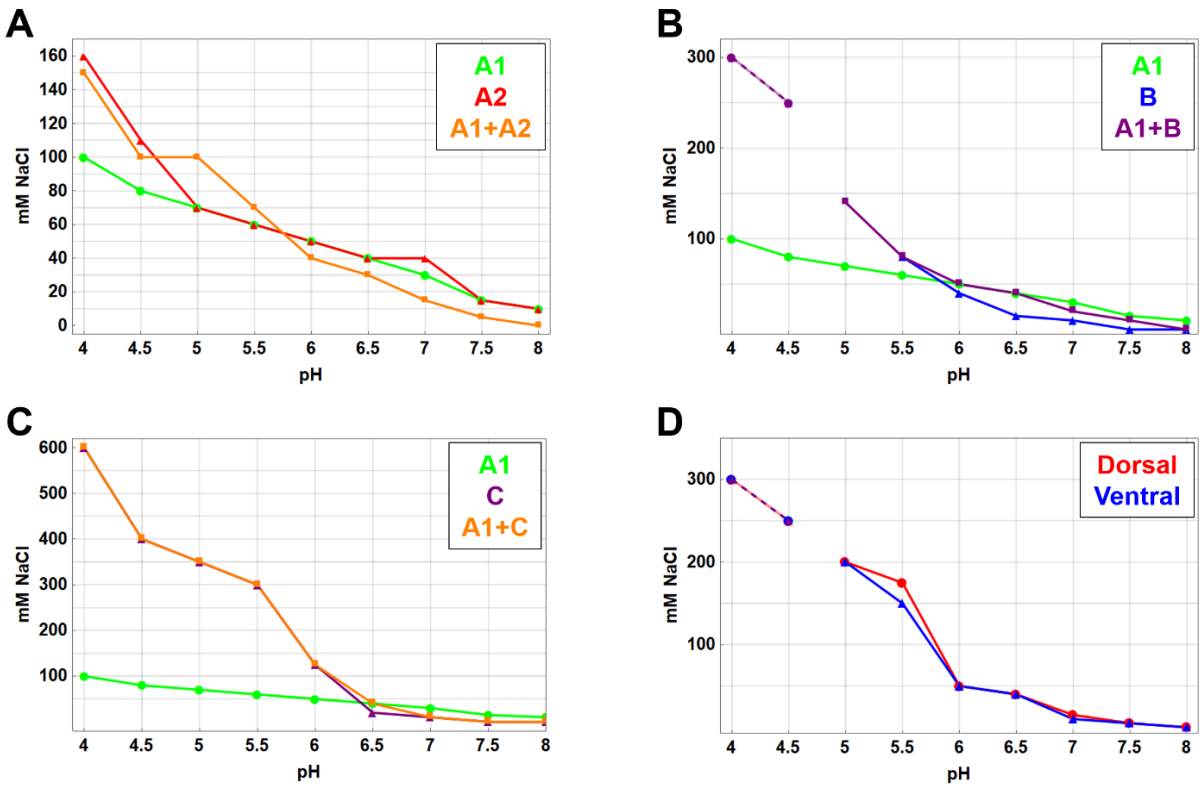

Figure A.5: Phase diagrams of (A) reflectin B and (B) zoom-in of reflectin B phase diagram for high pH values, as well as (C) reflectin C and (D) zoom-in of reflectin C phase diagram for high pH values. Black points denote the presence of droplets as detected by confocal microscopy and black points the absence of droplets. 100 μM stock protein concentration was diluted to final protein concentration of 4 μM in respective buffers.

Bibliography

[1] R. A. Cloney and S. L. Brocco, *Chromatophore Organs, Reflector Cells, Iridocytes and Leucophores in Cephalopods*, *American Zoologist* **23** (Aug., 1983) 581–592.

[2] T. L. Williams, S. L. Senft, J. Yeo, F. J. Martín-Martínez, A. M. Kuzirian, C. A. Martin, C. W. DiBona, C.-T. Chen, S. R. Dinneen, H. T. Nguyen, C. M. Gomes, J. J. C. Rosenthal, M. D. MacManes, F. Chu, M. J. Buehler, R. T. Hanlon, and L. F. Deravi, *Dynamic pigmentary and structural coloration within cephalopod chromatophore organs*, *Nature Communications* **10** (Dec., 2019) 1004.

[3] L. F. Deravi, A. P. Magyar, S. P. Sheehy, G. R. R. Bell, L. M. Mäthger, S. L. Senft, T. J. Wardill, W. S. Lane, A. M. Kuzirian, R. T. Hanlon, E. L. Hu, and K. K. Parker, *The structure–function relationships of a natural nanoscale photonic device in cuttlefish chromatophores*, *Journal of The Royal Society Interface* **11** (Apr., 2014) 20130942.

[4] L. M. Mathger, N. Shashar, and R. T. Hanlon, *Do cephalopods communicate using polarized light reflections from their skin?*, *Journal of Experimental Biology* **212** (July, 2009) 2133–2140.

[5] D. G. DeMartini, A. Ghoshal, E. Pandolfi, A. T. Weaver, M. Baum, and D. E. Morse, *Dynamic biophotonics: female squid exhibit sexually dimorphic tunable leucophores and iridocytes*, *Journal of Experimental Biology* **216** (Oct., 2013) 3733–3741.

[6] L. M. Mäthger, S. L. Senft, M. Gao, S. Karaveli, G. R. R. Bell, R. Zia, A. M. Kuzirian, P. B. Dennis, W. J. Crookes-Goodson, R. R. Naik, G. W. Kattawar, and R. T. Hanlon, *Bright White Scattering from Protein Spheres in Color Changing, Flexible Cuttlefish Skin*, *Advanced Functional Materials* **23** (Aug., 2013) 3980–3989.

[7] S. Brocco and R. Cloney, *Reflector cells in the skin of Octopus dofleini*, *Cell and Tissue Research* **205** (Feb., 1980).

[8] L. M. Mathger, G. R. R. Bell, A. M. Kuzirian, J. J. Allen, and R. T. Hanlon, *How does the blue-ringed octopus (Hapalochlaena lunulata) flash its blue rings?*, *Journal of Experimental Biology* **215** (Nov., 2012) 3752–3757.

[9] A. R. Tao, D. G. DeMartini, M. Izumi, A. M. Sweeney, A. L. Holt, and D. E. Morse, *The role of protein assembly in dynamically tunable bio-optical tissues*, *Biomaterials* **31** (Feb., 2010) 793–801.

[10] A. Ghoshal, D. G. DeMartini, E. Eck, and D. E. Morse, *Optical parameters of the tunable Bragg reflectors in squid*, *Journal of The Royal Society Interface* **10** (June, 2013) 20130386–20130386.

[11] A. Ghoshal, D. G. DeMartini, E. Eck, and D. E. Morse, *Experimental determination of refractive index of condensed reflectin in squid iridocytes*, *Journal of The Royal Society Interface* **11** (Apr., 2014) 20140106–20140106.

[12] D. G. DeMartini, M. Izumi, A. T. Weaver, E. Pandolfi, and D. E. Morse, *Structures, Organization, and Function of Reflectin Proteins in Dynamically Tunable Reflective Cells*, *Journal of Biological Chemistry* **290** (June, 2015) 15238–15249.

[13] M. Izumi, A. M. Sweeney, D. DeMartini, J. C. Weaver, M. L. Powers, A. Tao, T. V. Silvas, R. M. Kramer, W. J. Crookes-Goodson, L. M. Mäthger, R. R. Naik, R. T. Hanlon, and D. E. Morse, *Changes in reflectin protein phosphorylation are associated with dynamic iridescence in squid*, *Journal of The Royal Society Interface* **7** (Mar., 2010) 549–560.

[14] R. T. Hanlon, K. M. Cooper, B. U. Budelmann, and T. C. Pappas, *Physiological color change in squid iridophores*, *Cell and Tissue Research* (1990), no. 259 3–14.

[15] T. J. Wardill, P. T. Gonzalez-Bellido, R. J. Crook, and R. T. Hanlon, *Neural control of tuneable skin iridescence in squid*, *Proc. R. Soc. B* **279** (Oct., 2012) 4243–4252.

[16] P. T. Gonzalez-Bellido, T. J. Wardill, K. C. Buresch, K. M. Ulmer, and R. T. Hanlon, *Expression of squid iridescence depends on environmental luminance and peripheral ganglion control*, *Journal of Experimental Biology* **217** (Mar., 2014) 850–858.

[17] L. M. Mathger, *The role of muscarinic receptors and intracellular Ca2+ in the spectral reflectivity changes of squid iridophores*, *Journal of Experimental Biology* **207** (May, 2004) 1759–1769.

[18] D. G. DeMartini, D. V. Krogstad, and D. E. Morse, *Membrane invaginations facilitate reversible water flux driving tunable iridescence in a dynamic biophotonic system*, *Proceedings of the National Academy of Sciences* **110** (Feb., 2013) 2552–2556.

[19] D. E. Morse and E. Taxon, *Reflectin needs its intensity amplifier: Realizing the potential of tunable structural biophotonics*, *Applied Physics Letters* **117** (Nov., 2020) 220501.

[20] W. J. Crookes, *Reflectins: The Unusual Proteins of Squid Reflective Tissues*, *Science* **303** (Jan., 2004) 235–238.

[21] R. Levenson, D. G. DeMartini, and D. E. Morse, *Molecular mechanism of reflectin's tunable biophotonic control: Opportunities and limitations for new optoelectronics*, *APL Materials* **5** (2017), no. 10 104801.

[22] R. Levenson, C. Bracken, N. Bush, and D. E. Morse, *Cyclable Condensation and Hierarchical Assembly of Metastable Reflectin Proteins, the Drivers of Tunable Biophotonics*, *Journal of Biological Chemistry* **291** (Feb., 2016) 4058–4068.

[23] J. Wang, J.-M. Choi, A. S. Holehouse, H. O. Lee, X. Zhang, M. Jahnel, S. Maharana, R. Lemaitre, A. Pozniakovsky, D. Drechsel, I. Poser, R. V. Pappu, S. Alberti, and A. A. Hyman, *A Molecular Grammar Governing the Driving Forces for Phase Separation of Prion-like RNA Binding Proteins*, *Cell* **174** (July, 2018) 688–699.e16.

[24] R. V. Pappu, S. R. Cohen, F. Dar, M. Farag, and M. Kar, *Phase Transitions of Associative Biomacromolecules*, *Chemical Reviews* (Mar., 2023) acs.chemrev.2c00814.

[25] C. C. Valley, A. Cembran, J. D. Perlmutter, A. K. Lewis, N. P. Labello, J. Gao, and J. N. Sachs, *The Methionine-aromatic Motif Plays a Unique Role in Stabilizing Protein Structure*, *Journal of Biological Chemistry* **287** (Oct., 2012) 34979–34991.

[26] E. A. Orabi and A. M. English, *Modeling Protein S–Aromatic Motifs Reveals Their Structural and Redox Flexibility*, *The Journal of Physical Chemistry B* **122** (Apr., 2018) 3760–3770.

[27] C. R. Forbes, S. K. Sinha, H. K. Ganguly, S. Bai, G. P. A. Yap, S. Patel, and N. J. Zondlo, *Insights into Thiol–Aromatic Interactions: A Stereoelectronic Basis for S–H/ Interactions*, *Journal of the American Chemical Society* **139** (Feb., 2017) 1842–1855.

[28] M. J. Umerani, P. Pratakshya, A. Chatterjee, J. A. Cerna Sanchez, H. S. Kim, G. Ilc, M. Kovačič, C. Magnan, B. Marmiroli, B. Sartori, A. L. Kwansa, H. Orins, A. W. Bartlett, E. M. Leung, Z. Feng, K. L. Naughton, B. Norton-Baker, L. Phan, J. Long, A. Allevato, J. E. Leal-Cruz, Q. Lin, P. Baldi, S. Bernstorff, J. Plavec, Y. G. Yingling, and A. A. Gorodetsky, *Structure, self-assembly, and properties of a truncated reflectin variant*, *Proceedings of the National Academy of Sciences* (Dec., 2020) 202009044.

[29] R. Levenson, C. Bracken, C. Sharma, J. Santos, C. Arata, B. Malady, and D. E. Morse, *Calibration between trigger and color: Neutralization of a genetically encoded coulombic switch and dynamic arrest precisely tune reflectin assembly*, *Journal of Biological Chemistry* **294** (Nov., 2019) 16804–16815.

[30] R. Levenson, B. Malady, T. Lee, Y. A. Sabeh, P. Kohl, Y. Li, and D. E. Morse, *Protein Charge Neutralization is the Proximate Driver Dynamically Tuning a Nanoscale Bragg Reflector*, *BioRxiv* (Apr., 2021) 9.

[31] Z. Guan, T. Cai, Z. Liu, Y. Dou, X. Hu, P. Zhang, X. Sun, H. Li, Y. Kuang, Q. Zhai, H. Ruan, X. Li, Z. Li, Q. Zhu, J. Mai, Q. Wang, L. Lai, J. Ji, H. Liu, B. Xia, T. Jiang, S.-J. Luo, H.-W. Wang, and C. Xie, *Origin of the Reflectin Gene and Hierarchical Assembly of Its Protein*, *Current Biology* **27** (Sept., 2017) 2833–2842.e6.

[32] S.-P. Liang, R. Levenson, B. Malady, M. J. Gordon, D. E. Morse, and L. Sepunaru, *Electrochemistry as a surrogate for protein phosphorylation: voltage-controlled assembly of reflectin A1*, *Journal of The Royal Society Interface* **17** (Dec., 2020) 20200774.

[33] Y.-C. Lin, E. Masquelier, Y. Al Sabeh, L. Sepunaru, M. J. Gordon, and D. E. Morse, *Voltage-calibrated, finely tunable protein assembly*, *Journal of The Royal Society Interface* **20** (July, 2023) 20230183.

[34] R. M. Kramer, W. J. Crookes-Goodson, and R. R. Naik, *The self-organizing properties of squid reflectin protein*, *Nature Materials* **6** (July, 2007) 533–538.

[35] C. Xu, G. T. Stiubianu, and A. A. Gorodetsky, *Adaptive infrared-reflecting systems inspired by cephalopods*, *Science* **359** (Mar., 2018) 1495–1500.

[36] D. D. Ordinario, L. Phan, W. G. Walkup IV, J.-M. Jocson, E. Karshalev, N. Hüsken, and A. A. Gorodetsky, *Bulk protonic conductivity in a cephalopod structural protein*, *Nature Chemistry* **6** (June, 2014) 596–602.

[37] D. D. Ordinario, E. M. Leung, L. Phan, R. Kautz, W. K. Lee, M. Naeim, J. P. Kerr, M. J. Aquino, P. E. Sheehan, and A. A. Gorodetsky, *Protochromic Devices from a Cephalopod Structural Protein*, *Advanced Optical Materials* (Aug., 2017) 1600751.

[38] O. Gliko, W. Pan, P. Katsonis, N. Neumaier, O. Galkin, S. Weinkauf, and P. G. Vekilov, *Metastable Liquid Clusters in Super- and Undersaturated Protein Solutions*, *The Journal of Physical Chemistry B* **111** (Mar., 2007) 3106–3114.

[39] F. Sciortino, S. Mossa, E. Zaccarelli, and P. Tartaglia, *Equilibrium Cluster Phases and Low-Density Arrested Disordered States: The Role of Short-Range Attraction and Long-Range Repulsion*, *Physical Review Letters* **93** (July, 2004) 055701.

[40] T. Gibaud and P. Schurtenberger, *A closer look at arrested spinodal decomposition in protein solutions*, *Journal of Physics: Condensed Matter* **21** (Aug., 2009) 322201.

[41] J. C. F. Toledano, F. Sciortino, and E. Zaccarelli, *Colloidal systems with competing interactions: from an arrested repulsive cluster phase to a gel*, *Soft Matter* **5** (2009), no. 12 2390. arXiv: 0903.2929.

[42] R. P. Sear, *Phase separation of equilibrium polymers of proteins in living cells*, *Faraday Discussions* **139** (2008) 21.

[43] A. Stradner, G. M. Thurston, and P. Schurtenberger, *Tuning short-range attractions in protein solutions: from attractive glasses to equilibrium clusters*, *Journal of Physics: Condensed Matter* **17** (Aug., 2005) S2805–S2816.

[44] M. Kar, F. Dar, T. J. Welsh, L. Vogel, R. Kühnemuth, A. Majumdar, G. Krainer, T. M. Franzmann, S. Alberti, C. A. M. Seidel, T. P. Knowles, A. A. Hyman, and R. V. Pappu, *Phase separating RNA binding proteins form heterogeneous distributions of clusters in subsaturated solutions*, preprint, Biophysics, Feb., 2022.

[45] A. Veis, *A review of the early development of the thermodynamics of the complex coacervation phase separation*, *Advances in Colloid and Interface Science* **167** (Sept., 2011) 2–11.

[46] A. E. Posey, A. S. Holehouse, and R. V. Pappu, *Phase Separation of Intrinsically Disordered Proteins*, in *Methods in Enzymology*, vol. 611, pp. 1–30. Elsevier, 2018.

[47] A. Abyzov, M. Blackledge, and M. Zweckstetter, *Conformational Dynamics of Intrinsically Disordered Proteins Regulate Biomolecular Condensate Chemistry*, *Chemical Reviews* **122** (Mar., 2022) 6719–6748.

[48] R. van der Lee, M. Buljan, B. Lang, R. J. Weatheritt, G. W. Daughdrill, A. K. Dunker, M. Fuxreiter, J. Gough, J. Gsponer, D. T. Jones, P. M. Kim, R. W. Kriwacki, C. J. Oldfield, R. V. Pappu, P. Tompa, V. N. Uversky, P. E. Wright, and M. M. Babu, *Classification of Intrinsically Disordered Regions and Proteins*, *Chemical Reviews* **114** (July, 2014) 6589–6631.

[49] Y. Shin and C. P. Brangwynne, *Liquid phase condensation in cell physiology and disease*, *Science* **357** (Sept., 2017) eaaf4382.

[50] A. K. Rai, J.-X. Chen, M. Selbach, and L. Pelkmans, *Kinase-controlled phase transition of membraneless organelles in mitosis*, *Nature* **559** (July, 2018) 211–216.

[51] J. Söding, D. Zwicker, S. Sohrabi-Jahromi, M. Boehning, and J. Kirschbaum, *Mechanisms for Active Regulation of Biomolecular Condensates*, *Trends in Cell Biology* **30** (Jan., 2020) 4–14.

[52] S. Alberti, *Phase separation in biology*, *Current Biology* **27** (Oct., 2017) R1097–R1102.

[53] S. Jain, J. Wheeler, R. Walters, A. Agrawal, A. Barsic, and R. Parker, *ATPase-Modulated Stress Granules Contain a Diverse Proteome and Substructure*, *Cell* **164** (Jan., 2016) 487–498.

[54] S. Elbaum-Garfinkle, Y. Kim, K. Szczepaniak, C. C.-H. Chen, C. R. Eckmann, S. Myong, and C. P. Brangwynne, *The disordered P granule protein LAF-1 drives phase separation into droplets with tunable viscosity and dynamics*, *Proceedings of the National Academy of Sciences* **112** (June, 2015) 7189–7194.

[55] X. Su, J. A. Ditlev, E. Hui, W. Xing, S. Banjade, J. Okrut, D. S. King, J. Taunton, M. K. Rosen, and R. D. Vale, *Phase separation of signaling molecules promotes T cell receptor signal transduction*, *Science* **352** (Apr., 2016) 595–599.

[56] S. Alberti and A. A. Hyman, *Biomolecular condensates at the nexus of cellular stress, protein aggregation disease and ageing*, *Nature Reviews Molecular Cell Biology* **22** (Mar., 2021) 196–213.

[57] S. Wegmann, B. Eftekharzadeh, K. Tepper, K. M. Zoltowska, R. E. Bennett, S. Dujardin, P. R. Laskowski, D. MacKenzie, T. Kamath, C. Commins, C. Vanderburg, A. D. Roe, Z. Fan, A. M. Molliex, A. Hernandez-Vega, D. Muller, A. A. Hyman, E. Mandelkow, J. P. Taylor, and B. T. Hyman, *Tau protein liquid–liquid phase separation can initiate tau aggregation*, *The EMBO Journal* **37** (Apr., 2018).

[58] T. Murakami, S. Qamar, J. Lin, G. Schierle, E. Rees, A. Miyashita, A. Costa, R. Dodd, F. Chan, C. Michel, D. Kronenberg-Versteeg, Y. Li, S.-P. Yang, Y. Wakutani, W. Meadows, R. Ferry, L. Dong, G. Tartaglia, G. Favrin, W.-L. Lin, D. Dickson, M. Zhen, D. Ron, G. Schmitt-Ulms, P. Fraser, N. Shneider, C. Holt, M. Vendruscolo, C. Kaminski, and P. St George-Hyslop, *ALS/FTD Mutation-Induced Phase Transition of FUS Liquid Droplets and Reversible Hydrogels into Irreversible Hydrogels Impairs RNP Granule Function*, *Neuron* **88** (Nov., 2015) 678–690.

[59] F. Kametani and M. Hasegawa, *Reconsideration of Amyloid Hypothesis and Tau Hypothesis in Alzheimer's Disease*, *Frontiers in Neuroscience* **12** (Jan., 2018) 25.

[60] T. Nott, E. Petsalaki, P. Farber, D. Jervis, E. Fussner, A. Plochowietz, T. D. Craggs, D. Bazett-Jones, T. Pawson, J. Forman-Kay, and A. Baldwin, *Phase Transition of a Disordered Nuage Protein Generates Environmentally Responsive Membraneless Organelles*, *Molecular Cell* **57** (Mar., 2015) 936–947.

[61] C. P. Brangwynne, P. Tompa, and R. V. Pappu, *Polymer physics of intracellular phase transitions*, *Nature Physics* **11** (Nov., 2015) nphys3532.

[62] A. S. Holehouse, G. M. Ginell, D. Griffith, and E. Böke, *Clustering of Aromatic Residues in Prion-like Domains Can Tune the Formation, State, and Organization of Biomolecular Condensates: Published as part of the Biochemistry virtual special issue "Protein Condensates"*, *Biochemistry* **60** (Nov., 2021) 3566–3581.

[63] E. W. Martin, A. S. Holehouse, I. Peran, M. Farag, J. J. Incicco, A. Bremer, C. R. Grace, A. Soranno, R. V. Pappu, and T. Mittag, *Valence and patterning of aromatic residues determine the phase behavior of prion-like domains*, *Science* **367** (Feb., 2020) 694–699.

[64] A. Ghosh and H. Zhou, *Determinants for Fusion Speed of Biomolecular Droplets*, *Angewandte Chemie International Edition* **59** (Nov., 2020) 20837–20840.

[65] J. P. Brady, P. J. Farber, A. Sekhar, Y.-H. Lin, R. Huang, A. Bah, T. J. Nott, H. S. Chan, A. J. Baldwin, J. D. Forman-Kay, and L. E. Kay, *Structural and hydrodynamic properties of an intrinsically disordered region of a germ cell-specific protein on phase separation*, *Proceedings of the National Academy of Sciences* **114** (Sept., 2017) E8194–E8203.

[66] T. Wunder, S. L. H. Cheng, S.-K. Lai, H.-Y. Li, and O. Mueller-Cajar, *The phase separation underlying the pyrenoid-based microalgal Rubisco supercharger*, *Nature Communications* **9** (Dec., 2018).

[67] B. S. Schuster, E. H. Reed, R. Parthasarathy, C. N. Jahnke, R. M. Caldwell, J. G. Bermudez, H. Ramage, M. C. Good, and D. A. Hammer, *Controllable protein phase separation and modular recruitment to form responsive membraneless organelles*, *Nature Communications* **9** (Dec., 2018) 2985.

[68] J. E. Kohn, I. S. Millett, J. Jacob, B. Zagrovic, T. M. Dillon, N. Cingel, R. S. Dothager, S. Seifert, P. Thiyagarajan, T. R. Sosnick, M. Z. Hasan, V. S. Pande, I. Ruczinski, S. Doniach, and K. W. Plaxco, *Random-coil behavior and the dimensions of chemically unfolded proteins*, *Proceedings of the National Academy of Sciences* **101** (Aug., 2004) 12491–12496.

[69] N. C. Fitzkee and G. D. Rose, *Reassessing random-coil statistics in unfolded proteins*, *Proceedings of the National Academy of Sciences* **101** (Aug., 2004) 12497–12502.

[70] A. Chin, D. Toptygin, W. Elam, T. Schrank, and V. Hilser, *Phosphorylation Increases Persistence Length and End-to-End Distance of a Segment of Tau Protein*, *Biophysical Journal* **110** (Jan., 2016) 362–371.

[71] I. Alshareedah, T. Kaur, J. Ngo, H. Seppala, L.-A. D. Kounatse, W. Wang, M. M. Moosa, and P. R. Banerjee, *Interplay between Short-Range Attraction and Long-Range Repulsion Controls Reentrant Liquid Condensation of*

Ribonucleoprotein–RNA Complexes, *Journal of the American Chemical Society* **141** (Sept., 2019) 14593–14602.

[72] A. Patel, H. Lee, L. Jawerth, S. Maharana, M. Jahnel, M. Hein, S. Stoynov, J. Mahamid, S. Saha, T. Franzmann, A. Pozniakovski, I. Poser, N. Maghelli, L. Royer, M. Weigert, E. Myers, S. Grill, D. Drechsel, A. Hyman, and S. Alberti, *A Liquid-to-Solid Phase Transition of the ALS Protein FUS Accelerated by Disease Mutation*, *Cell* **162** (Aug., 2015) 1066–1077.

[73] F. Zhang, F. Roosen-Runge, A. Sauter, M. Wolf, R. M. J. Jacobs, and F. Schreiber, *Reentrant condensation, liquid–liquid phase separation and crystallization in protein solutions induced by multivalent metal ions*, *Pure and Applied Chemistry* **86** (Feb., 2014) 191–202.

[74] S. Ranganathan and E. I. Shakhnovich, *Dynamic metastable long-living droplets formed by sticker-spacer proteins*, *eLife* **9** (June, 2020) e56159.

[75] P. Segrè, V. Prasad, A. Schofield, and D. Weitz, *Glasslike Kinetic Arrest at the Colloidal-Gelation Transition*, *Physical Review Letters* **86** (June, 2001) 6042–6045.

[76] J. Hansen, C. J. Moll, L. López Flores, R. Castañeda-Priego, M. Medina-Noyola, S. U. Egelhaaf, and F. Platten, *Phase separation and dynamical arrest of protein solutions dominated by short-range attractions*, *The Journal of Chemical Physics* **158** (Jan., 2023) 024904.

[77] G. Krainer, T. J. Welsh, J. A. Joseph, J. R. Espinosa, S. Wittmann, E. de Csilléry, A. Sridhar, Z. Toprakcioglu, G. Gudiškytė, M. A. Czekalska, W. E. Arter, J. Guillén-Boixet, T. M. Franzmann, S. Qamar, P. S. George-Hyslop, A. A. Hyman, R. Collepardo-Guevara, S. Alberti, and T. P. J. Knowles, *Reentrant liquid condensate phase of proteins is stabilized by hydrophobic and non-ionic interactions*, *Nature Communications* **12** (Dec., 2021) 1085.

[78] S. Kim, A. Faghihnejad, Y. Lee, Y. Jho, H. Zeng, and D. S. Hwang, *Cation–interaction in DOPA-deficient mussel adhesive protein mfp-1*, *Journal of Materials Chemistry B* **3** (2015), no. 5 738–743.

[79] M. V. Rapp, G. P. Maier, H. A. Dobbs, N. J. Higdon, J. H. Waite, A. Butler, and J. N. Israelachvili, *Defining the Catechol–Cation Synergy for Enhanced Wet Adhesion to Mineral Surfaces*, *Journal of the American Chemical Society* **138** (July, 2016) 9013–9016.

[80] N. A. Yewdall, A. A. André, T. Lu, and E. Spruijt, *Coacervates as models of membraneless organelles*, *Current Opinion in Colloid & Interface Science* **52** (Apr., 2021) 101416.

[81] S. Das, Y.-H. Lin, R. M. Vernon, J. D. Forman-Kay, and H. S. Chan, *Comparative roles of charge, , and hydrophobic interactions in sequence-dependent phase separation of intrinsically disordered proteins*, *Proceedings of the National Academy of Sciences* **117** (Nov., 2020) 28795–28805.

[82] P. W. Atkins and J. De Paula, *Physical chemistry*. W.H. Freeman, New York, 9th ed ed., 2010.

[83] J. Qi, D. Liu, X. Liu, S. Guan, F. Shi, H. Chang, H. He, and G. Yang, *Fluorescent pH Sensors for Broad-Range pH Measurement Based on a Single Fluorophore*, *Analytical Chemistry* **87** (June, 2015) 5897–5904.

[84] A. N. Kapanidis and S. Weiss, *Fluorescent probes and bioconjugation chemistries for single-molecule fluorescence analysis of biomolecules*, *The Journal of Chemical Physics* **117** (Dec., 2002) 10953–10964.

[85] Y. Lin, Y. Fichou, A. P. Longhini, L. C. Llanes, P. Yin, G. C. Bazan, K. S. Kosik, and S. Han, *Liquid-Liquid Phase Separation of Tau Driven by Hydrophobic Interaction Facilitates Fibrillization of Tau*, *Journal of Molecular Biology* **433** (Jan., 2021) 166731.

[86] S. Boyko, X. Qi, T.-H. Chen, K. Surewicz, and W. K. Surewicz, *Liquid–liquid phase separation of tau protein: The crucial role of electrostatic interactions*, *Journal of Biological Chemistry* **294** (July, 2019) 11054–11059.

[87] A. L. Lehninger, D. L. Nelson, and M. M. Cox, *Lehninger principles of biochemistry*. W.H. Freeman, New York, 5th ed ed., 2008.

[88] T. Creighton, *Proteins: Structures and molecular properties*. W.H. Freeman & Company, a Macmillan Education Imprint, 2 ed., 1993.

[89] P. C. Bressloff, *Active suppression of Ostwald ripening: Beyond mean-field theory*, *Physical Review E* **101** (Apr., 2020) 042804.

[90] D. Zwicker, A. A. Hyman, and F. Jülicher, *Suppression of Ostwald ripening in active emulsions*, *Physical Review E* **92** (July, 2015) 012317.

[91] T. M. Franzmann, M. Jahnel, A. Pozniakovsky, J. Mahamid, A. S. Holehouse, E. Nüske, D. Richter, W. Baumeister, S. W. Grill, R. V. Pappu, A. A. Hyman, and S. Alberti, *Phase separation of a yeast prion protein promotes cellular fitness*, *Science* **359** (Jan., 2018) eaao5654.

[92] K. Burke, A. Janke, C. Rhine, and N. Fawzi, *Residue-by-Residue View of In Vitro FUS Granules that Bind the C-Terminal Domain of RNA Polymerase II*, *Molecular Cell* **60** (Oct., 2015) 231–241.

[93] L. Pytowski, C. F. Lee, A. C. Foley, D. J. Vaux, and L. Jean, *Liquid–liquid phase separation of type II diabetes-associated IAPP initiates hydrogelation and aggregation*, *Proceedings of the National Academy of Sciences* (May, 2020) 201916716.

[94] D. W. Sanders, N. Kedersha, D. S. Lee, A. R. Strom, V. Drake, J. A. Riback, D. Bracha, J. M. Eeftens, A. Iwanicki, A. Wang, M.-T. Wei, G. Whitney, S. M. Lyons, P. Anderson, W. M. Jacobs, P. Ivanov, and C. P. Brangwynne, *Competing Protein-RNA Interaction Networks Control Multiphase Intracellular Organization*, *Cell* **181** (Apr., 2020) 306–324.e28.

[95] K. T. Delaney and G. H. Fredrickson, *Theory of polyelectrolyte complexation—Complex coacervates are self-coacervates*, *The Journal of Chemical Physics* **146** (June, 2017) 224902.

[96] J. A. Riback, L. Zhu, M. C. Ferrolino, M. Tolbert, D. M. Mitrea, D. W. Sanders, M.-T. Wei, R. W. Kriwacki, and C. P. Brangwynne, *Composition-dependent thermodynamics of intracellular phase separation*, *Nature* **581** (May, 2020) 209–214.

[97] J. B. Woodruff, B. Ferreira Gomes, P. O. Widlund, J. Mahamid, A. Honigmann, and A. A. Hyman, *The Centrosome Is a Selective Condensate that Nucleates Microtubules by Concentrating Tubulin*, *Cell* **169** (June, 2017) 1066–1077.e10.

[98] M. Feric, N. Vaidya, T. S. Harmon, D. M. Mitrea, L. Zhu, T. M. Richardson, R. W. Kriwacki, R. V. Pappu, and C. P. Brangwynne, *Coexisting Liquid Phases Underlie Nucleolar Subcompartments*, *Cell* **165** (June, 2016) 1686–1697.

[99] K. M. Ruff, F. Dar, and R. V. Pappu, *Ligand effects on phase separation of multivalent macromolecules*, *Proceedings of the National Academy of Sciences* **118** (Mar., 2021) e2017184118.

[100] D. S. Protter, B. S. Rao, B. Van Treeck, Y. Lin, L. Mizoue, M. K. Rosen, and R. Parker, *Intrinsically Disordered Regions Can Contribute Promiscuous Interactions to RNP Granule Assembly*, *Cell Reports* **22** (Feb., 2018) 1401–1412.

[101] P. Li, S. Banjade, H.-C. Cheng, S. Kim, B. Chen, L. Guo, M. Llaguno, J. V. Hollingsworth, D. S. King, S. F. Banani, P. S. Russo, Q.-X. Jiang, B. T. Nixon, and M. K. Rosen, *Phase transitions in the assembly of multivalent signalling proteins*, *Nature* **483** (Mar., 2012) 336–340.

[102] J. N. Israelachvili, *Intermolecular and Surface Forces*, .

[103] G. He, T. GrandPre, H. Wilson, Y. Zhang, M. C. Jonikas, N. S. Wingreen, and Q. Wang, *Phase-separating pyrenoid proteins form complexes in the dilute phase*, *Communications Biology* **6** (Jan., 2023) 19.

[104] A. Bremer, M. Farag, W. M. Borcherds, I. Peran, E. W. Martin, R. V. Pappu, and T. Mittag, *Deciphering how naturally occurring sequence features impact the phase behaviours of disordered prion-like domains*, *Nature Chemistry* **14** (Feb., 2022) 196–207.

[105] J. Berry, C. P. Brangwynne, and M. Haataja, *Physical principles of intracellular organization via active and passive phase transitions*, *Reports on Progress in Physics* **81** (Apr., 2018) 046601.

[106] C. A. Weber, D. Zwicker, F. Jülicher, and C. F. Lee, *Physics of active emulsions*, *Reports on Progress in Physics* **82** (June, 2019) 064601.

[107] A. Stradner, H. Sedgwick, F. Cardinaux, W. C. K. Poon, S. U. Egelhaaf, and P. Schurtenberger, *Equilibrium cluster formation in concentrated protein solutions and colloids*, *Nature* **432** (Nov., 2004) 492–495.

[108] K. Chen, S. K. Ballas, R. R. Hantgan, and D. B. Kim-Shapiro, *Aggregation of Normal and Sickle Hemoglobin in High Concentration Phosphate Buffer*, *Biophysical Journal* **87** (Dec., 2004) 4113–4121.

[109] W. Pan, O. Galkin, L. Filobelo, R. L. Nagel, and P. G. Vekilov, *Metastable Mesoscopic Clusters in Solutions of Sickle-Cell Hemoglobin*, *Biophysical Journal* **92** (Jan., 2007) 267–277.

[110] S. B. Hutchens and Z.-G. Wang, *Metastable cluster intermediates in the condensation of charged macromolecule solutions*, *The Journal of Chemical Physics* **127** (Aug., 2007) 084912.

[111] L. Porcar, P. Falus, W.-R. Chen, A. Faraone, E. Fratini, K. Hong, P. Baglioni, and Y. Liu, *Formation of the Dynamic Clusters in Concentrated Lysozyme Protein Solutions*, *The Journal of Physical Chemistry Letters* **1** (Jan., 2010) 126–129.

[112] R. Hanlon, C.-C. Chiao, L. Mäthger, A. Barbosa, K. Buresch, and C. Chubb, *Cephalopod dynamic camouflage: bridging the continuum between background matching and disruptive coloration*, *Philosophical Transactions of the Royal Society B: Biological Sciences* **364** (Feb., 2009) 429–437.

[113] A. Chatterjee, J. A. Cerna Sanchez, T. Yamauchi, V. Taupin, J. Couvrette, and A. A. Gorodetsky, *Cephalopod-inspired optical engineering of human cells*, *Nature Communications* **11** (Dec., 2020) 2708.

[114] J. Song, C. Liu, B. Li, L. Liu, L. Zeng, Z. Ye, T. Mao, W. Wu, and B. Hu, *Tunable Cellular Localization and Extensive Cytoskeleton-Interplay of Reflectins*, *Frontiers in Cell and Developmental Biology* **10** (June, 2022) 862011.

[115] J. Messenger, *Neurotransmitters of Cephalopods*, *Invertebrate Neuroscience* **2** (Sept., 1996) 95–114.

[116] M. Wu, G. Xu, C. Han, P.-F. Luan, Y.-H. Xing, F. Nan, L.-Z. Yang, Y. Huang, Z.-H. Yang, L. Shan, L. Yang, J. Liu, and L.-L. Chen, *lncRNA SLERT controls phase separation of FC/DFCs to facilitate Pol I transcription*, *Science* **373** (July, 2021) 547–555.

[117] J. Liu, M. Hebert, Y. Ye, D. Templeton, H. Kung, and A. Matera, *Cell cycle-dependent localization of the CDK2-cyclin E complex in Cajal (coiled) bodies*, *Journal of Cell Science* **113** (May, 2000) 1543–1552.

[118] J. T. Wang, J. Smith, B.-C. Chen, H. Schmidt, D. Rasoloson, A. Paix, B. G. Lambrus, D. Calidas, E. Betzig, and G. Seydoux, *Regulation of RNA granule dynamics by phosphorylation of serine-rich, intrinsically disordered proteins in C. elegans*, *eLife* **3** (Dec., 2014) e04591.

[119] A. P. Jalihal, S. Pitchiaya, L. Xiao, P. Bawa, X. Jiang, K. Bedi, A. Parolia, M. Cieslik, M. Ljungman, A. M. Chinnaiyan, and N. G. Walter, *Multivalent Proteins Rapidly and Reversibly Phase-Separate upon Osmotic Cell Volume Change*, *Molecular Cell* **79** (Sept., 2020) 978–990.e5.

[120] K. Watanabe, T. Umeda, K. Niwa, I. Naguro, and H. Ichijo, *A PP6-ASK3 Module Coordinates the Bidirectional Cell Volume Regulation under Osmotic Stress*, *Cell Reports* **22** (Mar., 2018) 2809–2817.

[121] F. Cardinaux, E. Zaccarelli, A. Stradner, S. Bucciarelli, B. Farago, S. U. Egelhaaf, F. Sciortino, and P. Schurtenberger, *Cluster-Driven Dynamical Arrest in Concentrated Lysozyme Solutions*, *The Journal of Physical Chemistry B* **115** (June, 2011) 7227–7237.

[122] A. Shukla, E. Mylonas, E. Di Cola, S. Finet, P. Timmins, T. Narayanan, and D. I. Svergun, *Absence of equilibrium cluster phase in concentrated lysozyme solutions*, *Proceedings of the National Academy of Sciences* **105** (Apr., 2008) 5075–5080.

[123] Y. Liu, L. Porcar, J. Chen, W.-R. Chen, P. Falus, A. Faraone, E. Fratini, K. Hong, and P. Baglioni, *Lysozyme Protein Solution with an Intermediate Range Order Structure*, *The Journal of Physical Chemistry B* **115** (June, 2011) 7238–7247.

[124] S. J. Piper, R. M. Johnson, D. Wootten, and P. M. Sexton, *Membranes under the Magnetic Lens: A Dive into the Diverse World of Membrane Protein Structures Using Cryo-EM*, *Chemical Reviews* **122** (Sept., 2022) 13989–14017.

[125] K. D. Sharma, F. A. Heberle, and M. N. Waxham, *Visualizing lipid membrane structure with cryo-EM: past, present, and future*, *Emerging Topics in Life Sciences* **7** (Mar., 2023) 55–65.

[126] P. S. Erdmann, Z. Hou, S. Klumpe, S. Khavnekar, F. Beck, F. Wilfling, J. M. Plitzko, and W. Baumeister, *In situ cryo-electron tomography reveals gradient organization of ribosome biogenesis in intact nucleoli*, *Nature Communications* **12** (Sept., 2021) 5364.

[127] M. Zhang, C. Díaz-Celis, B. Onoa, C. Cañari-Chumpitaz, K. I. Requejo, J. Liu, M. Vien, E. Nogales, G. Ren, and C. Bustamante, *Molecular organization of the early stages of nucleosome phase separation visualized by cryo-electron tomography*, *Molecular Cell* **82** (Aug., 2022) 3000–3014.e9.

[128] H. Le Ferrand, M. Duchamp, B. Gabryelczyk, H. Cai, and A. Miserez, *Time-Resolved Observations of Liquid–Liquid Phase Separation at the Nanoscale Using in Situ Liquid Transmission Electron Microscopy*, *Journal of the American Chemical Society* **141** (May, 2019) 7202–7210.